MODELLING OF AN ARTICULATED FLYING BODY AND CONTROL SYSTEM DESIGN

A THESIS SUBMITTED TO
THE GRADUATE SCHOOL OF NATURAL AND APPLIED SCIENCES
OF
MIDDLE EAST TECHNICAL UNIVERSITY

BY

BURÇİN TUTKU GÜZELCAN

IN PARTIAL FULFILLMENT OF THE REQUIREMENTS
FOR
THE DEGREE OF MASTER OF SCIENCE
IN
MECHANICAL ENGINEERING

DECEMBER 2022

Approval of the thesis:

MODELLING OF AN ARTICULATED FLYING BODY AND CONTROL SYSTEM DESIGN

submitted by **BURÇİN TUTKU GÜZELCAN** in partial fulfillment of the requirements for the degree of **Master of Science** i**n Mechanical Engineering, Middle East Technical University** by,

Prof. Dr. Halil Kalıpçılar
Dean, Graduate School of **Natural and Applied Sciences** _____

Prof. Dr. M. A. Sahir Arıkan
Head of the Department, **Mechanical Engineering** _____

Prof. Dr. Yiğit Yazıcıoğlu
Supervisor, **Mechanical Engineering, METU** _____

Prof. Dr. M. Kemal Özgören
Co-Supervisor, **Mechanical Engineering, METU** _____

Examining Committee Members:

Assoc. Prof. Dr. Ali Emre Turgut
Mechanical Engineering, METU _____

Prof. Dr. Yiğit Yazıcıoğlu
Mechanical Engineering, METU _____

Prof. Dr. M. Kemal Özgören
Mechanical Engineering, METU _____

Prof. Dr. M. Arif Adlı
Mechanical Engineering, Gazi University _____

Assoc. Prof. Dr. Mustafa Mert Ankaralı
Electrical - Electronics Engineering, METU _____

Date: 05.12.2022

I hereby declare that all information in this document has been obtained and presented in accordance with academic rules and ethical conduct. I also declare that, as required by these rules and conduct, I have fully cited and referenced all material and results that are not original to this work.

Name Last name : Burçin Tutku Güzelcan

Signature :

ABSTRACT

MODELLING OF AN ARTICULATED FLYING BODY AND CONTROL SYSTEM DESIGN

Güzelcan, Burçin Tutku
Master of Science, Mechanical Engineering
Supervisor : Prof. Dr. Yiğit Yazıcıoğlu
Co-Supervisor: Prof. Dr. M. Kemal Özgören

December 2022, 99 pages

This study presents the conceptual design of an articulated coaxial rotor Unmanned Air Vehicle (UAV) with three-dimensional dynamical models and a control strategy. Conventional rotary-wing aircrafts operate maneuvers via swashplates which is a complex mechanism adding bulky elements to the aircrafts. While designing light weight UAVs, there appears a need for less complex and compact mechanisms for maneuverability rather than swashplates. There are different methods and mechanisms to acquire maneuvering without swashplates. Three DoF Stewart Mechanism as means of articulation forms a base platform for the coaxial rotor in this design. The Steward Mechanism is designed to tilt the coaxial rotor shaft connected to its upper platform to perform maneuvers. The coaxial rotor tilted by the Steward Mechanism provides a beneficial design with reduced complexity, enhanced maneuverability and agility.

Keywords: Unmanned Air Vehicle, Coaxial UAV, Tilted coaxial rotor, Articulated body, Three DoF Stewart Mechanism

ÖZ

EKLEMLİ HAVA ARACI MODELLEME VE KONTROL SİSTEM TASARIMI

Güzelcan, Burçin Tutku
Yüksek Lisans, Makina Mühendisliği
Tez Yöneticisi: Prof. Dr. Yiğit Yazıcıoğlu
Ortak Tez Yöneticisi: Prof. Dr. M. Kemal Özgören

Aralık 2022, 99 sayfa

Bu çalışma, üç boyutlu dinamik modeller ve kontrol stratejileri kullanarak eklemli bir insansız hava aracı (İHA) modellemesi ve kontrol sistemi tasarımı yapmayı öne sürmektedir. Halihazırdaki döner kanatlı hava araçlarında, manevra amacıyla karmaşık bir mekanizma olan eğik plaka kullanılarak hantal bir yapı oluşturulmaktadır. Hafif İHAlar tasarlarken manevra kabiliyeti için daha az karmaşık ve daha kompakt bir mekanizmaya ihtiyaç doğmuştur. Bu tasarımda, Swashplate mekanizması yerine, zıt yönde dönen eş eksenli iki pervanenin ortak milini taşımak ve yölendirmek üzere üç eksenli bir Stewart mekanizması kullanılmıştır. Stewart mekanizması, pervanelerin bağlı olduğu platformu kendisiyle beraber eğerek aracın manevra yapmasını sağlamaktadır. Stewart mekanizması ile yönlendirilen pervane mili, tasarımda karmaşıklığı azaltıp manevra kabiliyeti ve çevikliği artırarak tasarıma fayda sağlayacaktır.

Anahtar Kelimeler: İHA, Eşeksenli İHA, Eğilmiş eşeksenli rotor, Eklemli cisim, 3 Serbestlik dereceli Stewart Mekanizması

To my mother Şule, the best teacher I have ever had,

My lovely father Kaya, my elder brother Orçun,

And Şener, my partner for life and beyond.

ACKNOWLEDGMENTS

First of all, I would like to express my deepest gratitude to my advisors Prof. Dr. Yiğit Yazıcıoğlu and M. Kemal Özgören for their guidance, advice and patience.

My dear uncle Özbek Göçmen who encouraged me to study mechanical engineering deserves a special thanks and will always be remembered.

I also would like to thank my friends Deniz Öner, Hakan Karakurt, Büşra Başkan, Cansu Çetinbaş, Dilara Başaran, Kardelen Yıldırım and Kübra Öztürk for motivating and supporting me throughout this thesis journey.

TABLE OF CONTENTS

ABSTRACT v

ÖZ vi

ACKNOWLEDGMENTS viii

TABLE OF CONTENTS ix

LIST OF TABLES xii

LIST OF FIGURES xiii

LIST OF ABBREVIATIONS xv

LIST OF SYMBOLS xvi

CHAPTERS

1 INTRODUCTION 1

1.1 Literature Survey 1

1.2 Research Objectives 8

1.3 Thesis Outline 10

2 KINEMATICS 11

2.1 Kinematic Features 11

2.2 Simplifications and Assumptions 13

2.3 Reference Frames and Transformation Matrices 15

2.4 Angular Velocity Expressions 18

2.5 Angular Acceleration Expressions 22

2.5.1 Closed Form Expressions for Angular Acceleration 25

2.6 Position Expressions 27

2.7 Linear Velocity Expressions 30

2.8 Linear Acceleration Expressions 32
2.8.1 Closed Form Expressions for Linear Acceleration 36
3 DYNAMICS 41
3.1 Vectorial Force and Moment Equation 41
3.1.1 Vectorial Force Equations 42
3.1.2 Vectorial Moment Equations 43
3.2 Resolution of the Interaction Forces and Moments 45
3.3 Resolution of the Aerodynamic Forces and Moments 48
3.3.1 Downwash Force and Moment 48
3.3.2 Lift Force 55
3.3.3 Drag Moment 58
3.4 Force and Moment Equations in Matrix Form 61
3.4.1 Force Equations in Matrix Form 61
3.4.2 Moment Equations in Matrix Form 62
3.5 Direct Dynamic Analysis 64
4 CONTROL SYSTEM DESIGN 67
4.1 Active Control Strategy 67
4.2 Passive Control Strategy 70
5 SERIAL TO PARALLEL MANIPULATOR CONVERSION 71
5.1 Actuation by Means of a Universal Joint 72
5.1.1 Kinematics for Actuation by a Universal Joint 72
5.1.2 Dynamics for Actuation by a Universal Joint 73
5.2 Actuation by Means of a 3-DoF Parallel Manipulator 76
5.2.1 Kinematics for Actuation by a 3-DoF Parallel Manipulator 76

5.2.2 Dynamics for Actuation by a 3-DoF Parallel Manipulator 78
6 SIMULATION RESULTS 81
6.1 Simulation Parameters 81
6.2 Open Loop Simulations 82
6.3 Closed Loop Simulations 86
6.3.1 Altitude Control 87
6.3.2 Yaw Motion Control 88
6.3.3 Motion Control in X-Y Plane 90
7 CONCLUSION AND FUTURE WORKS 93
7.1 Conclusion 93
7.2 Future Works 95
REFERENCES 97

LIST OF TABLES

TABLES

Table 6.1 Numerical Parameters of the UAV 82

LIST OF FIGURES

FIGURES

Figure 1.1. Curtiss N-9 Aerial Torpedo [2] 1
Figure 1.2. Classification of UAVs [4] 2
Figure 1.3. Rotor Control Through a Swashplate [6] 3
Figure 1.4. The X-4 Flyer [7] 4
Figure 1.5. A Coaxial Drone [8] 5
Figure 1.6. The UAV Tricopter [9] 5
Figure 1.7. A Tri-rotor Coaxial UAV [10] 6
Figure 1.8. A Coaxial MAV with flaps [11] 6
Figure 1.9. A Coaxial Rotor Spherical UAV [12] 7
Figure 1.10. A Coaxial UAV with Cyclic Torque Actuation [13] 7
Figure 1.11. Motor-tilting Coaxial NAV [14] 8
Figure 1.12. Conceptual Design of the Proposed UAV with 3-DoF Stewart Mechanism 9
Figure 2.1. Bodies and Joints Representation of the Model with Isometric View . 13
Figure 2.2. Bodies and Reference Frames Representation on the Simplified Model with Isometric View 15
Figure 3.1. Downwash Effect on the Bodies 49
Figure 3.2. Top View of the Base Platform 52
Figure 3.3. Vectorial Representations of the Downwash Effect on the Base Platform 53
Figure 3.4. Representation of Lift Forces and Drag Moments 56
Figure 3.5. Curve-fit of Lift Force vs Rotational Velocity Plot 57
Figure 3.6. Curve-fit of Drag Moment vs Low Rotational Velocity Plot 59
Figure 3.7. Curve-fit of Drag Moment vs High Rotational Velocity Plot 59
Figure 5.1. Actuation by Means of a Universal Joint 72
Figure 5.2. Actuation by Means of a 3-DoF Parallel Manipulator 76
Figure 6.1. Screen Shot Taken from MATLAB Mechanics Explorer Animation .. 81

Figure 6.2. Input Torques for the OL Simulation 83
Figure 6.3. First Set of Position States for the OL Simulation 84
Figure 6.4. Second Set of Position States for the OL Simulation 85
Figure 6.5. First Set of Velocity States for the OL Simulation 85
Figure 6.6. Second Set of Velocity States for the OL Simulation 86
Figure 6.7. Third Set of Velocity States for the OL Simulation 86
Figure 6.8. Reference Altitude Position Tracking of the UAV 87
Figure 6.9. Reference Velocity Tracking of the UAV in Z Direction 88
Figure 6.10. Reference Yaw Angle Tracking of the UAV 89
Figure 6.11. Reference Yaw Angular Velocity Tracking of the UAV 90
Figure 6.12. Reference X Position Tracking of the UAV 91
Figure 6.13. Reference X Velocity Tracking of the UAV 91

LIST OF ABBREVIATIONS

ABBREVIATIONS

UAV: Unmanned Aerial Vehicle

PID: Proportional Integral Derivative

MAV: Micro Air Vehicle

NAV: Nano Air Vehicle

DOF: Degree of Freedom

SSM: Skew Symmetric Matrix

COLM: Column

RFB: Rotated Frame Based

3-D: Three Dimensional

PS: Propeller Shaft

OL: Open Loop

CL: Closed Loop

LIST OF SYMBOLS

SYMBOLS

L_k : The k^{th} link

B : Origin of the base platform

D_k : Origins of the k^{th} universal joints on the base platform

E_k : Origins of the k^{th} spherical joints under the upper platform

Q : Origin of the central spherical joint under the upper platform

P_k : Origins of the k^{th} revolute joints on the propeller shaft

μ : Degree of Freedom

j_k : Number of joints with a relative mobility of k

n_m : Number of the moving links

s_k : The k^{th} prismatic joint variable

x , y , z : Translational generalized coordinates of the base platform

ϕ_3' , ϕ_2' , ϕ_1' : Euler yaw, pitch and roll angles of the base platform

ϕ_2 , ϕ_3 : Angles of the propeller shaft with respect to the base platform

θ_3 , θ_4 : Spinning angles of the propellers

B_k : The k^{th} body

$F_a(A)$: Reference frame with the origin A and unit vector triad $\left\{\vec{u}_1^{(a)}, \vec{u}_2^{(a)}, \vec{u}_3^{(a)}\right\}$

$\vec{u}_1^{(a)}, \vec{u}_2^{(a)}, \vec{u}_3^{(a)}$: Unit basis vectors of reference frame $F_a(A)$

$\bar{u}_1, \bar{u}_2, \bar{u}_3$: Basic column matrices, i.e., $[1 \quad 0 \quad 0]^t, [0 \quad 1 \quad 0]^t, [0 \quad 0 \quad 1]^t$

$\tilde{u}_1, \tilde{u}_2, \tilde{u}_3$: Skew symmetric cross product matrices of the basic column matrices

$\hat{C}^{(a,b)}$: Transformation matrix from the body B_b reference frame to the body B_a reference frame

$\hat{C}^{(a,b)t}$: Transpose of the transformation matrix from the body B_a reference frame to the body B_b reference frame

$\vec{r}_{AB}$: Position vector from the point A to the point B

$\overset{\vee}{J}_k$: Inertia tensor for the body B_k

$\hat{M}^{(a)}$: Matrix representation of a tensor $\overset{\vee}{M}$ in the frame $F_a(A)$

$\hat{J}_k$: Inertia matrix for the body B_k represented in the body-fixed frame

$\bar{r}_{AB}^{(a)}$: Column matrix of the position vector from the point A to the point B represented in the frame $F_a(A)$

$D_a \vec{r}_{AB}$: Derivative of the position vector $\vec{r}_{AB}$ taken with respect to the frame $F_a(A)$

$\bar{v}_a$: Column matrix that represents the velocity of the point A in the frame $F_a(A)$

$\tilde{\omega}_{a/b}^{(a)}$: Skew symmetric cross product matrix of the angular velocity of the body B_a with respect to the body B_b, represented in the frame $F_a(A)$

CHAPTER 1

INTRODUCTION

1.1 Literature Survey

A UAV (Unmanned Aerial Vehicle) is an autonomous flying system which is operated without an on-board pilot. As a UAV consists of a control system with sensors, actuators and communication unit, it can be controlled remotely or autonomously. Americans Lawrance and Sperryen produced the first UAV named as Curtiss N-9 Aerial Torpedo during World War 1 in 1918. UAVs have started to be utilized for non-military objectives such as agriculture, meteorology, territory reconnaissance, surveillance, security and surveillance after 2004 [1].

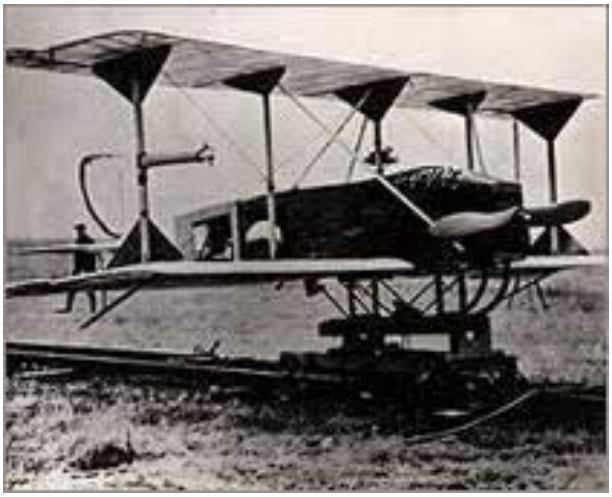

Figure 1.1. Curtiss N-9 Aerial Torpedo [2]

UAVs are classified as fixed-wing and rotary-wing aircrafts considering their wing types, seen in Figure 1.2. Rotary wing aircrafts have relatively more capabilities than fixed-wing aircrafts such as hovering, vertical take-off and landing, etc. That is why

they have been utilized extensively in numerous areas like urban mapping, search and rescue, disaster emergency and territory reconnaissance [3]. A helicopter with two rotors, a main rotor producing the thrust and a tail rotor generating anti-torque, is one of the common instances of rotary wing UAVs [4]. Helicopters also have swashplate mechanisms under the main rotor to realize maneuvering, which is seen in Figure 1.3. Frankly, it is a highly complex and bulky mechanism that is difficult to miniaturize for smaller UAVs. Consequently, among UAVs, quadrotors have turned out to be more common due to their simpler structure, easier control system and better load carrying capability [3].

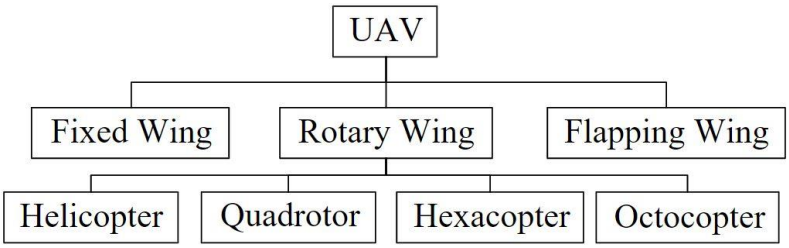

Figure 1.2. Classification of UAVs [4]

The other reasons why quadrotors have become popular is their highly maneuverable, straightforwardly controllable and small-scale sizing nature. Quadrotors are actuated and maneuvered through adjustable rotational speed of four rotors which is simpler and applicable solution for small-sized UAVs compared to swashplates. They have also various applications benefiting from their miniature size; for example, military missions such as patrolling borders and surveilling a target [4].

To continue with the control systems of quadrotors, various PID control algorithms have been utilized extensively in quadrotors due to the algorithm's straightforward, reliable and very stable features. Nowadays, PID is still preferred extensively as a control algorithm in various applications. In time, there appeared different variations of PID, some of which are nonlinear PID controllers, fuzzy PID control and linearizing feedback control with PID [3]. Linearizing feedback control has other

names such as computed torque method and method of inverse dynamics control. It is also partially utilized technique along with PID in this study, because it has a relatively simpler procedure of linearization before applying PID control.

Before proposing a coaxial UAV design without a swashplate in this study, it will be explained in detail, why swashplate mechanisms are necessary for helicopters but avoided while designing miniature UAVs. A swashplate mechanism appears as an articulated rotor hub. It enables pitch motion of the blade for collective and cyclic control inputs [5]. Collective control applies the same pitch angle to all blades for direct thrust control on the rotor. Cyclic control operates by tilting the swashplate creating a one-per-revolution sinusoidal variation in blade pitch. The rotor reacts to both collective and cyclic inputs by flapping in coning and tilting modes [6]. Flapping dynamics of the rotor affects the handling qualities of the aircraft. A swashplate design consists of three bearings (flap, lag and feather), lag dampers, rotating and non-rotating links as seen in Figure 1.3. It is mechanically complex and requires high level of maintenance, since the bearings operate in a highly stress environment [5]. In addition, it is not possible to minimize a bulky and complex mechanism such as swashplate while designing a mini-UAV, whose size is small compared to a helicopter. Therefore, there is a need to find a different method or to design a new mechanism suitable for mini-UAVs.

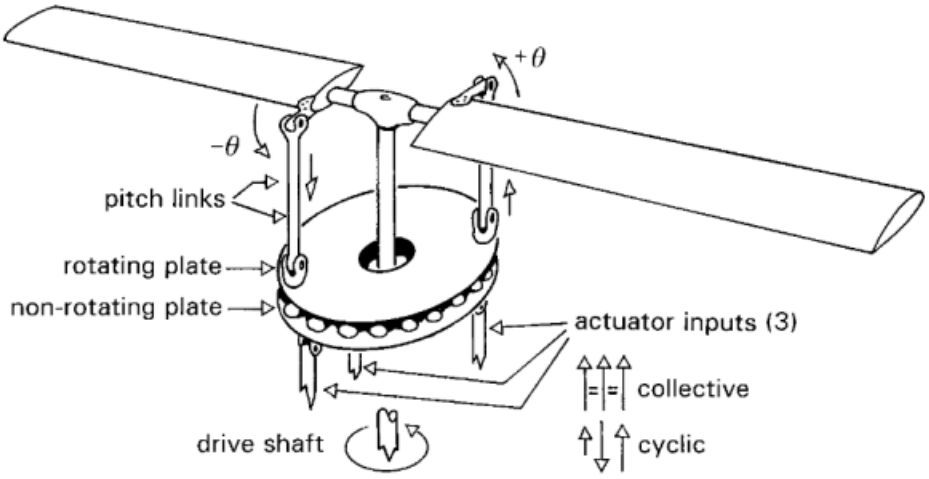

Figure 1.3. Rotor Control Through a Swashplate [6]

Motion control for coaxial rotor helicopters and their advantages over other configurations are explained to understand the reason why coaxial rotor configuration is chosen for the UAV design of concern. There are various rotor types for helicopters. A single main rotor and tail rotor is the most common type. The tail rotor is counter-rotating to the main rotor for torque balance and yaw control. The tandem rotor and side by side configurations have two contra-rotating main rotors with longitudinal and lateral separations respectively. The coaxial rotor helicopter has two contra rotating main rotors with concentric shafts. Pitch and roll motion are acquired by cyclic control, and direct thrust vector control is achieved by collective control as in the single main rotor configuration. Yaw control is acquired by differential torque of the two rotors. This configuration has symmetrical control which is easier to control. Additionally, it is more compact because of the absence of tail rotor [5]. The advantages of coaxial rotor configuration in helicopters lead to the idea that, it is a suitable configuration for the UAV design of concern.

Various UAV designs without swashplates utilize different mechanisms and control methods to perform maneuvers. Featured UAV designs without swashplates are covered here to show the current state of the art. One alternative for UAV designs without swashplates is a quadrotor having rpm-controlled rotors for maneuverability and reduced mechanical complexity [7].

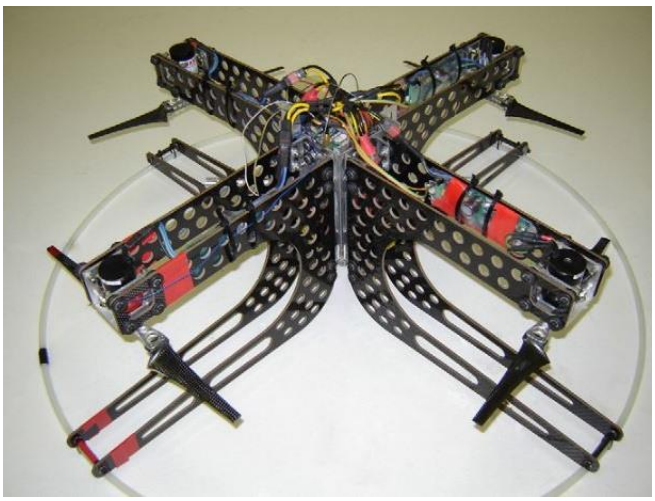

Figure 1.4. The X-4 Flyer [7]

There is another study which modifies a conventional quadrotor. Adjustable and fixed pitch propellers are utilized for a coaxial quadrotor to increase efficiency and flight performance in the existence of different flight conditions, such as turbulent wind [8].

Figure 1.5. A Coaxial Drone [8]

There are even more compact designs decreasing the number of rotors. For example, a tri-rotor UAV design benefits from rpm variation in each rotor to maneuver. Two of the rotors rotate in the same direction while the third one contra-rotates. The rotors are tilt-free which reduce mechanical complexity even more [9].

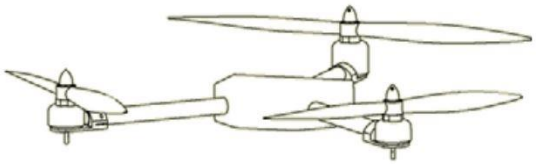

Figure 1.6. The UAV Tricopter [9]

Similarly, contra-rotating rotors are added coaxially to a tri-rotor UAV in a different study. Three coaxial rotors are used in the UAV design for heavy lifting tasks. The rotors provide higher thrust-to-volume ratio while requiring more power due to the aerodynamic effects of the contra-rotating propellers on each other [10].

Figure 1.7. A Tri-rotor Coaxial UAV [10]

There are single coaxial rotor UAV designs without swashplates in the literature as well, which use various methods and mechanisms for maneuverability as required by different tasks. One of the initial studies propose an MAV (Micro Air Vehicle) design having a coaxial rotor with rpm control for yaw and vertical motion. The blades are rigidly attached to the hub which means the rotors are tilt-free. Thus, roll and pitch motions are achieved by controlling aerodynamic surfaces (flaps). The coaxial rotor is driven by two motors with a transmission system. The design is highly compact and foldable, since it is designed for the task of surveillance and monitoring in urban areas [11].

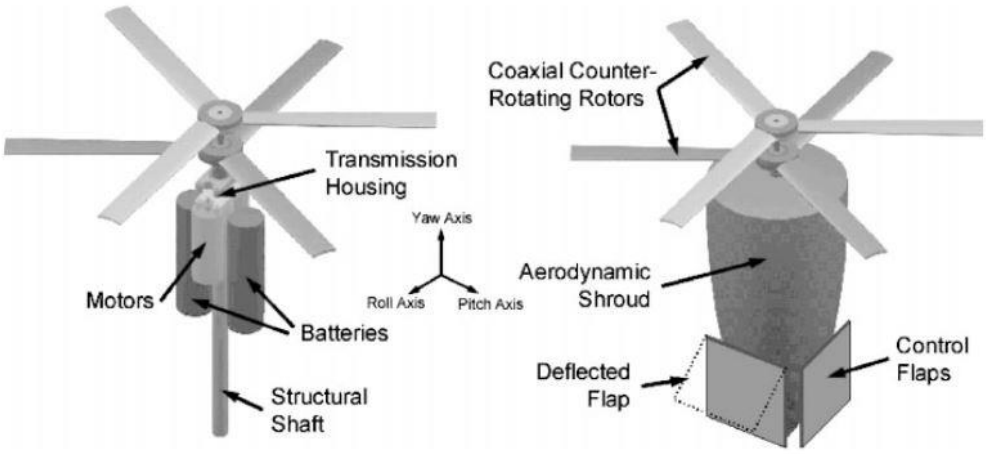

Figure 1.8. A Coaxial MAV with flaps [11]

In one of the studies, a coaxial rotor UAV design is maneuvered via actuated flaps positioned below the coaxial rotors. The UAV is placed inside a spherical cage protecting the propellers, so that it is able to operate in complex environments [12]. The design has one contra-rotating motor to drive coaxial rotor, which seems like an improvement compared to the previous study mentioned.

Figure 1.9. A Coaxial Rotor Spherical UAV [12]

Another way of controlling roll and pitch motion of a MAV is studied recently. The MAV has coaxial rotor with two actuators only. There is no tilting mechanism or flaps. Instead, the MAV has special articulated blades and is electronically driven by modulated cyclic torque to perform maneuvers [13].

Figure 1.10. A Coaxial UAV with Cyclic Torque Actuation [13]

The last highlighted study is related to a NAV (Nano Air Vehicle) which has coaxial rotors with tilting mechanism, developed for indoor and outdoor military missions for delivering sensor packages. The NAV has a combination of rotor cyclic and rpm control for maneuvering and vertical motion. Rotor cyclic and rpm can be controlled independently. Rotor cyclic is achieved by placing two motors in the rotor hub and tilting the plane of motors like a swashplate [14].

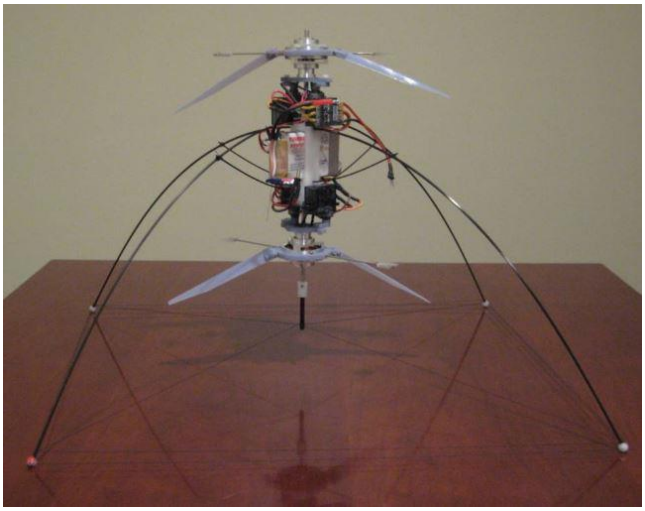

Figure 1.11. Motor-tilting Coaxial NAV [14]

1.2 Research Objectives

The main objective of this study is to design a UAV without a swashplate, because of the disadvantages of the swashplate mechanisms mentioned in the previous section. Another objective is to achieve the rolling and pitching motions of the UAV with a special parallel manipulator, which is a 3-DoF Stewart mechanism used for tilting the coaxial rotor. In addition, the yawing motion is achieved with the speed control of the coaxial propellers. Comparing this study with the other studies from the literature, some of which are covered in the previous section, the NAV in Figure 1.11 is found to be the most similar one to the UAV of concern in this study. That is because it has similar maneuvering method, which is speed control with tilting mechanism without a swashplate. However, the UAV of this study has some

differences compared to the mentioned NAV, which lead to contributions to the literature. The scales of the two designs are the most obvious difference because there is no similar study in the regular-size UAV field. The overall structure of this study is also different in a way to improve the landing performance by placing both of the coaxial rotors at the top the UAV. Actually, this study finds its inspiration from some of the hobbyist prototypes using actuators for tilting the coaxial rotor hub without any linkage system [15], [16]. However, there are no mathematical models and control strategies developed for the above-mentioned prototypes in the literature so far. On the other hand, the 3-DoF Stewart mechanism of this study which is seen in Figure 1.12 benefits the UAV design in terms of agility, compactness and improved maneuverability compared to the hobbyist prototypes mentioned earlier.

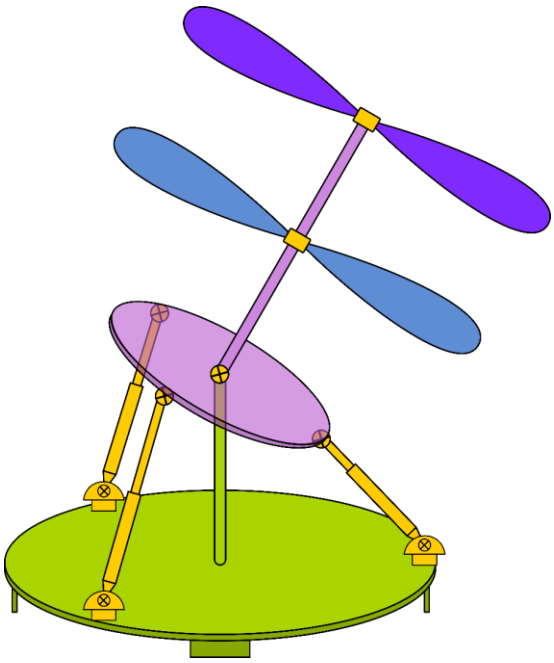

Figure 1.12. Conceptual Design of the Proposed UAV with 3-DoF Stewart Mechanism

1.3 Thesis Outline

First of all, kinematic features of the UAV design are explained briefly. Afterwards, the simplifications and assumptions necessary for the mathematical model are stated. After that, kinematic analysis for the simplified model is performed. Once the angular and linear acceleration expressions are derived, dynamic analysis part comes next. After acquiring the necessary matrices in the dynamic analysis part, they are related to the control strategy. Computed torque method with PID as a means of controlling the UAV is explained in the control part. Then, transition from the simplified model to the actual system is shown analytically. Completing the analytical part of the study, MATLAB, Simulink and Simscape simulation results are illustrated and discussed for both open loop and closed loop actuation modes of the UAV. In the end, the agreement between the analytical and simulation results are shown, and the future studies are discussed in the conclusion part.

CHAPTER 2

KINEMATICS

2.1 Kinematic Features

Proposed UAV design consists of two platforms connected to each other by a 3-DoF parallel manipulator as a mean of tilting mechanism and two propellers as a mean of actuation. The 3-DoF parallel manipulator is installed on the base platform L_1 and consists of 7 moving links which are link pairs $\{L_2, L_2'\}$, $\{L_3, L_3'\}$, $\{L_4, L_4'\}$ and the upper platform L_5. Since the base platform is also moving, it is named as L_1 rather than L_0. To express the DoF or mobility (μ) of the UAV, *Kutzbach-Gruebler formula* [17] is applied as seen below.

$$\mu = 6n_m - (5j_1 + 4j_2 + 3j_3) \tag{2.1}$$

The links are represented by different colors and the joints are represented by yellow color as seen in Figure 2.1. To continue with the joints, 3 universal joints (j_2) are installed on the base platform at the points D_1, D_2 and D_3. In addition, 3 spherical joints (j_3) are installed under the upper platform at the points E_1, E_2 and E_3. The 3 legs of the parallel manipulator consist of 3 prismatic joints (j_1). 1 spherical joint (j_3) connects base platform L_1 directly to the upper platform L_5 at the point Q. Moreover, 2 propellers are connected to the shaft of the upper platform with 2 revolute joints (j_1) at the points P_1 and P_2. Thus, Eq. (2.1) become as seen below.

$$\mu = 6\times10 - (5\times5 + 4\times3 + 3\times4) = 60 - 49 = 11 \tag{2.2}$$

Eq. (2.2) tells that the considered UAV has 11 DoF. 6 DoF belong to L_1 for describing its position (location and orientation) in the 3-D space, 3 DoF belong to

L_5 for describing its orientation with respect to L_1, and 2 DoF belong to the propellers for describing their angular positions with respect to the propeller shaft (PS) attached rigidly to L_5.

On the other hand, 3 prismatic joint variables (s_1, s_2, and s_3) and 2 revolute joint variables (θ_3 and θ_4) are actuated, which are sufficient to orient L_5 and the propellers with respect to L_1. This actuation scheme leaves L_1 with 6 DoF in the 3-D space. However, the mentioned 5 actuators lead to 4 effective control parameters for L_1, which are F_{net} (net aerodynamic force along PS), τ_{net} (net actuation torque about PS), ϕ_3 (azimuth angle of PS relative to L_1), and ϕ_2 (pitch angle of PS relative to L_1). The 5th parameter provided by the 5 actuators is ineffective because it indicates the insignificant spinning rotation of PS about itself.

By means of the 4 effective control parameters, it becomes possible to make the UAV move with a desired translational acceleration vector ($\vec{a}_{C_1}$) of C_1 (mass center of L_1) and a desired yaw acceleration ($\ddot{\phi}_3'$) of L_1. As for the pitch and roll accelerations ($\ddot{\phi}_2'$ and $\ddot{\phi}_1'$) of L_1, they cannot be commanded as desired by the available actuators. However, the pitch and roll motions of L_1 can at least be stabilized owing to the gravitational force and the downwash air flow of the propellers.

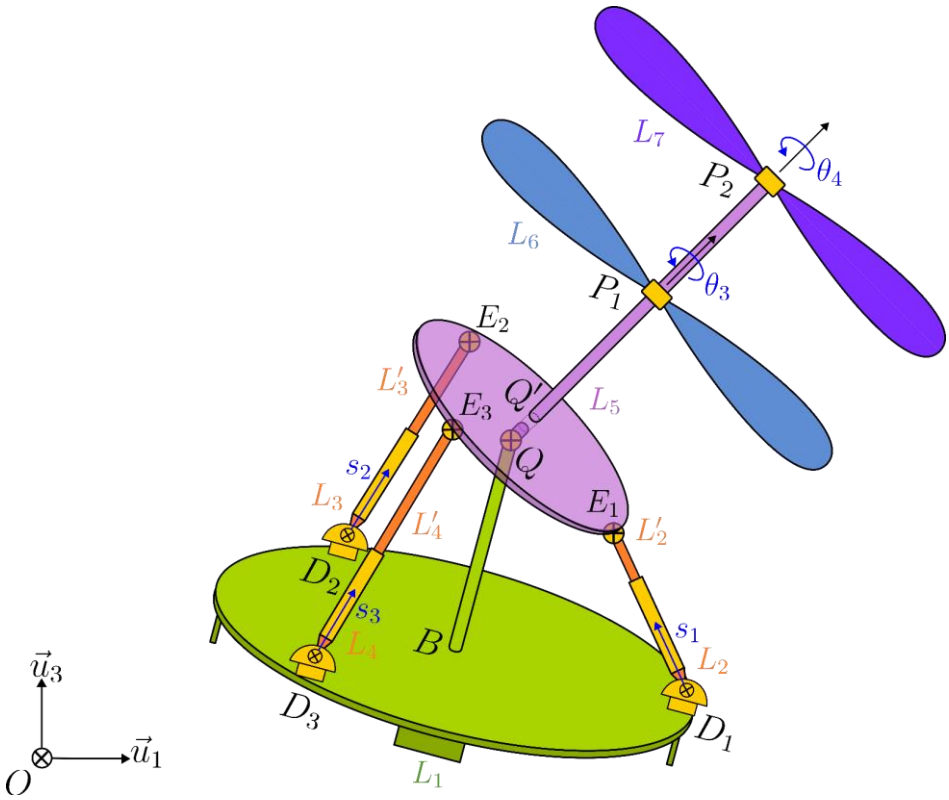

Figure 2.1. Bodies and Joints Representation of the Model with Isometric View

2.2 Simplifications and Assumptions

Since, the 3 DoF parallel manipulator of the UAV has 3 kinematic loops which means 3 times more equations are required than a UAV with a serial manipulator. The model with the parallel manipulator explained previously in Section 2.1 is a complex system in terms of dynamical analysis. To overcome the complexity and to model the UAV more conveniently, the 3 kinematic loops are simplified to a single branch as seen in Figure 2.2 like in the serial manipulators.

In the serial version of the UAV in Figure 2.2, the spherical joint at the point Q is replaced with a universal joint. In this version, the universal joint variables (ϕ_2 and ϕ_3) are actuated instead of the 3 prismatic joint variables of the previous version. Thus, the tilting motion of the upper platform L_5 can be realised by actuating only

2 joint variables instead of 3. It means that one of the actuated prismatic joints in the parallel manipulator version of the UAV in Figure 2.1 is redundant as discussed before. As mentioned in previous Section 2.1, the parallel manipulator version of the UAV has 11 DoF, one of which is associated with the insignificant spinning rotation of the propeller shaft and it is redundant. On the other hand, the serial manipulator version has 10 DoF without any redundancy. Moreover, 7 links in the parallel manipulator version decreases to 4 links and they are called as bodies rather than links in the serial manipulator version. The equivalency between the parallel manipulator version and the serial manipulator version of the UAV will be dealt with in detail later in Chapter 5.

For the sake of simplicity, following reasonable assumptions are made in the mathematical model of the UAV.

1) The masses of all the joints are neglected.
2) Cross-link in the universal joint is assumed to be massless.
3) Joints are frictionless.
4) The distance $|QQ'|$ is assumed to be zero thus, point Q is the joint origin.
5) Center of masses of the propellers L_6 and L_7 are assumed to be at the joint origins P_1 and P_2.
6) Masses of the stabilizing fins in the base platform L_1 are neglected.
7) Aerodynamic interaction between the two propellers is neglected.
8) Downwash effect on the upper platform L_5 is neglected.
9) The overall angular velocities of the propellers L_6 and L_7 are assumed to be $\dot{\theta}_3$ and $\dot{\theta}_4$ in the calculations of lift forces and drag moments. Because they are much larger than the angular velocity components of the other bodies in the system.

2.3 Reference Frames and Transformation Matrices

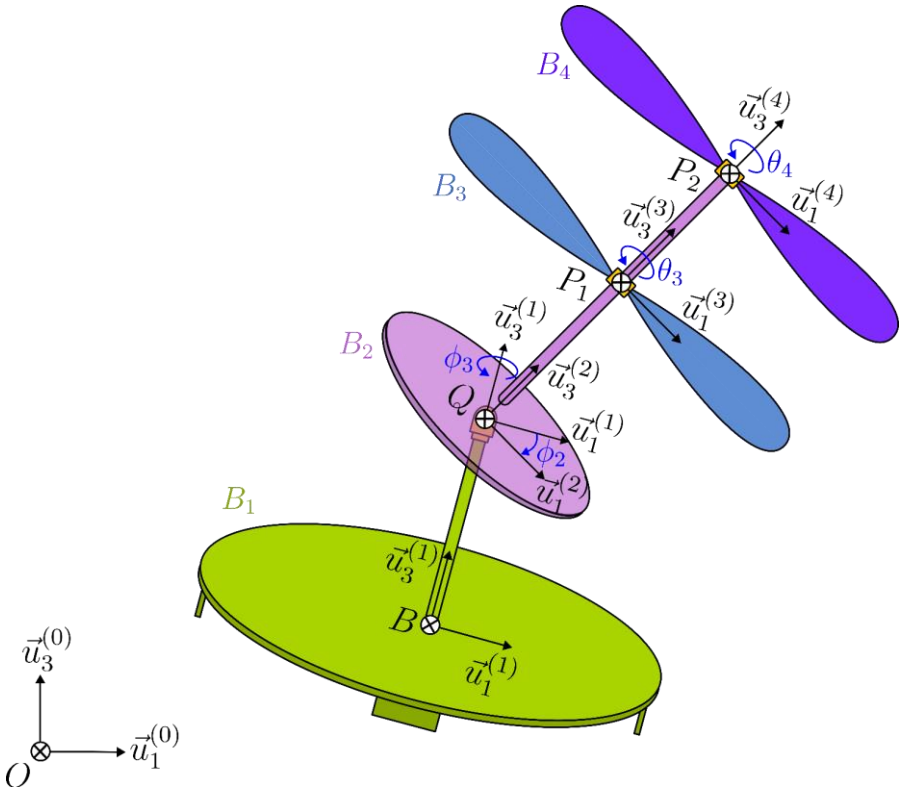

Figure 2.2. Bodies and Reference Frames Representation on the Simplified Model with Isometric View

In Figure 2.2, the right-handed earth fixed reference frame $F_0(O)$ is oriented in the East-North-Up directions. There are 4 bodies shown in different colors. The reference frame of the base platform B_1 is $F_1(B)$. The reference frame of the upper platform B_2 is $F_2(Q)$. The joint center of the universal joint which connects B_1 to B_2 is also located at point Q. The reference frame of the lower propeller B_3 is $F_3(P_1)$. B_3 is connected to B_2 with the revolute joint centered at point P_1. At last, the reference frame of the upper propeller B_4 is $F_4(P_2)$. B_4 is connected to B_2 with the revolute joint centered at point P_2.

Kinematic equations for all bodies will be expressed in their body frames because the inertia matrices are constant in the body frames. This is a convenient property for the calculations. Moreover, the common reference frame for the propellers (B_3 and B_4) is selected as the non-spinning reference frame attached to the propeller shaft, owing to the fact that propellers are inertially symmetric about the axis of rotation. These frames can be denoted as $F_{n3}(P_1)$ and $F_{n4}(P_2)$. Since frames $F_{n3}(P_1)$ and $F_{n4}(P_2)$ have same orientation as the frame $F_2(Q)$ but have position offsets in the direction of the propeller shaft, the following equations can be written for them.

$$\begin{aligned} F_{n3}(P_1) &= F_2(P_1) \\ F_{n4}(P_2) &= F_2(P_2) \end{aligned} \tag{2.3}$$

To express the DoF of the simplified serial manipulator model, Eq. (2.1) is applied again.

$$\mu = 6\times 4 - (5\times 2 + 4\times 1) = 24 - 14 = 10 \tag{2.4}$$

Since there are 10 DoF for the simplified model, there must be 10 generalized coordinates as indicated below.

$$\bar{q} = \begin{bmatrix} x \\ y \\ z \\ \phi_1' \\ \phi_2' \\ \phi_3' \\ \phi_2 \\ \phi_3 \\ \theta_3 \\ \theta_4 \end{bmatrix} \tag{2.5}$$

The first 6 generalized coordinates ($q_1, q_2, \ldots q_6$) describe the motion of the body B_1 relative to $F_0(O)$. The next two (q_7 and q_8) express the angles of the body B_2

relative to B_1. Finally, q_9 expresses the angle of the body B_3 relative to B_2 and q_{10} express angle of the body B_4 relative to B_2.

Proceeding with the transformation matrices, they are applied to express the rotation of one body relative to another body via *Rodrigues Equation* [17] as seen below.

$$\hat{R} = \hat{R}(\tilde{n}, \theta) = \hat{I} + \tilde{n}\sin\theta + \tilde{n}^2(1 - \cos\theta) \tag{2.6}$$

The term $\tilde{n}$ is the outcome of the skew symmetric matrix (ssm) operator which converts a column matrix to a skew symmetric matrix as seen below[17].

$$\begin{aligned} ssm(\bar{n}) &= \tilde{n} \\ ssm\left(\begin{bmatrix} n_1 \\ n_2 \\ n_3 \end{bmatrix}\right) &= \begin{bmatrix} 0 & -n_3 & n_2 \\ n_3 & 0 & -n_1 \\ -n_2 & n_1 & 0 \end{bmatrix} \end{aligned} \tag{2.7}$$

Eq. (2.6) expresses the rotation of angle θ about the vector $\vec{n}$. As such, $\hat{R}$ is the rotation matrix and it can be represented in exponential form [17] as seen below.

$$\hat{R} = \hat{R}(\tilde{n}, \theta) = e^{\tilde{n}\theta} \tag{2.8}$$

The transformation matrices for the rotation of the body frames are expressed conveniently as exponential rotation matrices. The rotation of B_1 relative to $F_0(O)$ is expressed below via the RFB-321 sequence of generalized coordinates q_4, q_5 and q_6, which are indicated in Eq. (2.5).

$$\hat{C}^{(0,1)} = e^{\tilde{u}_3\phi_3'} e^{\tilde{u}_2\phi_2'} e^{\tilde{u}_1\phi_1'} \tag{2.9}$$

Here, RFB stands for "Rotating Frame Based"[17], which implies that each successive rotation is carried out about an axis of the preceding rotated frame.

The rotation of B_2 relative to B_1 is expressed below via the RFB-32 sequence of generalized coordinates q_7 and q_8 which are indicated in Eq. (2.5).

$$\hat{C}^{(1,2)} = e^{\tilde{u}_3\phi_3} e^{\tilde{u}_2\phi_2} \tag{2.10}$$

The rotation of B_3 relative to B_2 is expressed as shown below.

$$\hat{C}^{(2,3)} = e^{\tilde{u}_3\theta_3} \tag{2.11}$$

The rotation of B_4 relative to B_2 is expressed as shown below.

$$\hat{C}^{(2,4)} = e^{\tilde{u}_3\theta_4} \tag{2.12}$$

The overall rotations relative to $F_0(O)$ are expressed as seen below.

$$\begin{aligned}
\hat{C}^{(0,2)} &= \hat{C}^{(0,1)}\hat{C}^{(1,2)} = e^{\tilde{u}_3\phi_3'}e^{\tilde{u}_2\phi_2'}e^{\tilde{u}_1\phi_1'}e^{\tilde{u}_3\phi_3}e^{\tilde{u}_2\phi_2} \\
\hat{C}^{(0,3)} &= \hat{C}^{(0,2)}\hat{C}^{(2,3)} = e^{\tilde{u}_3\phi_3'}e^{\tilde{u}_2\phi_2'}e^{\tilde{u}_1\phi_1'}e^{\tilde{u}_3\phi_3}e^{\tilde{u}_2\phi_2}e^{\tilde{u}_3\theta_3} \\
\hat{C}^{(0,4)} &= \hat{C}^{(0,2)}\hat{C}^{(2,4)} = e^{\tilde{u}_3\phi_3'}e^{\tilde{u}_2\phi_2'}e^{\tilde{u}_1\phi_1'}e^{\tilde{u}_3\phi_3}e^{\tilde{u}_2\phi_2}e^{\tilde{u}_3\theta_4}
\end{aligned} \tag{2.13}$$

2.4 Angular Velocity Expressions

The expression below is applied to derive the angular velocity equations for the bodies of the system [17].

$$\bar{\omega}_{k/0}^{(k)} = colm\left[\tilde{\omega}_{k/0}^{(k)}\right] = colm\left[\hat{C}^{(0,k)t}\dot{\hat{C}}^{(0,k)}\right] \qquad k = 1,2,3,4. \tag{2.14}$$

The column operation (colm) above creates a column matrix from a skew symmetric matrix which is the opposite of the ssm operation mentioned before in Eq. (2.7). Colm operation is expressed as shown below [17].

$$\begin{aligned}
&colm(\tilde{n}) = \bar{n} \\
&colm\left(\begin{bmatrix} 0 & -n_3 & n_2 \\ n_3 & 0 & -n_1 \\ -n_2 & n_1 & 0 \end{bmatrix}\right) = \begin{bmatrix} n_1 \\ n_2 \\ n_3 \end{bmatrix}
\end{aligned} \tag{2.15}$$

Continuing with the angular velocity of B_1,

$$\vec{\omega}_1 = \vec{\omega}_{1/0} \tag{2.16}$$

Matrix equations in $F_1(B)$ are shown below.

$$\bar{\omega}_1^{(1)} = colm\left[\tilde{\omega}_1^{(1)}\right] = colm\left[\hat{C}^{(0,1)t}\dot{\hat{C}}^{(0,1)}\right] \tag{2.17}$$

Since, $\hat{C}^{(0,1)}$ is a function of joint variables q_4, q_5 and q_6 (ϕ_1', ϕ_2' and ϕ_3'), expressions are seen as below.

$$\begin{aligned}\dot{\hat{C}}^{(0,1)} &= \left(\partial\hat{C}^{(0,1)} / \partial\phi_1'\right)\dot{\phi}_1' + \left(\partial\hat{C}^{(0,1)} / \partial\phi_2'\right)\dot{\phi}_2' + \left(\partial\hat{C}^{(0,1)} / \partial\phi_3'\right)\dot{\phi}_3' \\ \bar{\omega}_1^{(1)} &= colm\left[\sum_{k=4}^{k=6}\hat{C}^{(0,1)t}\left(\partial\hat{C}^{(0,1)} / \partial q_k\right)\dot{q}_k\right]\end{aligned} \tag{2.18}$$

$$\bar{\omega}_1^{(1)} = \sum_{k=4}^{k=6}\bar{\Omega}_{1k}\dot{q}_k = \bar{\Omega}_{14}\dot{\phi}_1' + \bar{\Omega}_{15}\dot{\phi}_2' + \bar{\Omega}_{16}\dot{\phi}_3' \tag{2.19}$$

In the above equation, $\bar{\Omega}_{1k}$ is called the angular velocity influence coefficient of $\dot{q}_k$ for B_1. It is the effect of the term $\dot{q}_k$ on the angular velocity of B_1. It is expressed as seen below.

$$\bar{\Omega}_{1k} = colm\left[\hat{C}^{(0,1)t}\left(\partial\hat{C}^{(0,1)} / \partial q_k\right)\right] \qquad \text{for } k = 4,5,6. \tag{2.20}$$

Proceeding with the angular velocity of B_2,

$$\vec{\omega}_2 = \vec{\omega}_{2/0} \tag{2.21}$$

Matrix equations in $F_2(Q)$ are seen as below.

$$\bar{\omega}_2^{(2)} = colm\left[\tilde{\omega}_2^{(2)}\right] = colm\left[\hat{C}^{(0,2)t}\dot{\hat{C}}^{(0,2)}\right] \tag{2.22}$$

Since, $\hat{C}^{(0,2)}$ is a function of joint variables q_4, q_5, q_6, q_7 and q_8 (ϕ_1', ϕ_2', ϕ_3', ϕ_2 and ϕ_3), expressions are seen as below.

$$\dot{\hat{C}}^{(0,2)} = \left(\partial \hat{C}^{(0,2)} / \partial \phi_1'\right)\dot{\phi}_1' + \left(\partial \hat{C}^{(0,2)} / \partial \phi_2'\right)\dot{\phi}_2' + \left(\partial \hat{C}^{(0,2)} / \partial \phi_3'\right)\dot{\phi}_3'$$
$$+\left(\partial \hat{C}^{(0,2)} / \partial \phi_2\right)\dot{\phi}_2 + \left(\partial \hat{C}^{(0,2)} / \partial \phi_3\right)\dot{\phi}_3 \qquad (2.23)$$
$$\bar{\omega}_2^{(2)} = colm\left[\sum_{k=4}^{k=8} \hat{C}^{(0,2)t}\left(\partial \hat{C}^{(0,2)} / \partial q_k\right)\dot{q}_k\right]$$

$$\bar{\omega}_2^{(2)} = \sum_{k=4}^{k=8} \bar{\Omega}_{2k}\dot{q}_k = \bar{\Omega}_{24}\dot{\phi}_1' + \bar{\Omega}_{25}\dot{\phi}_2' + \bar{\Omega}_{26}\dot{\phi}_3' + \bar{\Omega}_{27}\dot{\phi}_2 + \bar{\Omega}_{28}\dot{\phi}_3 \qquad (2.24)$$

In the above equation, $\bar{\Omega}_{2k}$ is called the angular velocity influence coefficient of $\dot{q}_k$ for B_2. It is the effect of the term $\dot{q}_k$ on the angular velocity of B_2. It is expressed as seen below.

$$\bar{\Omega}_{2k} = colm\left[\hat{C}^{(0,2)t}\left(\partial \hat{C}^{(0,2)} / \partial q_k\right)\right] \qquad \text{for } k = 4,5,6,7,8. \qquad (2.25)$$

Continuing with the angular velocity of B_3,

$$\vec{\omega}_3 = \vec{\omega}_{3/0} \qquad (2.26)$$

Matrix equation in $F_3\left(P_1\right)$ is seen as below.

$$\bar{\omega}_3^{(3)} = colm\left[\tilde{\omega}_3^{(3)}\right] = colm\left[\hat{C}^{(0,3)t}\dot{\hat{C}}^{(0,3)}\right] \qquad (2.27)$$

On the other hand, it is necessary to express $\bar{\omega}_3^{(3)}$ in the nonrotating frame $F_{n3}(P_1)$ which is equivalent to the frame $F_2\left(P_1\right)$. Thus, matrix equations in $F_2\left(P_1\right)$ are seen as below.

$$\bar{\omega}_3^{(2)} = \hat{C}^{(2,3)}\bar{\omega}_3^{(3)}$$
$$\bar{\omega}_3^{(2)} = \hat{C}^{(2,3)}colm\left[\tilde{\omega}_3^{(3)}\right] = \hat{C}^{(2,3)}colm\left[\hat{C}^{(0,3)t}\dot{\hat{C}}^{(0,3)}\right] \qquad (2.28)$$

Since, $\hat{C}^{(0,3)}$ is a function of joint variables q_4, q_5, q_6, q_7, q_8 and q_9 (ϕ_1', ϕ_2', ϕ_3', ϕ_2, ϕ_3 and θ_3), expressions are seen as below.

$$\dot{\hat{C}}^{(0,3)} = \left(\partial \hat{C}^{(0,3)} / \partial \phi_1'\right)\dot{\phi}_1' + \left(\partial \hat{C}^{(0,3)} / \partial \phi_2'\right)\dot{\phi}_2' + \left(\partial \hat{C}^{(0,3)} / \partial \phi_3'\right)\dot{\phi}_3'$$
$$+\left(\partial \hat{C}^{(0,3)} / \partial \phi_2\right)\dot{\phi}_2 + \left(\partial \hat{C}^{(0,3)} / \partial \phi_3\right)\dot{\phi}_3 + \left(\partial \hat{C}^{(0,3)} / \partial \theta_3\right)\dot{\theta}_3 \qquad (2.29)$$
$$\bar{\omega}_3^{(2)} = \hat{C}^{(2,3)} colm\left[\sum_{k=4}^{k=9} \hat{C}^{(0,3)t}\left(\partial \hat{C}^{(0,3)} / \partial q_k\right)\dot{q}_k\right]$$

$$\bar{\omega}_3^{(2)} = \sum_{k=4}^{k=9} \bar{\Omega}_{3k}^{(2)}\dot{q}_k = \bar{\Omega}_{34}^{(2)}\dot{\phi}_1' + \bar{\Omega}_{35}^{(2)}\dot{\phi}_2' + \bar{\Omega}_{36}^{(2)}\dot{\phi}_3' + \bar{\Omega}_{37}^{(2)}\dot{\phi}_2 + \bar{\Omega}_{38}^{(2)}\dot{\phi}_3 + \bar{\Omega}_{39}^{(2)}\dot{\theta}_3 \qquad (2.30)$$

$$\bar{\Omega}_{3k} = \bar{\Omega}_{3k}^{(2)} \qquad (2.31)$$

In the above equation, $\bar{\Omega}_{3k}$ is called the angular velocity influence coefficient of $\dot{q}_k$ for B_3. It is the effect of the term $\dot{q}_k$ on the angular velocity of B_3. It is expressed as seen below.

$$\bar{\Omega}_{3k} = \hat{C}^{(2,3)} colm\left[\hat{C}^{(0,3)t}\left(\partial \hat{C}^{(0,3)} / \partial q_k\right)\right] \qquad \text{for } k = 4,5,6,...9. \qquad (2.32)$$

Proceeding with the angular velocity of B_4,

$$\vec{\omega}_4 = \vec{\omega}_{4/0} \qquad (2.33)$$

Matrix equation in $F_4\left(P_2\right)$ is seen as below.

$$\bar{\omega}_4^{(4)} = colm\left[\tilde{\omega}_4^{(4)}\right] = colm\left[\hat{C}^{(0,4)t}\dot{\hat{C}}^{(0,4)}\right] \qquad (2.34)$$

However, it is necessary to express $\bar{\omega}_4^{(4)}$ in the nonrotating frame $F_{n4}(P_2)$ which is equivalent to the frame $F_2\left(P_2\right)$. Thus, matrix equations in $F_2\left(P_2\right)$ are seen as below.

$$\bar{\omega}_4^{(2)} = \hat{C}^{(2,4)}\bar{\omega}_4^{(4)}$$
$$\bar{\omega}_4^{(2)} = \hat{C}^{(2,4)} colm\left[\tilde{\omega}_4^{(4)}\right] = \hat{C}^{(2,4)} colm\left[\hat{C}^{(0,4)t}\dot{\hat{C}}^{(0,4)}\right] \qquad (2.35)$$

Since, $\hat{C}^{(0,4)}$ is a function of joint variables q_4, q_5, q_6, q_7, q_8 and q_{10} (ϕ_1', ϕ_2', ϕ_3', ϕ_2, ϕ_3 and θ_4), expressions are seen as below.

$$\dot{\hat{C}}^{(0,4)} = \left(\partial \hat{C}^{(0,4)} / \partial \phi_1'\right)\dot{\phi}_1' + \left(\partial \hat{C}^{(0,4)} / \partial \phi_2'\right)\dot{\phi}_2' + \left(\partial \hat{C}^{(0,4)} / \partial \phi_3'\right)\dot{\phi}_3'$$
$$+\left(\partial \hat{C}^{(0,4)} / \partial \phi_2\right)\dot{\phi}_2 + \left(\partial \hat{C}^{(0,4)} / \partial \phi_3\right)\dot{\phi}_3 + \left(\partial \hat{C}^{(0,4)} / \partial \theta_3\right)\dot{\theta}_3 \qquad (2.36)$$
$$\bar{\omega}_4^{(2)} = \hat{C}^{(2,4)} colm\left[\sum_{k=4}^{k=10} \hat{C}^{(0,4)t}\left(\partial \hat{C}^{(0,4)} / \partial q_k\right)\dot{q}_k\right]$$

$$\bar{\omega}_4^{(2)} = \sum_{k=4}^{k=10} \bar{\Omega}_{4k}^{(2)}\dot{q}_k = \bar{\Omega}_{44}^{(2)}\dot{\phi}_1' + \bar{\Omega}_{45}^{(2)}\dot{\phi}_2' + \bar{\Omega}_{46}^{(2)}\dot{\phi}_3' + \bar{\Omega}_{47}^{(2)}\dot{\phi}_2 + \bar{\Omega}_{48}^{(2)}\dot{\phi}_3 + \bar{\Omega}_{4,10}^{(2)}\dot{\theta}_4 \qquad (2.37)$$

$$\bar{\Omega}_{4k} = \bar{\Omega}_{4k}^{(2)} \qquad (2.38)$$

In the above equation, $\bar{\Omega}_{4k}$ is called the angular velocity influence coefficient of $\dot{q}_k$ for B_4. It is the effect of the term $\dot{q}_k$ on the angular velocity of B_4. It is expressed as seen below. Moreover, the term $\bar{\Omega}_{49}$ does not appear in the equation because it is zero as the rate of joint variable $\dot{q}_9\,(\dot{\theta}_3)$ has no effect on the B_4.

$$\bar{\Omega}_{4k} = \hat{C}^{(2,4)} colm\left[\hat{C}^{(0,4)t}\left(\partial \hat{C}^{(0,4)} / \partial q_k\right)\right] \qquad \text{for } k = 4,5,6,7,8,10. \qquad (2.39)$$

2.5 Angular Acceleration Expressions

To start with the angular acceleration of the B_1, the basic expressions are as seen below.

$$\vec{\alpha}_1 = \vec{\alpha}_{1/0} = D_0\vec{\omega}_{1/0} = D_1\vec{\omega}_{1/0} \qquad (2.40)$$

Here, $D_k = (d/dt)|_k$ indicates the differentiation of a vector with respect to a reference frame F_k, i.e., taking derivative as if F_k is fixed [17].

Matrix equations in $F_1(B)$ are seen as below.

$$\bar{\alpha}_1^{(1)} = D_1\bar{\omega}_1^{(1)} = \dot{\bar{\omega}}_1^{(1)} \qquad (2.41)$$

$\bar{\alpha}_1^{(1)}$ is also expressed with the influence coefficients as seen below.

$$\bar{\alpha}_1^{(1)} = \sum_{k=4}^{k=6}\left[\bar{\Omega}_{1k}\ddot{q}_k\right] + \sum_{k=4}^{k=6}\sum_{j=4}^{j=6}\left[\bar{\Gamma}_{1kj}\dot{q}_k\dot{q}_j\right] \tag{2.42}$$

In the above equation, the term $\bar{\Omega}_{1k}$ is the acceleration-to-acceleration influence coefficient for B_1 which is the same as the velocity-to-velocity influence coefficient for B_1. The term $\bar{\Gamma}_{1kj}$ is the velocity-to-acceleration influence coefficient for B_1 which is expressed as shown below.

$$\bar{\Gamma}_{1kj} = \partial\bar{\Omega}_{1k} / \partial q_j \qquad k = 4,5,6\ ;\ j = 4,5,6. \tag{2.43}$$

To continue with the angular acceleration of B_2, expressions are as seen below.

$$\vec{\alpha}_2 = \vec{\alpha}_{2/0} = D_0\vec{\omega}_{2/0} = D_2\vec{\omega}_{2/0} \tag{2.44}$$

Matrix equations in $F_2(Q)$ are seen as below.

$$\bar{\alpha}_2^{(2)} = D_2\bar{\omega}_2^{(2)} = \dot{\bar{\omega}}_2^{(2)} \tag{2.45}$$

$\bar{\alpha}_2^{(2)}$ is expressed with the influence coefficients as seen below.

$$\bar{\alpha}_2^{(2)} = \sum_{k=4}^{k=8}\left[\bar{\Omega}_{2k}\ddot{q}_k\right] + \sum_{k=4}^{k=8}\sum_{j=4}^{j=8}\left[\bar{\Gamma}_{2kj}\dot{q}_k\dot{q}_j\right] \tag{2.46}$$

In the above equation, the term $\bar{\Omega}_{2k}$ is the acceleration-to-acceleration influence coefficient for B_2 which is the same as the velocity-to-velocity influence coefficient for B_2. The term $\bar{\Gamma}_{2kj}$ is the velocity-to-acceleration influence coefficient for B_2 which is expressed as shown below.

$$\bar{\Gamma}_{2kj} = \partial\bar{\Omega}_{2k} / \partial q_j \qquad k = 4,5,\ldots 8\ ;\ j = 4,5,\ldots 8. \tag{2.47}$$

Proceeding with the angular acceleration of B_3, expressions are as seen below.

$$\begin{aligned} &\vec{\alpha}_3 = \vec{\alpha}_{3/0} = D_0\vec{\omega}_{3/0} = D_3\vec{\omega}_{3/0} \\ &D_3\vec{\omega}_{3/0} = D_2\vec{\omega}_{3/0} + \vec{\omega}_{2/3}\times\vec{\omega}_{3/0} = D_2\vec{\omega}_{3/0} - \vec{\omega}_{3/2}\times\vec{\omega}_{3/0} \end{aligned} \tag{2.48}$$

Above expression represents *Coriolis Transport Theorem* [17] which is applied to take derivative of an expression with respect to different frames.

Matrix equations in $F_2\left(P_1\right)$ are seen as below.

$$\begin{aligned}
&\bar{\alpha}_3^{(2)} = D_0\bar{\omega}_3^{(2)} = D_2\bar{\omega}_3^{(2)} - \tilde{\omega}_{3/2}^{(2)}\bar{\omega}_3^{(2)} \\
&D_2\bar{\omega}_3^{(2)} = D_2\bar{\omega}_{3/0}^{(2)} = D_2\left(\bar{\omega}_{3/2}^{(2)} + \bar{\omega}_{2/0}^{(2)}\right) = D_2\bar{\omega}_{3/2}^{(2)} + D_2\bar{\omega}_{2/0}^{(2)} = \bar{\alpha}_{3/2}^{(2)} + \bar{\alpha}_{2/0}^{(2)} \\
&\bar{\alpha}_3^{(2)} = \bar{\alpha}_{3/2}^{(2)} + \bar{\alpha}_{2/0}^{(2)} - \tilde{\omega}_{3/2}^{(2)}\bar{\omega}_3^{(2)}
\end{aligned} \tag{2.49}$$

$\bar{\alpha}_3^{(2)}$ is expressed with the influence coefficients as seen below.

$$\begin{aligned}
\bar{\alpha}_3^{(2)} &= \sum_{k=4}^{k=9}\left[\bar{\Omega}_{3k}\ddot{q}_k\right] + \sum_{k=4}^{k=9}\left[\dot{\bar{\Omega}}_{3k}\dot{q}_k\right] - \sum_{k=9}^{k=9}\sum_{j=4}^{j=9}\left[\tilde{\Omega}_{3k}\bar{\Omega}_{3j}\dot{q}_k\dot{q}_j\right] \\
\bar{\alpha}_3^{(2)} &= \sum_{k=4}^{k=9}\left[\bar{\Omega}_{3k}\ddot{q}_k\right] + \sum_{k=4}^{k=9}\sum_{j=4}^{j=9}\left[\bar{\Gamma}_{3kj}\dot{q}_k\dot{q}_j\right] - \sum_{k=9}^{k=9}\sum_{j=4}^{j=9}\left[\tilde{\Omega}_{3k}\bar{\Omega}_{3j}\dot{q}_k\dot{q}_j\right] \\
\bar{\alpha}_3^{(2)} &= \sum_{k=4}^{k=9}\left[\bar{\Omega}_{3k}\ddot{q}_k\right] + \sum_{k=4}^{k=8}\sum_{j=4}^{j=9}\left[\bar{\Gamma}_{3kj}\dot{q}_k\dot{q}_j\right] + \sum_{k=9}^{k=9}\sum_{j=4}^{j=9}\left[\left(\bar{\Gamma}_{3kj} - \tilde{\Omega}_{3k}\bar{\Omega}_{3j}\right)\dot{q}_k\dot{q}_j\right]
\end{aligned} \tag{2.50}$$

In the above equation, the term $\bar{\Omega}_{3k}$ is the acceleration-to-acceleration influence coefficient for B_3 which is the same as the velocity-to-velocity influence coefficient for B_3. The terms $\bar{\Gamma}_{2kj}$ and $\bar{\Gamma}_{2kj}^{*}$ are the velocity-to-acceleration influence coefficients for B_3 which are expressed as below.

$$\begin{aligned}
&\bar{\Gamma}_{3kj} = \partial\bar{\Omega}_{3k} / \partial q_j \qquad k = 4,5,...9\ ;\ j = 4,5,...9. \\
&\bar{\Gamma}_{3kj}^{*} = \bar{\Gamma}_{3kj} - \tilde{\Omega}_{3k}\bar{\Omega}_{3j} \qquad k = 9\ ;\ j = 4,5,...9
\end{aligned} \tag{2.51}$$

Continuing with the angular acceleration of B_4, expressions are as seen below.

$$\begin{aligned}
&\vec{\alpha}_4 = \vec{\alpha}_{4/0} = D_0\vec{\omega}_{4/0} = D_4\vec{\omega}_{4/0} \\
&D_4\vec{\omega}_{4/0} = D_2\vec{\omega}_{4/0} + \vec{\omega}_{2/4}\times\vec{\omega}_{4/0} = D_2\vec{\omega}_{4/0} - \vec{\omega}_{4/2}\times\vec{\omega}_{4/0}
\end{aligned} \tag{2.52}$$

Above expression represents *Coriolis Transport Theorem* [17] which is applied to take derivative of an expression with respect to different frames.

Matrix equations in $F_2\left(P_2\right)$ are seen as below.

$$\begin{aligned}
&\bar{\alpha}_4^{(2)} = D_0\bar{\omega}_4^{(2)} = D_2\bar{\omega}_4^{(2)} - \tilde{\omega}_{4/2}^{(2)}\bar{\omega}_4^{(2)} \\
&D_2\bar{\omega}_4^{(2)} = D_2\bar{\omega}_{4/0}^{(2)} = D_2\left(\bar{\omega}_{4/2}^{(2)} + \bar{\omega}_{2/0}^{(2)}\right) = D_2\bar{\omega}_{4/2}^{(2)} + D_2\bar{\omega}_{2/0}^{(2)} = \bar{\alpha}_{4/2}^{(2)} + \bar{\alpha}_{2/0}^{(2)} \\
&\bar{\alpha}_4^{(2)} = \bar{\alpha}_{4/2}^{(2)} + \bar{\alpha}_{2/0}^{(2)} - \tilde{\omega}_{4/2}^{(2)}\bar{\omega}_4^{(2)}
\end{aligned} \tag{2.53}$$

$\bar{\alpha}_4^{(2)}$ is expressed with the influence coefficients as seen below.

$$\begin{aligned}
\bar{\alpha}_4^{(2)} &= \sum_{k=4}^{k=10}\left[\bar{\Omega}_{4k}\ddot{q}_k\right] + \sum_{k=4}^{k=10}\left[\dot{\bar{\Omega}}_{4k}\dot{q}_k\right] - \sum_{k=10}^{k=10}\sum_{j=4}^{j=10}\left[\tilde{\Omega}_{4k}\bar{\Omega}_{4j}\dot{q}_k\dot{q}_j\right] \\
\bar{\alpha}_4^{(2)} &= \sum_{k=4}^{k=10}\left[\bar{\Omega}_{4k}\ddot{q}_k\right] + \sum_{k=4}^{k=10}\sum_{j=4}^{j=10}\left[\bar{\Gamma}_{4kj}\dot{q}_k\dot{q}_j\right] - \sum_{k=10}^{k=10}\sum_{j=4}^{j=10}\left[\tilde{\Omega}_{4k}\bar{\Omega}_{4j}\dot{q}_k\dot{q}_j\right] \\
\bar{\alpha}_4^{(2)} &= \sum_{k=4}^{k=10}\left[\bar{\Omega}_{4k}\ddot{q}_k\right] + \sum_{k=4}^{k=9}\sum_{j=4}^{j=10}\left[\bar{\Gamma}_{4kj}\dot{q}_k\dot{q}_j\right] + \sum_{k=10}^{k=10}\sum_{j=4}^{j=10}\left[\left(\bar{\Gamma}_{4kj} - \tilde{\Omega}_{4k}\bar{\Omega}_{4j}\right)\dot{q}_k\dot{q}_j\right]
\end{aligned} \tag{2.54}$$

In the above equation, the term $\bar{\Omega}_{4k}$ is the acceleration-to-acceleration influence coefficient for B_4 which is the same as velocity-to-velocity influence coefficient for B_4. The terms $\bar{\Gamma}_{4kj}$ and $\bar{\Gamma}_{4kj}^{*}$ are the velocity-to-acceleration influence coefficients for B_4 which are expressed as shown below.

$$\begin{aligned}
&\bar{\Gamma}_{4kj} = \partial\bar{\Omega}_{4k} / \partial q_j \qquad k = 4,5,...10\ ;\ j = 4,5,...10. \\
&\bar{\Gamma}_{4kj}^{*} = \bar{\Gamma}_{4kj} - \tilde{\Omega}_{4k}\bar{\Omega}_{4j} \qquad k = 10\ ;\ j = 4,5,...10.
\end{aligned} \tag{2.55}$$

2.5.1 Closed Form Expressions for Angular Acceleration

Angular acceleration equation for the bodies B_k $(k = 1,2,3,4.)$ is seen as below.

$$\bar{\alpha}_k^{(k)} = \bar{\alpha}_k^{(k)}\left(\bar{q},\dot{\bar{q}},\ddot{\bar{q}},t\right) = \hat{\Omega}_k\left(\bar{q},t\right)\ddot{\bar{q}} + \bar{\alpha}_k^{0}\left(\bar{q},\dot{\bar{q}},t\right) \qquad k = 1,2,3,4. \tag{2.56}$$

The terms $\bar{\alpha}_k^{0}$ $(k = 1,2,3,4.)$ are called biased terms of the angular accelerations which are left in the closed form since they are computed simultaneously via a computer program. On the other hand, influence coefficients of acceleration-to-

acceleration $\hat{\Omega}_k$ $(k=1,2,3,4.)$ are expressed in the open form. Scalar equations of the angular acceleration for B_1 are seen as below. Abbreviation of s and c stands for sine and cosine functions.

$$\begin{aligned}
\alpha_{11} &= \ddot{\phi}_1' - \ddot{\phi}_3'\left(s\phi_2'\right) + \alpha_{11}^0 \\
\alpha_{12} &= \ddot{\phi}_2'\left(c\phi_1'\right) + \ddot{\phi}_3'\left(c\phi_2' s\phi_1'\right) + \alpha_{12}^0 \\
\alpha_{13} &= -\ddot{\phi}_2'\left(s\phi_1'\right) + \ddot{\phi}_3'\left(c\phi_1' c\phi_2'\right) + \alpha_{13}^0
\end{aligned} \tag{2.57}$$

Scalar equations of angular acceleration for B_2 are seen as below.

$$\begin{aligned}
\alpha_{21} &= \ddot{\phi}_1'\left(c\phi_2 c\phi_3\right) + \ddot{\phi}_2'\left(s\phi_2 s\phi_1' + c\phi_2 c\phi_1' s\phi_3\right) + \ddot{\phi}_3'\left(\Omega_{2,16}\right) - \ddot{\phi}_3\left(s\phi_2\right) + \alpha_{21}^0 \\
\alpha_{22} &= -\ddot{\phi}_1'\left(s\phi_3\right) + \ddot{\phi}_2'\left(c\phi_3 c\phi_1'\right) + \ddot{\phi}_3'\left(s\phi_3 s\phi_2' + c\phi_3 c\phi_2' s\phi_1'\right) + \ddot{\phi}_2 + \alpha_{22}^0 \\
\alpha_{23} &= \ddot{\phi}_1'\left(c\phi_3 s\phi_2\right) + \ddot{\phi}_2'\left(c\phi_1' s\phi_2 s\phi_3 - c\phi_2 s\phi_1'\right) + \ddot{\phi}_3'\left(\Omega_{2,36}\right) + \ddot{\phi}_3\left(c\phi_2\right) + \alpha_{23}^0 \\
\Omega_{2,16} &= c\phi_2 c\phi_2' s\phi_3 s\phi_1' - c\phi_1' c\phi_2' s\phi_2 - c\phi_2 c\phi_3 s\phi_2' \\
\Omega_{2,36} &= c\phi_2 c\phi_1' c\phi_2' - c\phi_3 s\phi_2 s\phi_2' + c\phi_2' s\phi_2 s\phi_3 s\phi_1'
\end{aligned} \tag{2.58}$$

The term $\Omega_{j,kl}$ $\left(j=1,2,3,4;\ k=1,2,3;\ l=1,2...10.\right)$ indicates lengthy expressions with trigonometric functions. It is used for ease of reading the equations.

Scalar equations of angular acceleration for B_3 are seen as below.

$$\begin{aligned}
\alpha_{31} &= \ddot{\phi}_1'\left(c\phi_2 c\phi_3\right) + \ddot{\phi}_2'\left(s\phi_2 s\phi_1' + c\phi_2 c\phi_1' s\phi_3\right) + \ddot{\phi}_3'\left(\Omega_{3,16}\right) - \ddot{\phi}_3\left(s\phi_2\right) + \alpha_{31}^0 \\
\alpha_{32} &= -\ddot{\phi}_1'\left(s\phi_3\right) + \ddot{\phi}_2'\left(c\phi_3 c\phi_1'\right) + \ddot{\phi}_3'\left(s\phi_3 s\phi_2' + c\phi_3 c\phi_2' s\phi_1'\right) + \ddot{\phi}_2 + \alpha_{32}^0 \\
\alpha_{33} &= \ddot{\phi}_1'\left(c\phi_3 s\phi_2\right) + \ddot{\phi}_2'\left(c\phi_1' s\phi_2 s\phi_3 - c\phi_2 s\phi_1'\right) + \ddot{\phi}_3'\left(\Omega_{3,36}\right) + \ddot{\phi}_3\left(c\phi_2\right) + \ddot{\theta}_3 + \alpha_{33}^0 \\
\Omega_{3,16} &= c\phi_2 c\phi_2' s\phi_3 s\phi_1' - c\phi_1' c\phi_2' s\phi_2 - c\phi_2 c\phi_3 s\phi_2' \\
\Omega_{3,36} &= c\phi_2 c\phi_1' c\phi_2' - c\phi_3 s\phi_2 s\phi_2' + c\phi_2' s\phi_2 s\phi_3 s\phi_1'
\end{aligned} \tag{2.59}$$

Scalar equations of angular acceleration for B_4 are seen as below.

$$
\begin{aligned}
\alpha_{41} &= \ddot{\phi}_1'\left(c\phi_2 c\phi_3\right) + \ddot{\phi}_2'\left(s\phi_2 s\phi_1' + c\phi_2 c\phi_1' s\phi_3\right) + \ddot{\phi}_3'\left(\Omega_{4,16}\right) - \ddot{\phi}_3\left(s\phi_2\right) + \alpha_{41}^0 \\
\alpha_{42} &= -\ddot{\phi}_1'\left(s\phi_3\right) + \ddot{\phi}_2'\left(c\phi_3 c\phi_1'\right) + \ddot{\phi}_3'\left(s\phi_3 s\phi_2' + c\phi_3 c\phi_2' s\phi_1'\right) + \ddot{\phi}_2 + \alpha_{42}^0 \\
\alpha_{43} &= \ddot{\phi}_1'\left(c\phi_3 s\phi_2\right) + \ddot{\phi}_2'\left(c\phi_1' s\phi_2 s\phi_3 - c\phi_2 s\phi_1'\right) + \ddot{\phi}_3'\left(\Omega_{4,36}\right) + \ddot{\phi}_3\left(c\phi_2\right) + \ddot{\theta}_4 + \alpha_{43}^0 \\
\Omega_{4,16} &= c\phi_2 c\phi_2' s\phi_3 s\phi_1' - c\phi_1' c\phi_2' s\phi_2 - c\phi_2 c\phi_3 s\phi_2' \\
\Omega_{4,36} &= c\phi_2 c\phi_1' c\phi_2' - c\phi_3 s\phi_2 s\phi_2' + c\phi_2' s\phi_2 s\phi_3 s\phi_1'
\end{aligned}
\tag{2.60}
$$

2.6 Position Expressions

The points expressed below are seen in Figure 2.2. Offset vectors are indicated below.

$$
\begin{aligned}
\overrightarrow{OB} &= x\vec{u}_1^{(0)} + y\vec{u}_2^{(0)} + z\vec{u}_3^{(0)} \\
\overrightarrow{BQ} &= l_0\vec{u}_3^{(1)} \\
\overrightarrow{QP_1} &= h_0\vec{u}_3^{(2)} \\
\overrightarrow{P_1P_2} &= h_1\vec{u}_3^{(2)}
\end{aligned}
\tag{2.61}
$$

Mass center (C_k) position vectors ($\vec{c}_k$) which are shown below are constant within the body frames.

$$
\begin{aligned}
\vec{c}_1 &= \overrightarrow{BC_1} = c_1\vec{u}_3^{(1)} \\
\vec{c}_2 &= \overrightarrow{QC_2} = c_2\vec{u}_3^{(2)} \\
\vec{c}_3 &= \overrightarrow{P_1C_3} = c_3\vec{u}_3^{(3)} \\
\vec{c}_4 &= \overrightarrow{P_2C_4} = c_4\vec{u}_3^{(4)}
\end{aligned}
\tag{2.62}
$$

Mass center position of B_1 from the frame $F_0\left(O\right)$ are expressed below.

$$
\begin{aligned}
\vec{r}_1 &= \vec{r}_{OB} + \vec{r}_{BC_1} \\
\vec{r}_{OB} &= x\vec{u}_1^{(0)} + y\vec{u}_2^{(0)} + z\vec{u}_3^{(0)} \\
\vec{r}_{BC_1} &= \vec{c}_1 = c_1\vec{u}_3^{(1)} \\
\vec{r}_1 &= x\vec{u}_1^{(0)} + y\vec{u}_2^{(0)} + z\vec{u}_3^{(0)} + c_1\vec{u}_3^{(1)}
\end{aligned}
\tag{2.63}
$$

Matrix equations in frame $F_1\left(B\right)$ are expressed below.

$$
\begin{aligned}
&\overline{r}_1^{(1)} = \overline{r}_{OB}^{(0/1)} + \overline{r}_{BC_1}^{(1/1)} \\
&\overline{r}_{OB}^{(0/1)} = \overline{r}_{OB}^{(1)} = \hat{C}^{(1,0)}\overline{r}_{OB}^{(0)} \\
&\overline{r}_{OB}^{(0)} = x\overline{u}_1 + y\overline{u}_2 + z\overline{u}_3 \\
&\hat{C}^{(1,0)} = \hat{C}^{(0,1)t} \\
&\overline{r}_{BC_1}^{(1/1)} = \overline{r}_{BC_1}^{(1)} = c_1\overline{u}_3 \\
&\overline{r}_1^{(1)} = \hat{C}^{(0,1)t}\overline{r}_{OB}^{(0)} + \overline{r}_{BC_1}^{(1)}
\end{aligned}
\tag{2.64}
$$

Mass center position of B_2 from the frame $F_0(O)$ are expressed below.

$$
\begin{aligned}
&\vec{r}_2 = \vec{r}_{OB} + \vec{r}_{BQ} + \vec{r}_{QC_2} \\
&\vec{r}_{BQ} = l_0\vec{u}_3^{(1)} \\
&\vec{r}_{QC_2} = \vec{c}_2 = c_2\vec{u}_3^{(2)} \\
&\vec{r}_2 = x\vec{u}_1^{(0)} + y\vec{u}_2^{(0)} + z\vec{u}_3^{(0)} + l_0\vec{u}_3^{(1)} + c_2\vec{u}_3^{(2)}
\end{aligned}
\tag{2.65}
$$

Matrix equations in frame $F_2(Q)$ are expressed below.

$$
\begin{aligned}
&\overline{r}_2^{(2)} = \overline{r}_{OB}^{(0/2)} + \overline{r}_{BQ}^{(1/2)} + \overline{r}_{QC_2}^{(2/2)} \\
&\overline{r}_{OB}^{(0/2)} = \overline{r}_{OB}^{(2)} = \hat{C}^{(2,0)}\overline{r}_{OB}^{(0)} \\
&\hat{C}^{(2,0)} = \hat{C}^{(0,2)t} \\
&\overline{r}_{BQ}^{(1/2)} = \hat{C}^{(2,1)}\overline{r}_{BQ}^{(1)} \\
&\overline{r}_{BQ}^{(1)} = l_0\overline{u}_3 \\
&\hat{C}^{(2,1)} = \hat{C}^{(1,2)t}
\end{aligned}
\tag{2.66}
$$

$$
\begin{aligned}
&\overline{r}_{QC_2}^{(2/2)} = \overline{r}_{QC_2}^{(2)} = c_2\overline{u}_3 \\
&\overline{r}_2^{(2)} = \hat{C}^{(0,2)t}\overline{r}_{OB}^{(0)} + \hat{C}^{(1,2)t}\overline{r}_{BQ}^{(1)} + \overline{r}_{QC_2}^{(2)}
\end{aligned}
\tag{2.67}
$$

Mass center position of B_3 from the frame $F_0(O)$ are expressed below.

$$
\begin{aligned}
&\vec{r}_3 = \vec{r}_{OB} + \vec{r}_{BQ} + \vec{r}_{QP_1} + \vec{r}_{P_1C_3} \\
&\vec{r}_{QP_1} = h_0\vec{u}_3^{(2)} \\
&\vec{r}_{P_1C_3} = \vec{c}_3 = c_3\vec{u}_3^{(3)} \\
&\vec{r}_3 = x\vec{u}_1^{(0)} + y\vec{u}_2^{(0)} + z\vec{u}_3^{(0)} + l_0\vec{u}_3^{(1)} + h_0\vec{u}_3^{(2)} + c_3\vec{u}_3^{(3)}
\end{aligned}
\tag{2.68}
$$

Because of the assumption about the mass center of B_3 stated before in Section 2.2, c_3 is assumed to be zero. In addition to this assumption, the length c_4 must be also exactly zero, either by proper manufacturing or by balancing afterward. Otherwise, there will be severe vibrations caused by the propellers.

Thus, the expression $\vec{r}_3$ is modified as below.

$$
\vec{r}_3 = x\vec{u}_1^{(0)} + y\vec{u}_2^{(0)} + z\vec{u}_3^{(0)} + l_0\vec{u}_3^{(1)} + h_0\vec{u}_3^{(2)} \tag{2.69}
$$

Matrix equations in frame $F_2(P_1)$ are expressed below.

$$
\begin{aligned}
&\overline{r}_3^{(2)} = \overline{r}_{OB}^{(0/2)} + \overline{r}_{BQ}^{(1/2)} + \overline{r}_{QP_1}^{(2/2)} \\
&\overline{r}_{QP_1}^{(2/2)} = \overline{r}_{QP_1}^{(2)} = h_0\overline{u}_3 \\
&\overline{r}_3^{(2)} = \hat{C}^{(0,2)t}\overline{r}_{OB}^{(0)} + \hat{C}^{(1,2)t}\overline{r}_{BQ}^{(1)} + \overline{r}_{QP_1}^{(2)}
\end{aligned}
\tag{2.70}
$$

Mass center position of B_4 from the frame $F_0(O)$ are expressed below.

$$
\begin{aligned}
&\vec{r}_4 = \vec{r}_{OB} + \vec{r}_{BQ} + \vec{r}_{QP_1} + \vec{r}_{P_1P_2} + \vec{r}_{P_2C_4} \\
&\vec{r}_{P_1P_2} = h_1\vec{u}_3^{(2)} \\
&\vec{r}_{P_2C_4} = \vec{c}_4 = c_4\vec{u}_3^{(4)} \\
&\vec{r}_4 = x\vec{u}_1^{(0)} + y\vec{u}_2^{(0)} + z\vec{u}_3^{(0)} + l_0\vec{u}_3^{(1)} + (h_0 + h_1)\vec{u}_3^{(2)}
\end{aligned}
\tag{2.71}
$$

Matrix equations in frame $F_2(P_2)$ are expressed below.

$$
\begin{aligned}
&\overline{r}_4^{(2)} = \overline{r}_{OB}^{(0/2)} + \overline{r}_{BQ}^{(1/2)} + \overline{r}_{QP_1}^{(2/2)} + \overline{r}_{P_1P_2}^{(2/2)} \\
&\overline{r}_{P_1P_2}^{(2/2)} = \overline{r}_{P_1P_2}^{(2)} = h_1\overline{u}_3 \\
&\overline{r}_4^{(2)} = \hat{C}^{(0,2)t}\overline{r}_{OB}^{(0)} + \hat{C}^{(1,2)t}\overline{r}_{BQ}^{(1)} + \overline{r}_{QP_1}^{(2)} + \overline{r}_{P_1P_2}^{(2)}
\end{aligned}
\tag{2.72}
$$

2.7 Linear Velocity Expressions

Mass center velocity of B_1 is expressed below.

$$\vec{v}_1 = D_0\vec{r}_1 = D_1\vec{r}_1 + \vec{\omega}_1 \times \vec{r}_1 \tag{2.73}$$

Coriolis Transport Theorem is applied in the above equation to take derivative in the body frame. Matrix equation in the frame $F_1(B)$ is expressed below.

$$\overline{v}_1 = \dot{\overline{r}}_1^{(1)} + \tilde{\omega}_1^{(1)}\overline{r}_1^{(1)} \tag{2.74}$$

Above expression is demonstrated with influence coefficients as seen below.

$$\begin{aligned}
\overline{v}_1 &= \sum_{k=1}^{k=6}\left[\left(\partial\overline{r}_1^{(1)} / \partial q_k\right)\dot{q}_k\right] + \sum_{k=4}^{k=6}\left[\left(\tilde{\Omega}_{1k}\overline{r}_1^{(1)}\right)\dot{q}_k\right] \\
\overline{v}_1 &= \sum_{k=1}^{k=6}\left[\overline{V}_{1k}\dot{q}_k\right] + \sum_{k=4}^{k=6}\left[\left(\tilde{\Omega}_{1k}\overline{r}_1^{(1)}\right)\dot{q}_k\right] \\
\overline{v}_1 &= \sum_{k=1}^{k=3}\left[\overline{V}_{1k}\dot{q}_k\right] + \sum_{k=4}^{k=6}\left[\left(\overline{V}_{1k} + \tilde{\Omega}_{1k}\overline{r}_1^{(1)}\right)\dot{q}_k\right]
\end{aligned} \tag{2.75}$$

The terms $\overline{V}_{1k}$ and $\overline{V}_{1k}^{*}$ are velocity-to-velocity influence coefficients of $\dot{\overline{q}}_k$ for the B_1 which are expressed as seen below.

$$\begin{aligned}
\overline{V}_{1k} &= \partial\overline{r}_1^{(1)} / \partial q_k \qquad \text{for } k = 1,2,...6. \\
\overline{V}_{1k}^{*} &= \overline{V}_{1k} + \tilde{\Omega}_{1k}\overline{r}_1^{(1)} \qquad \text{for } k = 4,5,6.
\end{aligned} \tag{2.76}$$

Mass center velocity of B_2 is expressed below.

$$\vec{v}_2 = D_0\vec{r}_2 = D_2\vec{r}_2 + \vec{\omega}_2 \times \vec{r}_2 \tag{2.77}$$

Coriolis Transport Theorem is applied in the above equation to take derivative in the body frame. Matrix equation in the frame $F_2(Q)$ is expressed below.

$$\overline{v}_2 = \dot{\overline{r}}_2^{(2)} + \tilde{\omega}_2^{(2)}\overline{r}_2^{(2)} \tag{2.78}$$

Above expression is demonstrated with influence coefficients as seen below.

$$\begin{aligned}
\bar{v}_2 &= \sum_{k=1}^{k=8}\left[\left(\partial \bar{r}_2^{(2)} / \partial q_k\right)\dot{q}_k\right] + \sum_{k=4}^{k=8}\left[\left(\tilde{\Omega}_{2k}\bar{r}_2^{(2)}\right)\dot{q}_k\right] \\
\bar{v}_2 &= \sum_{k=1}^{k=8}\left[\bar{V}_{2k}\dot{q}_k\right] + \sum_{k=4}^{k=8}\left[\left(\tilde{\Omega}_{2k}\bar{r}_2^{(2)}\right)\dot{q}_k\right] \\
\bar{v}_2 &= \sum_{k=1}^{k=3}\left[\bar{V}_{2k}\dot{q}_k\right] + \sum_{k=4}^{k=8}\left[\left(\bar{V}_{2k} + \tilde{\Omega}_{2k}\bar{r}_2^{(2)}\right)\dot{q}_k\right]
\end{aligned} \tag{2.79}$$

The terms $\bar{V}_{2k}$ and $\bar{V}_{2k}^{*}$ are velocity-to-velocity influence coefficients of $\dot{\bar{q}}_k$ for the B_2 which are expressed as seen below.

$$\begin{aligned}
\bar{V}_{2k} &= \partial \bar{r}_2^{(2)} / \partial q_k \qquad \text{for } k = 1, 2, \ldots 8. \\
\bar{V}_{2k}^{*} &= \bar{V}_{2k} + \tilde{\Omega}_{2k}\bar{r}_2^{(2)} \qquad \text{for } k = 4, 5, \ldots 8.
\end{aligned} \tag{2.80}$$

Mass center velocity of B_3 is expressed below.

$$\vec{v}_3 = D_0\vec{r}_3 = D_2\vec{r}_3 + \vec{\omega}_2 \times \vec{r}_3 \tag{2.81}$$

Coriolis Transport Theorem is applied in the above equation to take derivative in the body frame. Matrix equation in the frame $F_2\left(P_1\right)$ is expressed below.

$$\bar{v}_3 = \dot{\bar{r}}_3^{(2)} + \tilde{\omega}_2^{(2)}\bar{r}_3^{(2)} \tag{2.82}$$

Above expression is demonstrated with influence coefficients as seen below.

$$\begin{aligned}
\bar{v}_3 &= \sum_{k=1}^{k=9}\left[\left(\partial \bar{r}_3^{(2)} / \partial q_k\right)\dot{q}_k\right] + \sum_{k=4}^{k=8}\left[\left(\tilde{\Omega}_{2k}\bar{r}_3^{(2)}\right)\dot{q}_k\right] \\
\bar{v}_3 &= \sum_{k=1}^{k=9}\left[\bar{V}_{3k}\dot{q}_k\right] + \sum_{k=4}^{k=8}\left[\left(\tilde{\Omega}_{2k}\bar{r}_3^{(2)}\right)\dot{q}_k\right] \\
\bar{v}_3 &= \sum_{k=1}^{k=3}\left[\bar{V}_{3k}\dot{q}_k\right] + \sum_{k=4}^{k=8}\left[\left(\bar{V}_{3k} + \tilde{\Omega}_{2k}\bar{r}_3^{(2)}\right)\dot{q}_k\right] + \sum_{k=9}^{k=9}\left[\bar{V}_{3k}\dot{q}_k\right]
\end{aligned} \tag{2.83}$$

The terms $\bar{V}_{3k}$ and $\bar{V}_{3k}^{*}$ are velocity-to-velocity influence coefficients of $\dot{\bar{q}}_k$ for the B_3 which are expressed as seen below.

$$\begin{aligned}
\bar{V}_{3k} &= \partial \bar{r}_3^{(2)} / \partial q_k \qquad \text{for } k = 1, 2, \ldots 9. \\
\bar{V}_{3k}^{*} &= \bar{V}_{3k} + \tilde{\Omega}_{2k}\bar{r}_3^{(2)} \qquad \text{for } k = 4, 5, \ldots 8.
\end{aligned} \tag{2.84}$$

Mass center velocity of B_4 is expressed below.

$$\vec{v}_4 = D_0\vec{r}_4 = D_2\vec{r}_4 + \vec{\omega}_2 \times \vec{r}_4 \tag{2.85}$$

Coriolis Transport Theorem is applied in the above equation to take derivative in the body frame. Matrix equation in the frame $F_2\left(P_2\right)$ is expressed below.

$$\bar{v}_4 = \dot{\bar{r}}_4^{(2)} + \tilde{\omega}_2^{(2)}\bar{r}_4^{(2)} \tag{2.86}$$

Above expression is demonstrated with influence coefficients as seen below.

$$\begin{aligned}
\bar{v}_4 &= \sum_{k=1}^{k=10}\left[\left(\partial\bar{r}_4^{(2)} / \partial q_k\right)\dot{q}_k\right] + \sum_{k=4}^{k=8}\left[\left(\tilde{\Omega}_{2k}\bar{r}_4^{(2)}\right)\dot{q}_k\right] \\
\bar{v}_4 &= \sum_{k=1}^{k=10}\left[\bar{V}_{4k}\dot{q}_k\right] + \sum_{k=4}^{k=8}\left[\left(\tilde{\Omega}_{2k}\bar{r}_4^{(2)}\right)\dot{q}_k\right] \\
\bar{v}_4 &= \sum_{k=1}^{k=3}\left[\bar{V}_{4k}\dot{q}_k\right] + \sum_{k=4}^{k=8}\left[\left(\bar{V}_{4k} + \tilde{\Omega}_{2k}\bar{r}_4^{(2)}\right)\dot{q}_k\right] + \sum_{k=9}^{k=10}\left[\bar{V}_{4k}\dot{q}_k\right]
\end{aligned} \tag{2.87}$$

The terms $\bar{V}_{4k}$ and $\bar{V}^*_{4k}$ are velocity-to-velocity influence coefficients of $\dot{\bar{q}}_k$ for the B_4 which are expressed as seen below.

$$\begin{aligned}
\bar{V}_{4k} &= \partial\bar{r}_4^{(2)} / \partial q_k \qquad \text{for } k = 1,2,...10. \\
\bar{V}^*_{4k} &= \bar{V}_{4k} + \tilde{\Omega}_{2k}\bar{r}_4^{(2)} \qquad \text{for } k = 4,5,...8.
\end{aligned} \tag{2.88}$$

Since there are two different types of influence coefficients for each body, it is necessary to name the influence coefficients for each body as a new general term $\bar{V}'_{jk}$ $(j = 1,2,3,4;\ k = 1,2,3,...10)$. The general term represents a new matrix containing two different types of influence coefficients for each body. The term $\bar{V}'_{jk}$ will appear in the following Sections for the sake of writing simpler expressions.

2.8 Linear Acceleration Expressions

Mass center acceleration of B_1 is expressed below.

$$\vec{a}_1 = D_0\vec{v}_1 = D_1\vec{v}_1 + \vec{\omega}_1 \times \vec{v}_1 \tag{2.89}$$

Coriolis Transport Theorem is applied in the above equation to take derivative in the body frame. Matrix equation in the frame $F_1(B)$ is expressed below.

$$\bar{a}_1^{(1)} = \dot{\bar{v}}_1^{(1)} + \tilde{\omega}_1^{(1)}\bar{v}_1^{(1)} \tag{2.90}$$

Above expression is demonstrated with influence coefficients as seen below.

$$\begin{aligned}
\bar{a}_1^{(1)} &= \sum_{k=1}^{k=6}\left[\bar{V}'_{1k}\ddot{q}_k + \dot{\bar{V}}'_{1k}\dot{q}_k\right] + \sum_{k=4}^{k=6}\sum_{j=1}^{j=6}\left[\left(\tilde{\Omega}_{1k}\bar{V}'_{1j}\right)\dot{q}_k\dot{q}_j\right] \\
\sum_{k=1}^{k=6}\left[\dot{\bar{V}}'_{1k}\dot{q}_k\right] &= \sum_{k=1}^{k=6}\sum_{j=1}^{j=6}\left[\bar{A}_{1kj}\dot{q}_k\dot{q}_j\right] \\
\bar{a}_1^{(1)} &= \sum_{k=1}^{k=6}\left[\bar{V}'_{1k}\ddot{q}_k\right] + \sum_{k=1}^{k=6}\sum_{j=1}^{j=6}\left[\bar{A}_{1kj}\dot{q}_k\dot{q}_j\right] + \sum_{k=4}^{k=6}\sum_{j=1}^{j=6}\left[\left(\tilde{\Omega}_{1k}\bar{V}'_{1j}\right)\dot{q}_k\dot{q}_j\right] \\
\bar{a}_1^{(1)} &= \sum_{k=1}^{k=6}\left[\bar{V}'_{1k}\ddot{q}_k\right] + \sum_{k=1}^{k=3}\sum_{j=1}^{j=6}\left[\bar{A}_{1kj}\dot{q}_k\dot{q}_j\right] + \sum_{k=4}^{k=6}\sum_{j=1}^{j=6}\left[\left(\bar{A}_{1kj} + \tilde{\Omega}_{1k}\bar{V}'_{1j}\right)\dot{q}_k\dot{q}_j\right]
\end{aligned} \tag{2.91}$$

In the above equation, $\bar{V}'_{1k}$ is the acceleration-to-acceleration influence coefficient for the B_1, which is the same as the velocity-to-velocity influence coefficient for B_1. The terms $\bar{A}_{1kj}$ and $\bar{A}^*_{1kj}$ are velocity-to-acceleration influence coefficients for B_1 which are expressed as below.

$$\begin{aligned}
\bar{A}_{1kj} &= \partial\bar{V}'_{1k} / \partial q_j \qquad \text{for } k = 1,2,...6;\ j = 1,2,...6. \\
\bar{A}^*_{1kj} &= \bar{A}_{1kj} + \tilde{\Omega}_{1k}\bar{V}'_{1j} \qquad \text{for } k = 4,5,6;\ j = 1,2,...6.
\end{aligned} \tag{2.92}$$

Mass center acceleration of B_2 is expressed below.

$$\vec{a}_2 = D_0\vec{v}_2 = D_2\vec{v}_2 + \vec{\omega}_2 \times \vec{v}_2 \tag{2.93}$$

Coriolis Transport Theorem is applied in the above equation to take derivative in the body frame. Matrix equation in the frame $F_2(Q)$ is expressed below.

$$\bar{a}_2^{(2)} = \dot{\bar{v}}_2^{(2)} + \tilde{\omega}_2^{(2)}\bar{v}_2^{(2)} \tag{2.94}$$

Above expression is demonstrated with influence coefficients as seen below.

$$\begin{aligned}\bar{a}_2^{(2)} &= \sum_{k=1}^{k=8}\left[\bar{V}'_{2k}\ddot{q}_k + \dot{\bar{V}}'_{2k}\dot{q}_k\right] + \sum_{k=4}^{k=8}\sum_{j=1}^{j=8}\left[\left(\tilde{\Omega}_{2k}\bar{V}'_{2j}\right)\dot{q}_k\dot{q}_j\right] \\ \sum_{k=1}^{k=8}\left[\dot{\bar{V}}'_{2k}\dot{q}_k\right] &= \sum_{k=1}^{k=8}\sum_{j=1}^{j=8}\left[\bar{A}_{2kj}\dot{q}_k\dot{q}_j\right]\end{aligned} \tag{2.95}$$

$$\begin{aligned}\bar{a}_2^{(2)} &= \sum_{k=1}^{k=8}\left[\bar{V}'_{2k}\ddot{q}_k\right] + \sum_{k=1}^{k=8}\sum_{j=1}^{j=8}\left[\bar{A}_{2kj}\dot{q}_k\dot{q}_j\right] + \sum_{k=4}^{k=8}\sum_{j=1}^{j=8}\left[\left(\tilde{\Omega}_{2k}\bar{V}'_{2j}\right)\dot{q}_k\dot{q}_j\right] \\ \bar{a}_2^{(2)} &= \sum_{k=1}^{k=8}\left[\bar{V}'_{2k}\ddot{q}_k\right] + \sum_{k=1}^{k=3}\sum_{j=1}^{j=8}\left[\bar{A}_{2kj}\dot{q}_k\dot{q}_j\right] + \sum_{k=4}^{k=8}\sum_{j=1}^{j=8}\left[\left(\bar{A}_{2kj} + \tilde{\Omega}_{2k}\bar{V}'_{2j}\right)\dot{q}_k\dot{q}_j\right]\end{aligned} \tag{2.96}$$

In the above equation, $\bar{V}'_{2k}$ is the acceleration-to-acceleration influence coefficient for the B_2, which is the same as the velocity-to-velocity influence coefficient for B_2. The terms $\bar{A}_{2kj}$ and $\bar{A}^*_{2kj}$ are velocity-to-acceleration influence coefficients for B_2 which are expressed as below.

$$\begin{aligned}\bar{A}_{2kj} &= \partial\bar{V}'_{2k}/\partial q_j \qquad \text{for } k = 1,2,...8;\ j = 1,2,...8. \\ \bar{A}^*_{2kj} &= \bar{A}_{2kj} + \tilde{\Omega}_{2k}\bar{V}'_{2j} \qquad \text{for } k = 4,5,...8;\ j = 1,2,...8.\end{aligned} \tag{2.97}$$

Mass center acceleration of B_3 is expressed below.

$$\vec{a}_3 = D_0\vec{v}_3 = D_2\vec{v}_3 + \vec{\omega}_2 \times \vec{v}_3 \tag{2.98}$$

Coriolis Transport Theorem is applied in the above equation to take derivative in the body frame. Matrix equation in the frame $F_2\left(P_1\right)$ is expressed below.

$$\bar{a}_3^{(2)} = \dot{\bar{v}}_3^{(2)} + \tilde{\omega}_2^{(2)}\bar{v}_3^{(2)} \tag{2.99}$$

Above expression is demonstrated with influence coefficients as seen below.

$$\bar{a}_3^{(2)} = \sum_{k=1}^{k=9}\left[\bar{V}'_{3k}\ddot{q}_k + \dot{\bar{V}}'_{3k}\dot{q}_k\right] + \sum_{k=4}^{k=8}\sum_{j=1}^{j=9}\left[\left(\tilde{\Omega}_{2k}\bar{V}'_{3j}\right)\dot{q}_k\dot{q}_j\right]$$

$$\sum_{k=1}^{k=9}\left[\dot{\bar{V}}'_{3k}\dot{q}_k\right] = \sum_{k=1}^{k=9}\sum_{j=1}^{j=9}\left[\bar{A}_{3kj}\dot{q}_k\dot{q}_j\right]$$

$$\bar{a}_3^{(2)} = \sum_{k=1}^{k=9}\left[\bar{V}'_{3k}\ddot{q}_k\right] + \sum_{k=1}^{k=9}\sum_{j=1}^{j=9}\left[\bar{A}_{3kj}\dot{q}_k\dot{q}_j\right] + \sum_{k=4}^{k=8}\sum_{j=1}^{j=9}\left[\left(\tilde{\Omega}_{2k}\bar{V}'_{3j}\right)\dot{q}_k\dot{q}_j\right] \tag{2.100}$$

$$\bar{a}_3^{(2)} = \sum_{k=1}^{k=9}\left[\bar{V}'_{2k}\ddot{q}_k\right] + \sum_{k=1}^{k=3}\sum_{j=1}^{j=9}\left[\bar{A}_{3kj}\dot{q}_k\dot{q}_j\right] + \sum_{k=4}^{k=8}\sum_{j=1}^{j=9}\left[\left(\bar{A}_{3kj} + \tilde{\Omega}_{2k}\bar{V}'_{3j}\right)\dot{q}_k\dot{q}_j\right]$$

$$+\sum_{k=9}^{k=9}\sum_{j=1}^{j=9}\left[\bar{A}_{3kj}\dot{q}_k\dot{q}_j\right]$$

In the above equation, $\bar{V}'_{3k}$ is the acceleration-to-acceleration influence coefficient for the B_3, which is the same as the velocity-to-velocity influence coefficient for B_3. The terms $\bar{A}_{3kj}$ and $\bar{A}^*_{3kj}$ are velocity-to-acceleration influence coefficients for B_3 which are expressed as below.

$$\begin{aligned} \bar{A}_{3kj} &= \partial\bar{V}'_{3k} / \partial q_j \qquad \text{for } k = 1,2,...9;\ j = 1,2,...9. \\ \bar{A}^*_{3kj} &= \bar{A}_{3kj} + \tilde{\Omega}_{2k}\bar{V}'_{3j} \qquad \text{for } k = 4,5,...8;\ j = 1,2,...9. \end{aligned} \tag{2.101}$$

Mass center acceleration of B_4 is expressed below.

$$\vec{a}_4 = D_0\vec{v}_4 = D_2\vec{v}_4 + \vec{\omega}_2 \times \vec{v}_4 \tag{2.102}$$

Coriolis Transport Theorem is applied in the above equation to take derivative in the body frame. Matrix equation in the frame $F_2\left(P_2\right)$ is expressed below.

$$\bar{a}_4^{(2)} = \dot{\bar{v}}_4^{(2)} + \tilde{\omega}_2^{(2)}\bar{v}_4^{(2)} \tag{2.103}$$

Above expression is demonstrated with influence coefficients as seen below.

$$\bar{a}_4^{(2)} = \sum_{k=1}^{k=10}\left[\bar{V}'_{4k}\ddot{q}_k + \dot{\bar{V}}'_{4k}\dot{q}_k\right] + \sum_{k=4}^{k=8}\sum_{j=1}^{j=10}\left[\left(\tilde{\Omega}_{2k}\bar{V}'_{4j}\right)\dot{q}_k\dot{q}_j\right]$$

$$\sum_{k=1}^{k=10}\left[\dot{\bar{V}}'_{4k}\dot{q}_k\right] = \sum_{k=1}^{k=10}\sum_{j=1}^{j=10}\left[\bar{A}_{4kj}\dot{q}_k\dot{q}_j\right]$$

$$\bar{a}_4^{(2)} = \sum_{k=1}^{k=10}\left[\bar{V}'_{4k}\ddot{q}_k\right] + \sum_{k=1}^{k=10}\sum_{j=1}^{j=10}\left[\bar{A}_{4kj}\dot{q}_k\dot{q}_j\right] + \sum_{k=4}^{k=8}\sum_{j=1}^{j=10}\left[\left(\tilde{\Omega}_{2k}\bar{V}'_{4j}\right)\dot{q}_k\dot{q}_j\right] \qquad (2.104)$$

$$\bar{a}_4^{(2)} = \sum_{k=1}^{k=10}\left[\bar{V}'_{4k}\ddot{q}_k\right] + \sum_{k=1}^{k=3}\sum_{j=1}^{j=10}\left[\bar{A}_{4kj}\dot{q}_k\dot{q}_j\right] + \sum_{k=4}^{k=8}\sum_{j=1}^{j=10}\left[\left(\bar{A}_{4kj} + \tilde{\Omega}_{2k}\bar{V}'_{4j}\right)\dot{q}_k\dot{q}_j\right]$$

$$+\sum_{k=9}^{k=10}\sum_{j=1}^{j=9}\left[\bar{A}_{4kj}\dot{q}_k\dot{q}_j\right]$$

In the above equation, $\bar{V}'_{4k}$ is the acceleration-to-acceleration influence coefficient for the B_4, which is the same as the velocity-to-velocity influence coefficient for B_4. The terms $\bar{A}_{4kj}$ and $\bar{A}^*_{4kj}$ are velocity-to-acceleration influence coefficients for B_4 which are expressed as below.

$$\begin{aligned} \bar{A}_{4kj} &= \partial\bar{V}'_{4k} / \partial q_j \qquad \text{for } k = 1,2,...10;\ j = 1,2,...10. \\ \bar{A}^*_{4kj} &= \bar{A}_{4kj} + \tilde{\Omega}_{2k}\bar{V}'_{4j} \qquad \text{for } k = 4,5,...8;\ j = 1,2,...10. \end{aligned} \qquad (2.105)$$

2.8.1 Closed Form Expressions for Linear Acceleration

Linear acceleration equation for the bodies B_k $(k = 1,2,3,4.)$ is seen as below.

$$\bar{a}_k^{(k)} = \bar{a}_k^{(k)}\left(\bar{q},\dot{\bar{q}},\ddot{\bar{q}},t\right) = \hat{V}_k\left(\bar{q},t\right)\ddot{\bar{q}} + \bar{a}_k^0\left(\bar{q},\dot{\bar{q}},t\right) \qquad k = 1,2,3,4. \qquad (2.106)$$

The terms $\bar{a}_k^0$ $(k = 1,2,3,4.)$ are called biased terms of the linear accelerations which are left in the closed form since they are computed simultaneously via a computer program. On the other hand, influence coefficients of acceleration-to-acceleration $\hat{V}_k$ $(k = 1,2,3,4.)$ are expressed in the open form via scalar equations since they are unknown. Scalar equations of the linear acceleration for B_1 are seen as below. Abbreviation of s and c stands for sine and cosine functions.

$$
\begin{aligned}
a_{11} &= \ddot{x}\left(c\phi_2' c\phi_3'\right) + \ddot{y}\left(c\phi_2' s\phi_3'\right) - \ddot{z}\left(s\phi_2'\right) + \ddot{\phi}_2'\left(V_{1,15}\right) + \ddot{\phi}_3'\left(V_{1,16}\right) + a_{11}^0 \\
a_{12} &= \ddot{x}\left(c\phi_3' s\phi_1' s\phi_2' - c\phi_1' s\phi_3'\right) + \ddot{y}\left(c\phi_1' c\phi_3' + s\phi_1' s\phi_2' s\phi_3'\right) + \ddot{z}\left(c\phi_2' s\phi_1'\right) \\
&-\ddot{\phi}_1'\left(c_1\right) + \ddot{\phi}_2'\left(V_{1,25}\right) + \ddot{\phi}_3'\left(V_{1,26}\right) + a_{12}^0 \\
a_{13} &= \ddot{x}\left(s\phi_1' s\phi_3' + c\phi_1' c\phi_3' s\phi_2'\right) + \ddot{y}\left(c\phi_1' s\phi_2' s\phi_3' - c\phi_3' s\phi_1'\right) + \ddot{z}\left(c\phi_1' c\phi_2'\right) \\
&+\ddot{\phi}_3'\left(V_{1,36}\right) + a_{13}^0
\end{aligned}
\tag{2.107}
$$

$$
\begin{aligned}
&V_{1,15} = C_{1,15x} x + C_{1,15y} y + c\phi_1' c_1 \\
&\begin{cases}
C_{1,15x} = -s\phi_1'\left(c\phi_1' s\phi_3' - c\phi_3' s\phi_1' s\phi_2'\right) + c\phi_1'\left(s\phi_1' s\phi_3' + c\phi_1' c\phi_3' s\phi_2'\right) - c\phi_3' s\phi_2' \\
C_{1,15y} = s\phi_1'\left(c\phi_1' c\phi_3' + s\phi_1' s\phi_2' s\phi_3'\right) - c\phi_1'\left(c\phi_3' s\phi_1' - c\phi_1' s\phi_2' s\phi_3'\right) - s\phi_2' s\phi_3'
\end{cases} \\
&V_{1,16} = C_{1,16x} x + C_{1,16y} y + c\phi_2' s\phi_1' c_1 \\
&\begin{cases}
C_{1,16x} = c\phi_2' s\phi_1'\left(s\phi_1' s\phi_3' + c\phi_1' c\phi_3' s\phi_2'\right) + c\phi_1' c\phi_2'\left(c\phi_1' s\phi_3' - c\phi_3' s\phi_1' s\phi_2'\right) \\
-c\phi_2' s\phi_3' \\
C_{1,16y} = -c\phi_2' s\phi_1'\left(c\phi_3' s\phi_1' - c\phi_1' s\phi_2' s\phi_3'\right) - c\phi_1' c\phi_2'\left(c\phi_1' c\phi_3' + s\phi_1' s\phi_2' s\phi_3'\right) \\
+c\phi_2' c\phi_3'
\end{cases}
\end{aligned}
\tag{2.108}
$$

$$
\begin{aligned}
&V_{1,25} = C_{1,25x} x + C_{1,25y} y \\
&\begin{cases}
C_{1,25x} = c\phi_2' c\phi_3' s\phi_1' - s\phi_1' c\phi_2' c\phi_3' \\
C_{1,25y} = c\phi_2' s\phi_1' s\phi_3' - s\phi_1' c\phi_2' s\phi_3'
\end{cases} \\
&V_{1,26} = C_{1,26x} x + C_{1,26y} y + s\phi_2' c_1 \\
&\begin{cases}
C_{1,26x} = s\phi_2'\left(s\phi_1' s\phi_3' + c\phi_1' c\phi_3' s\phi_2' + s\phi_1' s\phi_3'\right) + c\phi_1' c\phi_3'\left(\left(c\phi_2'\right)^2 + 1\right) \\
C_{1,26y} = -s\phi_2'\left(c\phi_3' s\phi_1' - c\phi_1' s\phi_2' s\phi_3' + c\phi_3' s\phi_1'\right) + c\phi_1' s\phi_3'\left(\left(c\phi_2'\right)^2 - 1\right)
\end{cases}
\end{aligned}
\tag{2.109}
$$

$$
\begin{aligned}
&V_{1,36} = C_{1,36x} x + C_{1,36y} y \\
&\begin{cases}
C_{1,36x} = s\phi_2'\left(c\phi_1' s\phi_3' - c\phi_3' s\phi_1' s\phi_2' - c\phi_1' s\phi_3'\right) + c\phi_3' s\phi_1'\left(1 - \left(c\phi_2'\right)^2\right) \\
C_{1,36y} = -s\phi_2'\left(c\phi_1' c\phi_3' + s\phi_1' s\phi_2' s\phi_3' - c\phi_1' c\phi_3'\right) + s\phi_1' s\phi_3'\left(1 - \left(c\phi_2'\right)^2\right)
\end{cases}
\end{aligned}
\tag{2.110}
$$

The term $V_{j,kl}$ $\left(j = 1,2,3,4;\ k = 1,2,3;\ l = 1,2...10.\right)$ expresses more complicated trigonometric terms for ease of reading the equations. The terms $C_{j,klx}$ and $C_{j,kly}$ $\left(j = 1,2,3,4;\ k = 1,2,3;\ l = 1,2...10.\right)$ also express complicated trigonometric terms

in the expression of $V_{j,kl}$ which represents coefficients of the terms x, y and z. Scalar equations of the linear acceleration for B_2 are seen as below.

$$\begin{aligned}
&a_{21} = \ddot{x}\left(V_{2,11}\right) + \ddot{y}\left(V_{2,12}\right) + \ddot{z}\left(V_{2,13}\right) - \ddot{\phi}_1'\left(s\phi_3\left(c_2 + l_0 c\phi_2\right)\right) \\
&+\ddot{\phi}_2'\left(c\phi_3 c\phi_1'\left(c_2 + l_0 c\phi_2\right)\right) + \ddot{\phi}_3'\left(V_{2,16}\right) + \ddot{\phi}_2\left(c_2\right) + a_{21}^0 \\
&a_{22} = \ddot{x}\left(V_{2,21}\right) + \ddot{y}\left(V_{2,22}\right) + \ddot{z}\left(V_{2,23}\right) - \ddot{\phi}_1'\left(c\phi_3\left(l_0 + c_2 c\phi_2\right)\right) \\
&+\ddot{\phi}_2'\left(V_{2,25}\right) + \ddot{\phi}_3'\left(V_{2,26}\right) + \ddot{\phi}_3\left(c_2 s\phi_2\right) + a_{22}^0 \\
&a_{23} = \ddot{x}\left(V_{2,31}\right) + \ddot{y}\left(V_{2,32}\right) + \ddot{z}\left(V_{2,33}\right) - \ddot{\phi}_1'\left(l_0 s\phi_2 s\phi_3\right) \\
&+\ddot{\phi}_2'\left(l_0 s\phi_2 c\phi_3 c\phi_1'\right) + \ddot{\phi}_3'\left(V_{2,36}\right) + a_{23}^0
\end{aligned} \tag{2.111}$$

$$\begin{aligned}
&V_{2,11} = c\phi_2 c\phi_3 c\phi_2' c\phi_3' - c\phi_2 s\phi_3\left(c\phi_1' s\phi_3' - c\phi_3' s\phi_1' s\phi_2'\right) \\
&-s\phi_2\left(s\phi_1' s\phi_3' + c\phi_1' c\phi_3' s\phi_2'\right) \\
&V_{2,12} = c\phi_2 c\phi_3 c\phi_2' s\phi_3' + c\phi_2 s\phi_3\left(c\phi_1' c\phi_3' + s\phi_1' s\phi_2' s\phi_3'\right) \\
&+s\phi_2\left(c\phi_3' s\phi_1' - c\phi_1' s\phi_2' s\phi_3'\right) \\
&V_{2,13} = c\phi_2\left(c\phi_2' s\phi_3 s\phi_1' - c\phi_3 s\phi_2'\right) - c\phi_1' c\phi_2' s\phi_2 \\
&V_{2,16} = c_2\left(s\phi_3 s\phi_2' + c\phi_3 c\phi_2' s\phi_1'\right) + l_0 c\phi_2\left(s\phi_3 s\phi_2' + c\phi_3 c\phi_2' s\phi_1'\right)
\end{aligned} \tag{2.112}$$

$$\begin{aligned}
&V_{2,21} = -c\phi_3\left(c\phi_1' s\phi_3' - c\phi_3' s\phi_1' s\phi_2'\right) - s\phi_3 c\phi_2' c\phi_3' \\
&V_{2,22} = c\phi_3\left(c\phi_1' c\phi_3' + s\phi_1' s\phi_2' s\phi_3'\right) - s\phi_3 c\phi_2' s\phi_3' \\
&V_{2,23} = s\phi_3 s\phi_2' + c\phi_3 c\phi_2' s\phi_1' \\
&V_{2,25} = -l_0 c\phi_1' s\phi_3 - c_2\left(s\phi_2 s\phi_1' + c\phi_2 s\phi_3 c\phi_1'\right) \\
&V_{2,26} = l_0\left(c\phi_3 s\phi_2' - c\phi_2' s\phi_3 s\phi_1'\right) \\
&+c_2\left(c\phi_2 c\phi_3 s\phi_2' + c\phi_1' c\phi_2' s\phi_2 - c\phi_2 c\phi_2' s\phi_3 s\phi_1'\right)
\end{aligned} \tag{2.113}$$

$$\begin{aligned}
&V_{2,31} = c\phi_2\left(s\phi_1' s\phi_3' + c\phi_1' c\phi_3' s\phi_2'\right) - s\phi_2 s\phi_3\left(c\phi_1' s\phi_3' - c\phi_3' s\phi_1' s\phi_2'\right) \\
&+s\phi_2 c\phi_3 c\phi_2' c\phi_3' \\
&V_{2,32} = -c\phi_2\left(c\phi_3' s\phi_1' - c\phi_1' s\phi_2' s\phi_3'\right) + s\phi_2 s\phi_3\left(c\phi_1' c\phi_3' + s\phi_1' s\phi_2' s\phi_3'\right) \\
&+s\phi_2 c\phi_3 c\phi_2' s\phi_3' \\
&V_{2,33} = c\phi_2 c\phi_1' c\phi_2' - s\phi_2 c\phi_3 s\phi_2' + s\phi_2 s\phi_3 c\phi_2' s\phi_1' \\
&V_{2,36} = l_0\left(s\phi_2\left(s\phi_3 s\phi_2' + c\phi_3 c\phi_2' s\phi_1'\right)\right)
\end{aligned} \tag{2.114}$$

Scalar equations of the linear acceleration for B_3 are seen as below.

$$
\begin{aligned}
a_{31} &= \ddot{x}\left(V_{3,11}\right)+\ddot{y}\left(V_{3,12}\right)+\ddot{z}\left(V_{3,13}\right)-\ddot{\phi}_1'\left(s\phi_3\left(h_0+l_0c\phi_2\right)\right)\\
&+\ddot{\phi}_2'\left(c\phi_3c\phi_1'\left(h_0+l_0c\phi_2\right)\right)+\ddot{\phi}_3'\left(V_{3,16}\right)+\ddot{\phi}_2\left(h_0\right)+a_{31}^0\\
a_{32} &= \ddot{x}\left(V_{3,21}\right)+\ddot{y}\left(V_{3,22}\right)+\ddot{z}\left(V_{3,23}\right)-\ddot{\phi}_1'\left(c\phi_3\left(l_0+h_0c\phi_2\right)\right)\\
&+\ddot{\phi}_2'\left(V_{3,25}\right)+\ddot{\phi}_3'\left(V_{3,26}\right)+\ddot{\phi}_3\left(h_0s\phi_2\right)+a_{32}^0\\
a_{33} &= \ddot{x}\left(V_{3,31}\right)+\ddot{y}\left(V_{3,32}\right)+\ddot{z}\left(V_{3,33}\right)-\ddot{\phi}_1'\left(l_0s\phi_2s\phi_3\right)\\
&+\ddot{\phi}_2'\left(l_0s\phi_2c\phi_3c\phi_1'\right)+\ddot{\phi}_3'\left(V_{3,36}\right)+a_{33}^0
\end{aligned}
\tag{2.115}
$$

$$
\begin{aligned}
V_{3,11} &= c\phi_2c\phi_3c\phi_2'c\phi_3'-c\phi_2s\phi_3\left(c\phi_1's\phi_3'-c\phi_3's\phi_1's\phi_2'\right)\\
&-s\phi_2\left(s\phi_1's\phi_3'+c\phi_1'c\phi_3's\phi_2'\right)\\
V_{3,12} &= c\phi_2c\phi_3c\phi_2's\phi_3'+c\phi_2s\phi_3\left(c\phi_1'c\phi_3'+s\phi_1's\phi_2's\phi_3'\right)\\
&+s\phi_2\left(c\phi_3's\phi_1'-c\phi_1's\phi_2's\phi_3'\right)\\
V_{3,13} &= c\phi_2c\phi_2's\phi_3s\phi_1'-c\phi_1'c\phi_2's\phi_2-c\phi_2c\phi_3s\phi_2'\\
V_{3,16} &= h_0\left(s\phi_3s\phi_2'+c\phi_3c\phi_2's\phi_1'\right)+l_0\left(c\phi_2\left(s\phi_3s\phi_2'+c\phi_3c\phi_2's\phi_1'\right)\right)
\end{aligned}
\tag{2.116}
$$

$$
\begin{aligned}
V_{3,21} &= -c\phi_3c\phi_1's\phi_3'-c\phi_3's\phi_1's\phi_2'-c\phi_2'c\phi_3's\phi_3\\
V_{3,22} &= c\phi_3\left(c\phi_1'c\phi_3'+s\phi_1's\phi_2's\phi_3'\right)-c\phi_2's\phi_3s\phi_3'\\
V_{3,23} &= s\phi_3s\phi_2'+c\phi_3c\phi_2's\phi_1'\\
V_{3,25} &= -l_0c\phi_1's\phi_3-h_0\left(s\phi_2s\phi_1'+c\phi_2c\phi_1's\phi_3\right)\\
V_{3,26} &= l_0\left(c\phi_3s\phi_2'-c\phi_2's\phi_3s\phi_1'\right)\\
&+h_0\left(c\phi_2c\phi_3s\phi_2'+c\phi_1'c\phi_2's\phi_2-c\phi_2c\phi_2's\phi_3s\phi_1'\right)
\end{aligned}
\tag{2.117}
$$

$$
\begin{aligned}
V_{3,31} &= c\phi_2\left(s\phi_1's\phi_3'+c\phi_1'c\phi_3's\phi_2'\right)-s\phi_2s\phi_3\left(c\phi_1's\phi_3'-c\phi_3's\phi_1's\phi_2'\right)\\
&+s\phi_2c\phi_3c\phi_2'c\phi_3'\\
V_{3,32} &= s\phi_2s\phi_3\left(c\phi_1'c\phi_3'+s\phi_1's\phi_2's\phi_3'\right)-c\phi_2\left(c\phi_3's\phi_1'-c\phi_1's\phi_2's\phi_3'\right)\\
&+s\phi_2c\phi_3c\phi_2's\phi_3'\\
V_{3,33} &= c\phi_2c\phi_1'c\phi_2'-s\phi_2c\phi_3s\phi_2'+s\phi_2s\phi_3c\phi_2's\phi_1'\\
V_{3,36} &= l_0\left(s\phi_2s\phi_3s\phi_2'+s\phi_2c\phi_3c\phi_2's\phi_1'\right)
\end{aligned}
\tag{2.118}
$$

Scalar equations of the linear acceleration for B_4 are seen as below.

$$
\begin{aligned}
a_{41} &= \ddot{x}\left(V_{4,11}\right)+\ddot{y}\left(V_{4,12}\right)+\ddot{z}\left(V_{4,13}\right)-\ddot{\phi}_1'\left(s\phi_3\left(h_0+h_1+l_0c\phi_2\right)\right)\\
&+\ddot{\phi}_2'\left(c\phi_3c\phi_1'\left(h_0+h_1+l_0c\phi_2\right)\right)+\ddot{\phi}_3'\left(V_{4,16}\right)+\ddot{\phi}_2\left(h_0+h_1\right)+a_{41}^0\\
a_{42} &= \ddot{x}\left(V_{4,21}\right)+\ddot{y}\left(V_{4,22}\right)+\ddot{z}\left(V_{4,23}\right)-\ddot{\phi}_1'\left(c\phi_3\left(l_0+\left(h_0+h_1\right)c\phi_2\right)\right)\\
&+\ddot{\phi}_2'\left(V_{4,25}\right)+\ddot{\phi}_3'\left(V_{4,26}\right)+\ddot{\phi}_3\left(s\phi_2\left(h_0+h_1\right)\right)+a_{42}^0\\
a_{43} &= \ddot{x}\left(V_{4,31}\right)+\ddot{y}\left(V_{4,32}\right)+\ddot{z}\left(V_{4,33}\right)-\ddot{\phi}_1'\left(l_0s\phi_2s\phi_3\right)\\
&+\ddot{\phi}_2'\left(l_0s\phi_2c\phi_3c\phi_1'\right)+\ddot{\phi}_3'\left(V_{4,36}\right)+a_{43}^0
\end{aligned}
\tag{2.119}
$$

$$
\begin{aligned}
V_{4,11} &= c\phi_2c\phi_3c\phi_2'c\phi_3'-c\phi_2s\phi_3\left(c\phi_1's\phi_3'-c\phi_3's\phi_1's\phi_2'\right)\\
&-s\phi_2\left(s\phi_1's\phi_3'+c\phi_1'c\phi_3's\phi_2'\right)\\
V_{4,12} &= c\phi_2c\phi_3c\phi_2's\phi_3'+c\phi_2s\phi_3\left(c\phi_1'c\phi_3'+s\phi_1's\phi_2's\phi_3'\right)\\
&+s\phi_2\left(c\phi_3's\phi_1'-c\phi_1's\phi_2's\phi_3'\right)\\
V_{4,13} &= c\phi_2c\phi_2's\phi_3s\phi_1'-c\phi_1'c\phi_2's\phi_2-c\phi_2c\phi_3s\phi_2'\\
V_{4,16} &= l_0\left(c\phi_2s\phi_3s\phi_2'+c\phi_2c\phi_3c\phi_2's\phi_1'\right)\\
&+h_0\left(s\phi_3s\phi_2'+c\phi_3c\phi_2's\phi_1'\right)+h_1\left(s\phi_3s\phi_2'+c\phi_3c\phi_2's\phi_1'\right)
\end{aligned}
\tag{2.120}
$$

$$
\begin{aligned}
V_{4,21} &= -c\phi_3c\phi_1's\phi_3'-c\phi_3's\phi_1's\phi_2'-c\phi_2'c\phi_3's\phi_3\\
V_{4,22} &= c\phi_3\left(c\phi_1'c\phi_3'+s\phi_1's\phi_2's\phi_3'\right)-c\phi_2's\phi_3s\phi_3'\\
V_{4,23} &= s\phi_3s\phi_2'+c\phi_3c\phi_2's\phi_1'\\
V_{4,25} &= -l_0c\phi_1's\phi_3-\left(h_0+h_1\right)\left(s\phi_2s\phi_1'+c\phi_2c\phi_1's\phi_3\right)\\
V_{4,26} &= l_0\left(c\phi_3s\phi_2'-c\phi_2's\phi_3s\phi_1'\right)\\
&+\left(h_0+h_1\right)\left(c\phi_2c\phi_3s\phi_2'+s\phi_2c\phi_1'c\phi_2'-c\phi_2s\phi_3c\phi_2's\phi_1'\right)
\end{aligned}
\tag{2.121}
$$

$$
\begin{aligned}
V_{4,31} &= c\phi_2\left(s\phi_1's\phi_3'+c\phi_1'c\phi_3's\phi_2'\right)-s\phi_2s\phi_3\left(c\phi_1's\phi_3'-c\phi_3's\phi_1's\phi_2'\right)\\
&+s\phi_2c\phi_3c\phi_2'c\phi_3'\\
V_{4,32} &= s\phi_2s\phi_3\left(c\phi_1'c\phi_3'+s\phi_1's\phi_2's\phi_3'\right)-c\phi_2\left(c\phi_3's\phi_1'-c\phi_1's\phi_2's\phi_3'\right)\\
&+s\phi_2c\phi_3c\phi_2's\phi_3'\\
V_{4,33} &= c\phi_2c\phi_1'c\phi_2'-s\phi_2c\phi_3s\phi_2'+s\phi_2s\phi_3c\phi_2's\phi_1'\\
V_{4,36} &= l_0\left(s\phi_2s\phi_3s\phi_2'+s\phi_2c\phi_3c\phi_2's\phi_1'\right)
\end{aligned}
\tag{2.122}
$$

CHAPTER 3

DYNAMICS

In this chapter, Newton-Euler Equations are applied for the 5 bodies of the serial manipulator model. In addition to the 4 bodies which are illustrated in Figure 2.2, the cross-link of the universal joint between the base platform B_1 and the upper platform B_2 is included as the body B_c .Since the cross-link B_c is assumed to be massles, it was excluded in Chapter 2 of kinematics. Newton-Euler Equations consist of 1 vectorial force and 1 vectorial moment equations written per body. Then 30 scalar equations are generated by resolving the 6 vectorial force and moment equations per body either in their body frames or in their nonspinning body frames (if they are inertially symmetric). After that, the scalar equations are rearrenged into an augmented matrix equation that involves the array of the generalized acceleration ($\ddot{\bar{q}}$), the array of the generalized actuation forces ($\bar{Q}$), and the array of the structural interaction forces and moments ($\bar{R}$) arising at the joints. For a consequent direct dynamics analysis, especially with control applications, $\bar{R}$ is eliminated in order to set up the direct relationship between $\ddot{\bar{q}}$ and $\bar{Q}$.

3.1 Vectorial Force and Moment Equation

Masses of the bodies are denoted as m_k $(k = 1,2,3,4.)$ and moment of inertia tensors of the bodies are denoted as $\overset{\vee}{J}_k$ $(k = 1,2,3,4.)$. Since the rotors have inertial symmetry about their spin axes, their inertia tensors can be expressed equally in the shaft of the upper body B_2 frame instead of the separate rotor frames. Moreover, the products of inertia are assumed to be zero owing to perfect manifacturing. Therefore, the inertia tensors for the bodies can be expressed as seen below.

$$\begin{aligned}\overset{\vee}{J}_1 &= J_{1n}\left[\vec{u}_1^{(2)}\vec{u}_1^{(2)} + \vec{u}_2^{(2)}\vec{u}_2^{(2)}\right] + J_{1s}\vec{u}_3^{(2)}\vec{u}_3^{(2)} \\ \overset{\vee}{J}_2 &= J_{2n}\left[\vec{u}_1^{(2)}\vec{u}_1^{(2)} + \vec{u}_2^{(2)}\vec{u}_2^{(2)}\right] + J_{2s}\vec{u}_3^{(2)}\vec{u}_3^{(2)}\end{aligned} \tag{3.1}$$

$$\begin{aligned}\overset{\vee}{J}_3 &= J_{3n}\left[\vec{u}_1^{(2)}\vec{u}_1^{(2)} + \vec{u}_2^{(2)}\vec{u}_2^{(2)}\right] + J_{3s}\vec{u}_3^{(2)}\vec{u}_3^{(2)} \\ \overset{\vee}{J}_4 &= J_{4n}\left[\vec{u}_1^{(2)}\vec{u}_1^{(2)} + \vec{u}_2^{(2)}\vec{u}_2^{(2)}\right] + J_{4s}\vec{u}_3^{(2)}\vec{u}_3^{(2)}\end{aligned} \tag{3.2}$$

Kinematic terms at the left hand side of the N-E equations are acquired before in the previous chapter. Interaction forces are shown as $\vec{F}_{k(k+1)}$. The sequence $k,(k+1)$ is taken as the positive direction. Thus, whenever the term $\vec{F}_{(k+1)k}$ appears, it is turned into $-F_{k(k+1)}$.

3.1.1 Vectorial Force Equations

Vectorial force equation for B_1 is expressed as seen below.

$$\begin{aligned}m_1\vec{a}_1 &= \vec{F}_{c1} + m_1\vec{g} + \vec{F}_{dw} \\ m_1\vec{a}_1 &= -\vec{F}_{1c} - \vec{u}_3^{(0)}m_1 g + \vec{F}_{dw}\end{aligned} \tag{3.3}$$

The force $\vec{F}_{dw}$ is the downwash force exerted on B_1. This term will be discussed later in the Section 3.3.

Vectorial force equation for the cross-link B_c is written as follows.

$$\begin{aligned}\vec{0} &= \vec{F}_{1c} + \vec{F}_{2c} \\ \vec{0} &= \vec{F}_{1c} - \vec{F}_{c2}\end{aligned} \tag{3.4}$$

Vectorial force equation for B_2 is written as follows.

$$\begin{aligned}m_2\vec{a}_2 &= \vec{F}_{c2} + \vec{F}_{32} + \vec{F}_{42} + m_2\vec{g} \\ m_2\vec{a}_2 &= \vec{F}_{c2} - \vec{F}_{23} - \vec{F}_{24} - \vec{u}_3^{(0)}m_2 g\end{aligned} \tag{3.5}$$

Vectorial force equation for B_3 and B_4 are written as follows.

$$\begin{aligned} m_3\vec{a}_3 &= \vec{F}_{23} + m_3\vec{g} + \vec{F}_{L_3} \\ m_3\vec{a}_3 &= \vec{F}_{23} - \vec{u}_3^{(0)} m_3 g + \vec{F}_{L_3} \end{aligned} \tag{3.6}$$

$$\begin{aligned} m_4\vec{a}_4 &= \vec{F}_{24} + m_4\vec{g} + \vec{F}_{L_4} \\ m_4\vec{a}_4 &= \vec{F}_{24} - \vec{u}_3^{(0)} m_4 g + \vec{F}_{L_4} \end{aligned} \tag{3.7}$$

The force terms $\vec{F}_{L_k}$ $(k = 3,4)$ are the lift forces exerted on B_3 and B_4 by the surrounding air. They will also be discussed later in Section 3.3.

3.1.2 Vectorial Moment Equations

The vectorial moment equation for B_1 is shown below.

$$\begin{aligned} \overset{\vee}{J}_1 \cdot \vec{\alpha}_1 + \vec{\omega}_1 \times \overset{\vee}{J}_1 \cdot \vec{\omega}_1 &= \vec{M}_{c1} + \vec{M}_{dw} + \vec{r}_{C_1Q} \times \vec{F}_{c1} \\ \overset{\vee}{J}_1 \cdot \vec{\alpha}_1 + \vec{\omega}_1 \times \overset{\vee}{J}_1 \cdot \vec{\omega}_1 &= -\vec{M}_{1c} + \vec{M}_{dw} - \vec{r}_{C_1Q} \times \vec{F}_{1c} \end{aligned} \tag{3.8}$$

The distance $\vec{r}_{C_1Q}$ is defined as seen below.

$$\vec{r}_{C_1Q} = \vec{u}_3^{(1)} \left(l_0 - c_2 \right) \tag{3.9}$$

The term $\vec{M}_{dw}$ is the moment generated by the downwash force $\vec{F}_{dw}$ which will be discussed later in the Section 3.3.

The vectorial moment equation for the cross-link B_c is written as follows.

$$\begin{aligned} \vec{0} &= \vec{M}_{1c} + \vec{M}_{2c} \\ \vec{0} &= \vec{M}_{1c} - \vec{M}_{c2} \end{aligned} \tag{3.10}$$

The vectorial moment equation for B_2 is shown as follows.

$$\begin{aligned}\overset{\vee}{J}_2\cdot\vec{\alpha}_2+\vec{\omega}_2\times\overset{\vee}{J}_2\cdot\vec{\omega}_2&=\vec{M}_{c2}+\vec{M}_{32}+\vec{M}_{42}+\vec{r}_{C_2Q}\times\vec{F}_{c2}+\vec{r}_{C_2P_1}\times\vec{F}_{32}+\vec{r}_{C_2P_2}\times\vec{F}_{42}\\ \overset{\vee}{J}_2\cdot\vec{\alpha}_2+\vec{\omega}_2\times\overset{\vee}{J}_2\cdot\vec{\omega}_2&=\vec{M}_{c2}-\vec{M}_{23}-\vec{M}_{24}+\vec{r}_{C_2Q}\times\vec{F}_{c2}-\vec{r}_{C_2P_1}\times\vec{F}_{23}-\vec{r}_{C_2P_2}\times\vec{F}_{24}\end{aligned}\tag{3.11}$$

The vectors $\vec{r}_{C_2Q}$, $\vec{r}_{C_2P_1}$ and $\vec{r}_{C_2P_2}$ are expressed as seen below.

$$\begin{aligned}\vec{r}_{C_2Q}&=-c_2\vec{u}_3^{(2)}\\ \vec{r}_{C_2P_1}&=\left(h_0-c_2\right)\vec{u}_3^{(2)}\\ \vec{r}_{C_2P_2}&=\left(h_0+h_1-c_2\right)\vec{u}_3^{(2)}\end{aligned}\tag{3.12}$$

The vectorial moment equation for B_3 is shown below.

$$\overset{\vee}{J}_3\cdot\vec{\alpha}_3+\vec{\omega}_3\times\overset{\vee}{J}_3\cdot\vec{\omega}_3=\vec{M}_{23}+\vec{r}_{C_3P_1}\times\vec{F}_{23}+\vec{M}_{D_3}\tag{3.13}$$

Since $\vec{r}_{C_3P_1}=0$, the above equation reduces to

$$\overset{\vee}{J}_3\cdot\vec{\alpha}_3+\vec{\omega}_3\times\overset{\vee}{J}_3\cdot\vec{\omega}_3=\vec{M}_{23}+\vec{M}_{D_3}\tag{3.14}$$

The vectorial moment equation for B_4 is shown below.

$$\overset{\vee}{J}_4\cdot\vec{\alpha}_4+\vec{\omega}_4\times\overset{\vee}{J}_4\cdot\vec{\omega}_4=\vec{M}_{24}+\vec{r}_{C_4P_2}\times\vec{F}_{24}+\vec{M}_{D_4}\tag{3.15}$$

Since $\vec{r}_{C_4P_2}=0$, too, the above equation also reduces to

$$\overset{\vee}{J}_4\cdot\vec{\alpha}_4+\vec{\omega}_4\times\overset{\vee}{J}_4\cdot\vec{\omega}_4=\vec{M}_{24}+\vec{M}_{D_4}\tag{3.16}$$

The moment terms $\vec{M}_{D_k}$ $\left(k=3,4\right)$ are the drag moments exerted on B_3 and B_4. by the surrounding air. They will be discussed later in the Section 3.3.

3.2 Resolution of the Interaction Forces and Moments

The interaction force $\vec{F}_{k(k+1)}$ and moment $\vec{M}_{k(k+1)}$ are normally resolved in the reference frame of the $(k+1)$th body, on which they are applied. In other words, they are represented by the column matrices $\bar{F}_{k(k+1)} = \bar{F}^{(k+1)}_{k(k+1)}$ and $\bar{M}_{k(k+1)} = \bar{M}^{(k+1)}_{k(k+1)}$. To resolve $\vec{F}_{k(k+1)}$ and $\vec{M}_{k(k+1)}$ in the reference frame of the (k)th body, i.e., to obtain the column matrices $\bar{F}^{(k)}_{k(k+1)}$ and $\bar{M}^{(k)}_{k(k+1)}$, the transformation matrix $\hat{C}^{(k,k+1)}$ is utilized. On the other hand, since nonrotating frames of the bodies B_3 and B_4 have the same orientation as B_2, the interaction forces and moments $\bar{F}_{23}$, $\bar{M}_{23}$, $\bar{F}_{24}$ and $\bar{M}_{24}$ are resolved in the 2nd body frame. The components of $\bar{F}_{k(k+1)}$ and $\bar{M}_{k(k+1)}$ are denoted as $F_{k(k+1)j}$ and $M_{k(k+1)j}$ for $j = 1,2,3.$

Before resolving interaction forces and moments, transformation matrices for the body frame $F_c(Q_c)$ of the cross-link B_c are expressed as seen below.

$$\begin{aligned}
\hat{C}^{(0,1)} &= e^{\tilde{u}_3\phi_3'} e^{\tilde{u}_2\phi_2'} e^{\tilde{u}_1\phi_1'} \\
\hat{C}^{(1,c)} &= e^{\tilde{u}_3\phi_3} \\
\hat{C}^{(1,c)t} &= e^{-\tilde{u}_3\phi_3} \\
\hat{C}^{(0,c)} &= \hat{C}^{(0,1)}\hat{C}^{(1,c)} \\
\hat{C}^{(c,2)} &= e^{\tilde{u}_2\phi_2} \\
\hat{C}^{(1,2)} &= \hat{C}^{(1,c)}\hat{C}^{(c,2)} = e^{\tilde{u}_3\phi_3} e^{\tilde{u}_2\phi_2}
\end{aligned} \tag{3.17}$$

The expression for $\hat{C}^{(0,1)}$ indicated in Eq. (2.9) is written above for convenience. Moreover, it is seen that the expression for $C^{(1,2)}$ is same as the expression mentioned in Eq. (2.10)

The vectorial expressions for the interaction force and moment between B_1 and B_c are as seen below.

$$\begin{aligned}\vec{F}_{1c} &= \vec{u}_1^{(1)} F_{1c1} + \vec{u}_2^{(1)} F_{1c2} + \vec{u}_3^{(1)} F_{1c3} \\ \vec{M}_{1c} &= \vec{u}_1^{(1)} M_{1c1} + \vec{u}_2^{(1)} M_{1c2} + \vec{u}_3^{(1)} T_{1c3}\end{aligned} \tag{3.18}$$

In the above equations, the component T_{1c3} represents the actuation torque applied for the universal joint variable ϕ_3. The other force and moment components represent the structural interactions.

Matrix equations in the frame $F_c\left(Q_c\right)$ are expressed as seen below.

$$\begin{aligned}\bar{F}_{1c}^{(1)} &= \bar{u}_1 F_{1c1} + \bar{u}_2 F_{1c2} + \bar{u}_3 F_{1c3} \\ \bar{M}_{1c}^{(1)} &= \bar{u}_1 M_{1c1} + \bar{u}_2 M_{1c2} + \bar{u}_3 T_{1c3}\end{aligned} \tag{3.19}$$

Matrix equations in the frame $F_1\left(B\right)$ are expressed as seen below.

$$\begin{aligned}\bar{F}_{1c}^{(c)} &= \hat{C}^{(1,c)t} \bar{F}_{1c}^{(1)} \\ \bar{M}_{1c}^{(c)} &= \hat{C}^{(1,c)t} \bar{M}_{1c}^{(1)}\end{aligned} \tag{3.20}$$

The vectorial expressions for the interaction force and moment between the B_c and B_2 are as seen below.

$$\begin{aligned}\vec{F}_{c2} &= \vec{u}_1^{(2)} F_{c21} + \vec{u}_2^{(2)} F_{c22} + \vec{u}_3^{(2)} F_{c23} \\ \vec{M}_{c2} &= \vec{u}_1^{(2)} M_{c21} + \vec{u}_2^{(2)} T_{c22} + \vec{u}_3^{(2)} M_{c23}\end{aligned} \tag{3.21}$$

In the above equations, the component T_{c22} represents the actuation torque applied for the universal joint variable ϕ_2. The other force and moment components represent the structural interactions.

Matrix equations in the frame $F_2\left(Q\right)$ are expressed as seen below.

$$\begin{aligned}\bar{F}_{c2}^{(2)} &= \bar{u}_1 F_{c21} + \bar{u}_2 F_{c22} + \bar{u}_3 F_{c23} \\ \bar{M}_{c2}^{(2)} &= \bar{u}_1 M_{c21} + \bar{u}_2 T_{c22} + \bar{u}_3 M_{c23}\end{aligned} \tag{3.22}$$

Matrix equations in the frame $F_c\left(Q_c\right)$ are expressed below by applying the similar steps as in Eq. (3.20).

$$\begin{aligned}\bar{F}_{c2}^{(c)} &= \hat{C}^{(c,2)}\bar{F}_{c2}^{(2)} \\ \bar{M}_{c2}^{(c)} &= \hat{C}^{(c,2)}\bar{M}_{c2}^{(2)}\end{aligned} \tag{3.23}$$

The vectoral expressions for the interaction force and moement between the B_2 and B_3 are as seen below.

$$\begin{aligned}\vec{F}_{23} &= \vec{u}_1^{(2)}F_{231} + \vec{u}_2^{(2)}F_{232} + \vec{u}_3^{(2)}F_{233} \\ \vec{M}_{23} &= \vec{u}_1^{(2)}M_{231} + \vec{u}_2^{(2)}M_{232} + \vec{u}_3^{(2)}T_{233}\end{aligned} \tag{3.24}$$

In the above equations, the component T_{233} represents the actuation torque applied for the revolute joint variable θ_3. The other force and moment components represent the structural interactions.

Matrix equations in the frame $F_2\left(P_1\right)$ are expressed as seen below.

$$\begin{aligned}\bar{F}_{23}^{(2)} &= \bar{u}_1F_{231} + \bar{u}_2F_{232} + \bar{u}_3F_{233} \\ \bar{M}_{23}^{(2)} &= \bar{u}_1M_{231} + \bar{u}_2M_{232} + \bar{u}_3T_{233}\end{aligned} \tag{3.25}$$

The vectoral expressions for the interaction force and moment between the B_2 and B_4 are as seen below.

$$\begin{aligned}\vec{F}_{24} &= \vec{u}_1^{(2)}F_{241} + \vec{u}_2^{(2)}F_{242} + \vec{u}_3^{(2)}F_{243} \\ \vec{M}_{24} &= \vec{u}_1^{(2)}M_{241} + \vec{u}_2^{(2)}M_{242} + \vec{u}_3^{(2)}T_{243}\end{aligned} \tag{3.26}$$

In the above equations, the component T_{243} represents the actuation torque applied for the revolute joint variable θ_4. The other force and moment components represent the structural interactions.

Matrix equations in the frame $F_2\left(P_2\right)$ are expressed as seen below.

$$\bar{F}_{24}^{(2)} = \bar{u}_1 F_{241} + \bar{u}_2 F_{242} + \bar{u}_3 F_{243}$$
$$\bar{M}_{24}^{(2)} = \bar{u}_1 M_{241} + \bar{u}_2 M_{242} + \bar{u}_3 T_{243} \quad (3.27)$$

3.3 Resolution of the Aerodynamic Forces and Moments

As part of the aerodynamic forces and moments that appear in the N-E equations in the previous section, there are the downwash force $\vec{F}_{dw}$ exerted on B_1, lift forces $\vec{F}_{L_k}$ $(k=3,4)$ and the drag moments $\vec{M}_{D_k}$ $(k=3,4)$ exerted on B_3 and B_4. They are explained in the subsections presented below. However, the aerodynamic interactions between the two propellers B_3 and B_4 are neglected.

3.3.1 Downwash Force and Moment

The reason why the downwash force is particularly taken into account (while the other aerodynamic effects such as the interactions between the propellers are neglected) is that it has a passive stabilizing effect on the UAV. To give further detail, the downwash force in the model results from the *weathervane effect* [18]. It is explained as a body changing its direction of motion in the direction of the wind like a weathervane. In the UAV model, the *weathervane effect* creates a stabilizing effect especially on the base platform B_1, because the propellers create a wind in the downward direction and this wind pushes the base platform B_1 trying to align it in the same direction as the upper platform B_2. To benefit from the *weathervane effect* more, 4 fins are mounted at the bottom of the base platform B_1. They are also convenient in terms of landing the UAV. The pushing effect on the fins can be seen in Figure 3.1.

On the contrary to the base platform B_1, the downwash force on the upper platform B_2 is neglected, because the downwash force applied on the upper platform B_2 does

not create any stabilizing moment due to the fact that the orientation of the nonspinning frame of the propellers (B_3 and B_4) and the upper platform B_2 is the same.

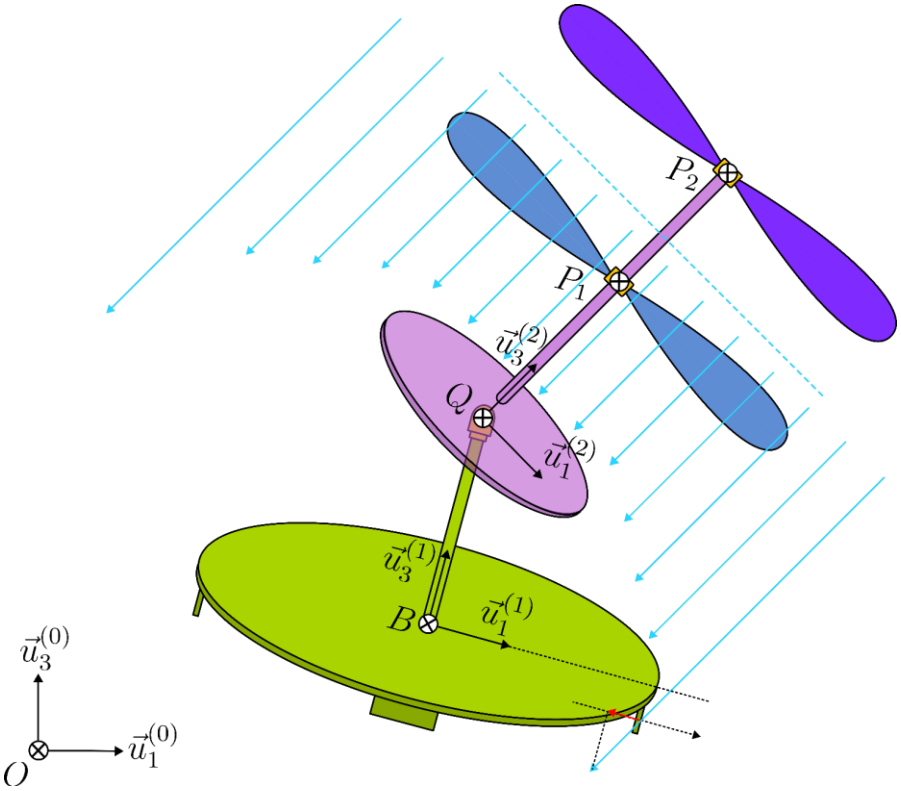

Figure 3.1. Downwash Effect on the Bodies

To calculate the downwash force exerted on the base platform B_1, two elements are necessary. First one is the magnitude of the force and second one is the direction of the force.

Continuing with the magnitude of the downwash force, the scalar value of the downwash force is calculated by the equation below. The expression is applicable when the air flow hits a surface perpendicularly [19]. That is why the projection of the downwash force on the normal of the fin surface is calculated as it indicates that decomposing the airflow vector in the fin frame and taking the component in the direction which is perpendicular to the fin surface.

$$f_{dw}(z) = -\frac{1}{2}\rho_{air} C_D A_{exert} v^2(z) \tag{3.28}$$

In the above equation, ρ_{air} is the air density, C_D is the drag coefficient and A_{exert} is the fin surface which can be expressed as seen below.

$$A_{exert} = l_f h_f \tag{3.29}$$

In the above equation, h_f is the height of the fin and l_f is the length of the fin.

Moreover, the function $v(z)$ appearing in Eq. (3.28) defines the air flow velocity depending on the distance z from the propeller and can be expressed as follows.

$$v(z) = \frac{10}{z}\sqrt{\frac{T_r}{\pi\rho_{air}}} \tag{3.30}$$

In the above equation, T_r is the thrust force generated by the propeller. If the above expression is inserted into Eq. (3.28), the relevant equation is derived as seen below.

$$f_{dw}(z) = \frac{50 C_D A_{exert}}{\pi}\frac{T_r}{z^2} \tag{3.31}$$

The distance z in the above expression is a variable. However, in the UAV model, it is assumed to have a constant value which is taken as the vertical distance from the middle of $|P_1P_2|$ to the point B_{f_k} which is the center of geometry for the surface of the stabilizing fins during hovering. Thus, the variable z is turned into the parameter h_z which is expressed as seen below.

$$h_z = h_1/2 + h_0 + l_0 + (t_p + h_f)/2 \tag{3.32}$$

Some of the parameters above are defined in Eq. (2.61). The parameter t_p represents thickness of the circular plate of the base and upper platforms B_1 and B_2.

Moreover, Eq. (3.31) becomes as seen below.

$$f_{dw} = \frac{50 C_D A_{exert}}{\pi} \frac{T_r}{h_z^2} \tag{3.33}$$

In Eq. (3.33), the thrust force T_r becomes the only variable which is expressed as seen below.

$$T_r\left(\dot{\theta}_3, \dot{\theta}_4\right) = F_{L_3}\left(\dot{\theta}_3\right) + F_{L_4}\left(\dot{\theta}_4\right) \tag{3.34}$$

As there are two propellers, thrust force T_r consists of lift forces F_{L_3} and F_{L_4} generated by the propellers B_3 and B_4. In addition, lift forces are depend on spinning velocities of the propellers ($\dot{\theta}_3$ and $\dot{\theta}_4$), which will be discussed in detail in the next section. Therefore, thrust force T_r is a function of $\dot{\theta}_3$ and $\dot{\theta}_4$ as seen in Eq. (3.34). Moreover, drag coefficient of the stabilizing fins C_D, is selected as 1.17 according to the conditions of a circular disc exposed by a perpendicular air flow for a low Reynolds number such as $\mathrm{Re} \cong 10^3$ [20].

Since the magnitude of the downwash force is determined, directional effects are considered now as a second element. The placement of the fins and the values of the constant angles λ_{f_k} $\left(k = 1, 2, 3, 4.\right)$ which are depicted in Figure 3.2 are seen as follows.

$$\measuredangle\left(\overrightarrow{BB_{f_k}}\right) = \lambda_{f_k} = \left(k-1\right)\pi/2 \qquad k = 1, 2, 3, 4. \tag{3.35}$$

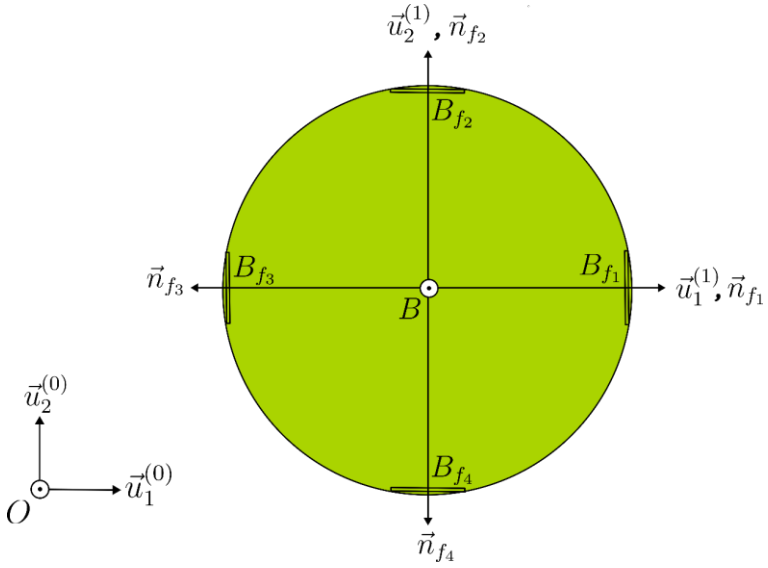

Figure 3.2. Top View of the Base Platform

The reference frames of the fins are denoted as $F_{f_k}\left(B_{f_k}\right)$ $\left(k=1,2,3,4.\right)$ and the transformation matrices for the fins are expressed as seen below.

$$\begin{aligned}
\hat{C}^{(1,f_k)} &= e^{\tilde{u}_3\lambda_{f_k}} \\
\hat{C}^{(1,2)} &= e^{\tilde{u}_3\phi_3}e^{\tilde{u}_2\phi_2} \\
\hat{C}^{(2,f_k)} &= \hat{C}^{(2,1)}\hat{C}^{(1,f_k)} \\
\hat{C}^{(2,f_k)} &= \hat{C}^{(1,2)t}\hat{C}^{(1,f_k)}
\end{aligned} \tag{3.36}$$

The transformation matrix $\hat{C}^{(1,2)}$ is expressed before in Eq. (2.10) of the Chapter 2.3 but it is written again in the above equation for convenience.

The unit vector of the downwash force is denoted as $\vec{n}_{dw}$ and basically in the reverse direction of the propeller shaft which is depicted in both Figure 3.1 and Figure 3.3. It is also expressed as seen below.

$$\vec{n}_{dw} = -\vec{u}_3^{(2)} \tag{3.37}$$

The normal unit vectors of the fin surfaces $\vec{n}_{f_k}$ $(k=1,2,3,4)$ can be seen in Figure 3.2, also $\vec{n}_{f_1}$ as an example is illustrated in Figure 3.3. The term $\vec{n}_{f_k}$ can be expressed as follows.

$$\vec{n}_{f_k} = \vec{u}_1^{(f_k)} \tag{3.38}$$

Projection of the downwash force on the normal unit vectors of the fin surfaces $\vec{n}_{f_k}$ is illustrated in Figure 3.3 and calculated as indicated below.

$$\vec{p}_{f_k} = \left(\vec{n}_{dw} \cdot \vec{n}_{f_k}\right)\vec{n}_{f_k} \tag{3.39}$$

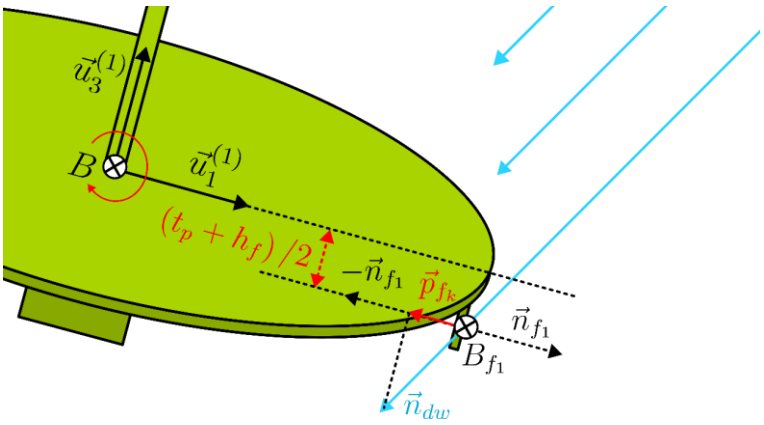

Figure 3.3. Vectorial Representations of the Downwash Effect on the Base Platform

If the scalar part of the vector $\vec{p}_{f_k}$, which is $\left(\vec{n}_{dw} \cdot \vec{n}_{f_k}\right)$, is a positive value, it represents the downwash effect on the fins which are in the opposite direction of the tilting. However, downwash effects on those fins are negligible since the air flow is prevented by the base platform and does not reach to those fins as seen in Figure 3.1. Therefore, when the value of $\left(\vec{n}_{dw} \cdot \vec{n}_{f_k}\right)$ is negative, it is indicated that the projection $\vec{p}_{f_k}$ is in the direction of $-\vec{n}_{f_k}$ as seen in Figure 3.3. In this case, downwash forces on those fins are taken into account.

The calculations mentioned above appear as matrix equations in the frame $F_{f_k}\left(B_{f_k}\right)$ below.

$$\begin{aligned}
&\overline{n}_{f_k}^{(f_k)} = \overline{u}_1^{(f_k/f_k)} = \overline{u}_1 \\
&\overline{n}_{dw}^{(f_k)} = -\overline{u}_3^{(2/f_k)} = -\hat{C}^{(f_k,2)}\overline{u}_3^{(2/2)} = -\hat{C}^{(2,f_k)t}\overline{u}_3 \\
&\overline{p}_{f_k}^{(f_k)} = \left(\overline{n}_{dw}^{(f_k)t}\overline{n}_{f_k}^{(f_k)}\right)\overline{n}_{f_k}^{(f_k)}
\end{aligned} \tag{3.40}$$

Matrix equation in the $F_1\left(B\right)$ can be seen as follows.

$$\overline{p}_{f_k}^{(1)} = C^{(1,f_k)}\overline{p}_{f_k}^{(f_k)} \tag{3.41}$$

Thus, downwash force can be expressed with the magnitude calculated before in Eq. (3.33) and the projection indicated above, as follows.

$$\overline{F}_{dw}^{(1)} = \sum_{k=1}^{k=4} f_{dw}\overline{p}_{f_k}^{(1)} \tag{3.42}$$

The vector equation of the above expression is indicated as seen below.

$$\vec{F}_{dw} = \sum_{k=1}^{k=4} f_{dw}\vec{p}_{f_k} \tag{3.43}$$

Thus, the downwash moment $\vec{M}_{dw}$ which is depicted in Figure 3.3 can be expressed by the following equation.

$$\vec{M}_{dw} = \sum_{k=1}^{k=4} \vec{r}_{C_1B_{f_k}} \times \left[\, f_{dw}\vec{p}_{f_k} \,\right] \tag{3.44}$$

The position vector $\vec{r}_{C_1B_{f_k}}$ seen in the above equation can be expressed as follows.

$$\begin{aligned}
&\vec{r}_{C_1B_{f_k}} = \vec{r}_{C_1B} + \vec{r}_{BB_{f_k}} \\
&\vec{r}_{C_1B} = -c_1\vec{u}_3^{(1)} \\
&\vec{r}_{BB_{f_k}} = b_0\vec{u}_1^{(f_k)} - \left(\left(t_p + h_f\right)/2\right)\vec{u}_3^{(1)} \\
&\vec{r}_{C_1B_{f_k}} = -\left(c_1 + \left(t_p + h_f\right)/2\right)\vec{u}_3^{(1)} + b_0\vec{u}_1^{(f_k)}
\end{aligned} \tag{3.45}$$

The scalar term b_0 represents the radius of the circular base platform which can be seen in Figure 3.2. The other scalar term t_p represents thickness of the circular plate of the base and upper platforms.

Matrix equations in $F_1(B)$ are indicated as follows.

$$\begin{aligned}
\bar{r}^{(1)}_{C_1B_{f_k}} &= -\left(c_1 + h_f\right)\bar{u}_3^{(1/1)} + b_0\bar{u}_1^{(f_k/1)} = -\left(c_1 + h_f\right)\bar{u}_3^{(1/1)} + b_0\hat{C}^{(1,f_k)}\bar{u}_1^{(f_k/f_k)} \\
\bar{r}^{(1)}_{C_1B_{f_k}} &= -\left(c_1 + h_f\right)\bar{u}_3 + b_0\hat{C}^{(1,f_k)}\bar{u}_1 \\
\bar{M}^{(1)}_{dw} &= \sum_{k=1}^{k=4}\tilde{r}^{(1)}_{C_1B_{f_k}}\left[\, f_{dw}\bar{p}^{(1)}_{f_k}\right]
\end{aligned} \tag{3.46}$$

3.3.2 Lift Force

Lift Forces $\vec{F}_{L_3}$ and $\vec{F}_{L_4}$ are generated due to the aerodynamic effects of spinning motion of the propellers (B_3 and B_4) and applied in the direction of the shaft of the upper body B_2 is illustrated in Figure 3.4.

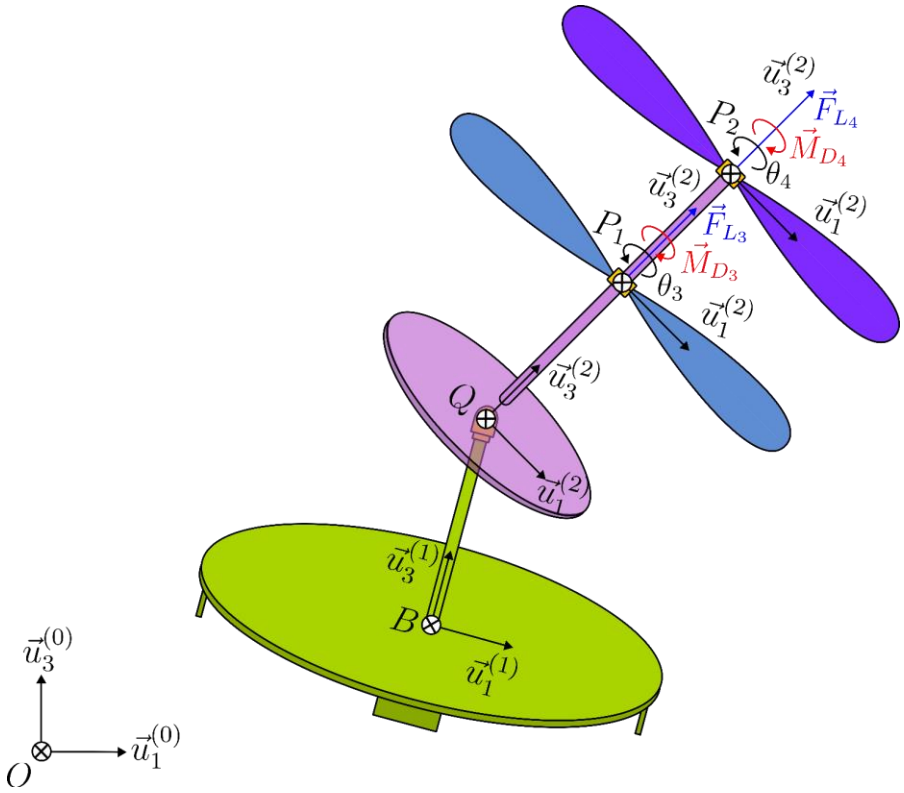

Figure 3.4. Representation of Lift Forces and Drag Moments

Magnitude of the lift forces F_{L_3} and F_{L_4} are calculated through the test data of the selected propeller which will be mentioned in detail later in Chapter 6. The two propeller blades are symmetrical with respect to xy plane. Thus, the test data is applicable to both propellers. The test data consisting of the rotational velocity of the propellers versus the lift forces are utilized for curve-fitting which can be seen in Figure 3.5.

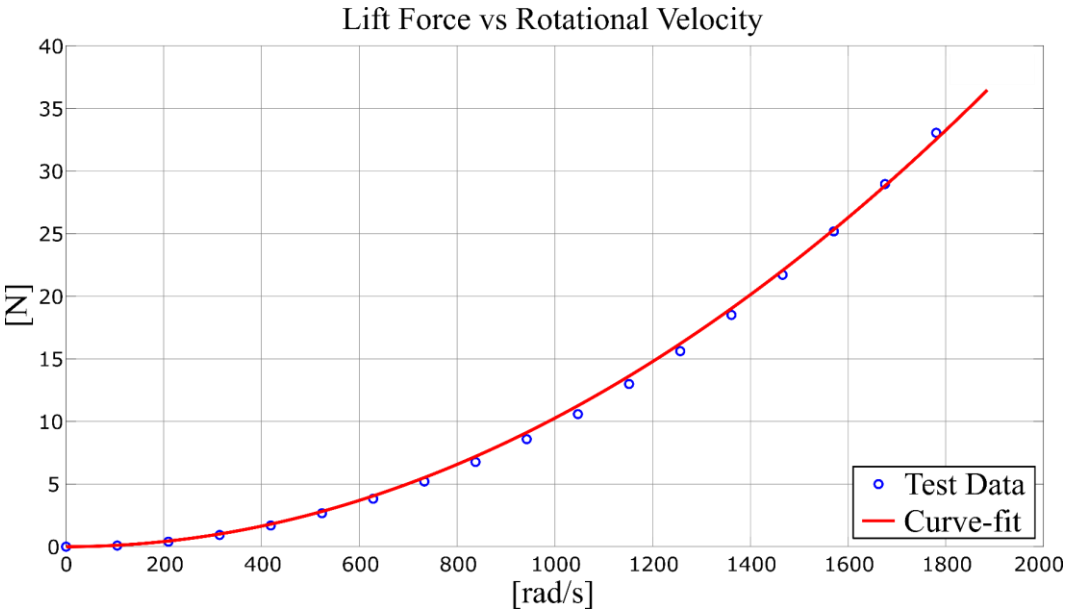

Figure 3.5. Curve-fit of Lift Force vs Rotational Velocity Plot

Then, the second order polynomials which are expressed as seen below are generated from the curve-fitted test data which is illustrated in Figure 3.5.

$$\begin{aligned} F_{L_3} &= p_{F,2}\left|\dot{\theta}_3\right|^2 + p_{F,1}\left|\dot{\theta}_3\right| \\ F_{L_4} &= p_{F,2}\left|\dot{\theta}_4\right|^2 + p_{F,1}\left|\dot{\theta}_4\right| \end{aligned} \tag{3.47}$$

Here, absolute values of the angular velocities are used in Eq. (3.47) because one of the two propellers is driven to spin in the reverse direction by applying negative torque to achieve torque cancellation in the UAV. Moreover, angular velocities of the propellers are assumed to be $\dot{\theta}_3$ and $\dot{\theta}_4$ in calculations of the lift force since rotor speeds are very much larger than the other angular velocity components. Thus, the terms other than $\dot{\theta}_3$ and $\dot{\theta}_4$, are neglected in the expressions for angular velocities of the propellers. Coefficients in the above equation are indicated as seen below.

$$\begin{aligned} p_{F,1} &= 1.346\times10^{-10} \\ p_{F,2} &= 1.027\times10^{-5} \end{aligned} \tag{3.48}$$

To express the lift forces as vectors, the equations are written as seen below.

$$\vec{F}_{L_3} = F_{L_3}\vec{u}_3^{(2)}$$
$$\vec{F}_{L_4} = F_{L_4}\vec{u}_3^{(2)} \tag{3.49}$$

The lift forces can also be expressed in the following matrix forms in the frames $F_2(P_1)$ and $F_2(P_2)$.

$$\bar{F}_{L_3}^{(2)} = F_{L_3}\bar{u}_3$$
$$\bar{F}_{L_4}^{(2)} = F_{L_4}\bar{u}_3 \tag{3.50}$$

3.3.3 Drag Moment

The drag moment results from the spinning motion of the propellers (B_3 and B_4) due to the aerodynamic effects. It is applied in the opposite direction of the spinning motion of the propellers as seen in Figure 3.4.

Magnitude of the drag moments M_{D_3} and M_{D_4} are calculated through the test data of the selected propeller. The test data consisting of the rotational velocity of the propellers versus the drag moments are separated into two collections of data points for curve-fitting, since 2 different second order polynomials give better curve-fitting results. Thus, there are two curve-fitted plots, the first one for low rotational velocities and the second one for high rotational velocities which can be seen in Figure 3.6 and Figure 3.7.

The second order polynomials which are expressed as seen below are generated from the curve-fitted test data for low rotational velocities which can be seen in Figure 3.6.

$$M_{D_3} = p_{M,2}\left|\dot{\theta}_3\right|^2 + p_{M,1}\left|\dot{\theta}_3\right|$$
$$M_{D_4} = p_{M,2}\left|\dot{\theta}_4\right|^2 + p_{M,1}\left|\dot{\theta}_4\right| \tag{3.51}$$

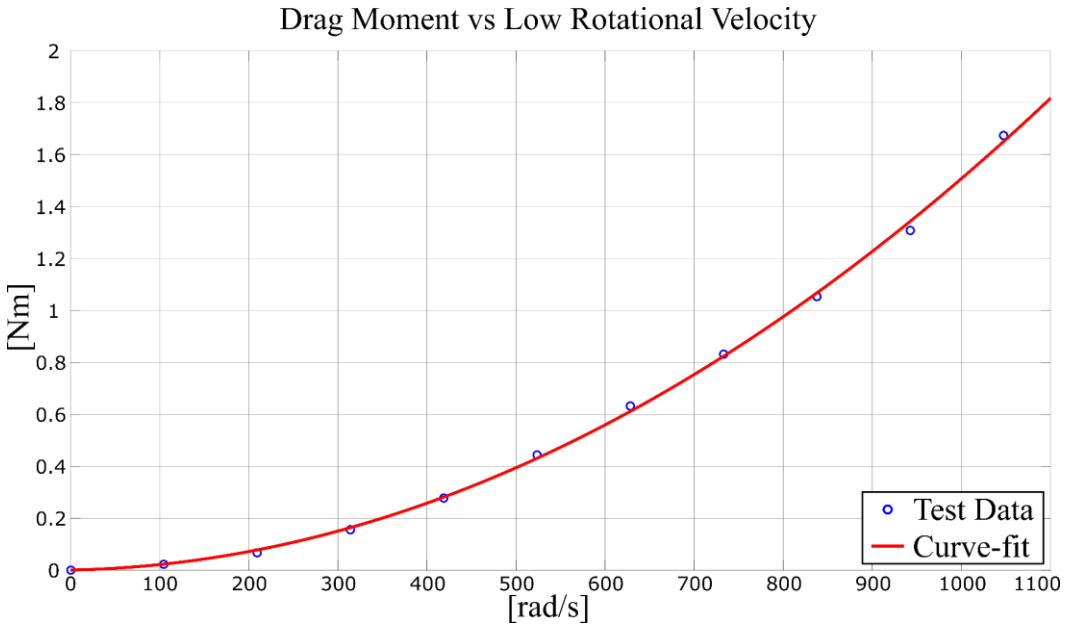

Figure 3.6. Curve-fit of Drag Moment vs Low Rotational Velocity Plot

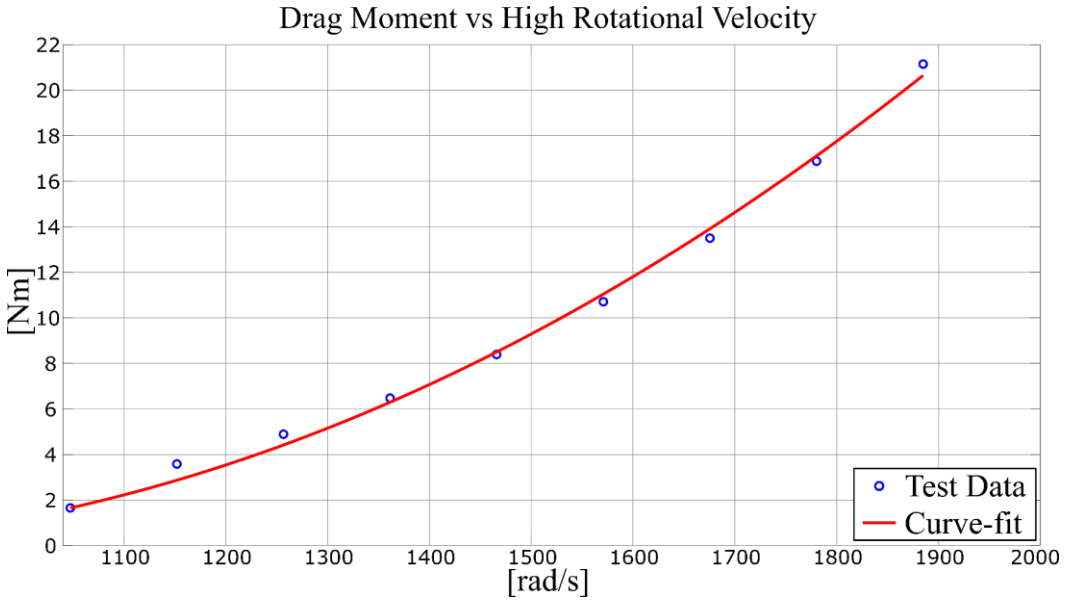

Figure 3.7. Curve-fit of Drag Moment vs High Rotational Velocity Plot

The curve-fitted test data for high rotational velocities which can be seen in Figure 3.7 is utilized to generate another second order polynomial which can be seen as follows.

$$M_{D_3} = p_{M,2,h}\left|\dot{\theta}_3\right|^2 + p_{M,1,h}\left|\dot{\theta}_3\right| + p_{M,0,h}$$
$$M_{D_4} = p_{M,2,h}\left|\dot{\theta}_4\right|^2 + p_{M,1,h}\left|\dot{\theta}_4\right| + p_{M,0,h} \tag{3.52}$$

The coefficients seen in Eq. (3.51) and (3.52) are expressed as seen below.

$$\begin{aligned} p_{M,1} &= 6.779\times10^{-5} \\ p_{M,2} &= 1.44\times10^{-6} \\ p_{M,0,h} &= 7.674 \\ p_{M,1,h} &= -0.02154 \\ p_{M,2,h} &= 1.508\times10^{-5} \end{aligned} \tag{3.53}$$

In Eqs. (3.51) and (3.52), the angular velocities of the propellers are assumed to be $\dot{\theta}_3$ and $\dot{\theta}_4$ in the calculations of the drag moment since the angular velocities of the propellers are greater than the angular velocities of the base and upper platforms. Thus, the terms other than $\dot{\theta}_3$ and $\dot{\theta}_4$, are neglected in the expressions for the angular velocities of the propellers just as they are neglected before in the calculations of the lift force.

To express the drag moments as vectors, equations can be written as follows.

$$\vec{M}_{D_3} = -\mathrm{sgn}\left(\dot{\theta}_3\right) M_{D_3} \vec{u}_3^{(2)}$$
$$\vec{M}_{D_4} = -\mathrm{sgn}\left(\dot{\theta}_4\right) M_{D_4} \vec{u}_3^{(2)} \tag{3.54}$$

The drag moments can also be expressed in the following matrix forms in the frames $F_2\left(P_1\right)$ and $F_2\left(P_2\right)$.

$$\bar{M}_{D_3}^{(2)} = -\mathrm{sgn}\left(\dot{\theta}_3\right) M_{D_3} \bar{u}_3$$
$$\bar{M}_{D_4}^{(2)} = -\mathrm{sgn}\left(\dot{\theta}_4\right) M_{D_4} \bar{u}_3 \tag{3.55}$$

The signum function (sgn) gives the sign of a variable. Here, the sgn function seen in Eqs. (3.54) and (3.55) expresses the direction of the spinning motion of the propellers (B_3 and B_4). Since there are minus signs in the expressions, it means that

drag moments are applied in the opposite direction of the spinning motion just as mentioned in the beginning of this section.

3.4 Force and Moment Equations in Matrix Form

In this section, the vectorial force and moment equations which are explained in Section 3.1 are written as matrix equations by resolving them in the appropriate body frames.

3.4.1 Force Equations in Matrix Form

The vectorial force equations for B_1, B_c, B_2, B_3 and B_4 that are given in Eqs. (3.3) -(3.7) are written again as seen below for convenience.

$$m_1\vec{a}_1 = -\vec{F}_{1c} - \vec{u}_3^{(0)} m_1 g + \vec{F}_{dw} \tag{3.56}$$

$$\vec{0} = \vec{F}_{1c} - \vec{F}_{c2} \tag{3.57}$$

$$m_2\vec{a}_2 = \vec{F}_{c2} - \vec{F}_{23} - \vec{F}_{24} - \vec{u}_3^{(0)} m_2 g \tag{3.58}$$

$$m_3\vec{a}_3 = \vec{F}_{23} - \vec{u}_3^{(0)} m_3 g + \vec{F}_{L_3} \tag{3.59}$$

$$m_4\vec{a}_4 = \vec{F}_{24} + \vec{u}_3^{(0)} m_4 g + \vec{F}_{L_4} \tag{3.60}$$

The resolution of Eq (3.56) is expressed in $F_1(B)$ as seen below.

$$m_1\bar{a}_1^{(1)} = -\bar{F}_{1c}^{(1)} - \hat{C}^{(0,1)t}\bar{u}_3 m_1 g + \bar{F}_{dw}^{(1)} \tag{3.61}$$

The resolution of Eq (3.57) is expressed in $F_c(Q_c)$ as seen below.

$$\bar{0} = \bar{F}_{1c}^{(c)} - \bar{F}_{c2}^{(c)} \;\Rightarrow\; \bar{F}_{1c}^{(c)} = \hat{C}^{(c,2)}\bar{F}_{c2}^{(2)} \tag{3.62}$$

The resolution of Eq (3.58) is expressed in $F_2(Q)$ as seen below.

$$m_2\bar{a}_2^{(2)} = \bar{F}_{c2}^{(2)} - \bar{F}_{23}^{(2)} - \bar{F}_{24}^{(2)} - \hat{C}^{(0,2)t}\bar{u}_3 m_2 g \tag{3.63}$$

The resolution of Eq (3.59) is expressed in $F_2\left(P_1\right)$ as seen below.

$$m_3\bar{a}_3^{(2)} = \bar{F}_{23}^{(2)} - \hat{C}^{(0,2)t}\bar{u}_3 m_3 g + \bar{F}_{L_3}^{(2)} \tag{3.64}$$

The resolution of Eq (3.60) is expressed in $F_2\left(P_2\right)$ as seen below.

$$m_4\bar{a}_4^{(2)} = \bar{F}_{24}^{(2)} - \hat{C}^{(0,2)t}\bar{u}_3 m_4 g + \bar{F}_{L_4}^{(2)} \tag{3.65}$$

3.4.2 Moment Equations in Matrix Form

As the inertia matrices are constant in the body frames, they are expressed in the body frames, except those of the propellers B_3 and B_4. They are expressed in the body frame of B_2 which is a non-spinning frame for B_3 and B_4 due to the property of being symmetric along the spinning axis.

The vectorial moment equations for B_1, B_c, B_2, B_3, B_4 and the required position vectors that are given in Eqs. (3.8)-(3.16) are written again as seen below for convenience.

$$\overset{\vee}{J}_1\cdot\vec{\alpha}_1 + \vec{\omega}_1\times\overset{\vee}{J}_1\cdot\vec{\omega}_1 = -\vec{M}_{1c} + \vec{M}_{dw} - \vec{r}_{C_1Q}\times\vec{F}_{1c} \tag{3.66}$$

$$\vec{r}_{C_1Q} = \vec{u}_3^{(1)}\left(l_0 - c_2\right) \tag{3.67}$$

$$\vec{0} = \vec{M}_{1c} - \vec{M}_{c2} \tag{3.68}$$

$$\begin{aligned}&\overset{\vee}{J}_2\cdot\vec{\alpha}_2 + \vec{\omega}_2\times\overset{\vee}{J}_2\cdot\vec{\omega}_2 = \vec{M}_{c2} - \vec{M}_{23} - \vec{M}_{24}\\ &+\vec{r}_{C_2Q}\times\vec{F}_{c2} - \vec{r}_{C_2P_1}\times\vec{F}_{23} - \vec{r}_{C_2P_2}\times\vec{F}_{24}\end{aligned} \tag{3.69}$$

$$\begin{aligned}\vec{r}_{C_2Q} &= -c_2\vec{u}_3^{(2)}\\ \vec{r}_{C_2P_1} &= \left(h_0 - c_2\right)\vec{u}_3^{(2)}\\ \vec{r}_{C_2P_2} &= \left(h_0 + h_1 - c_2\right)\vec{u}_3^{(2)}\end{aligned} \tag{3.70}$$

$$\overset{\vee}{J}_3 \cdot \vec{\alpha}_3 + \vec{\omega}_3 \times \overset{\vee}{J}_3 \cdot \vec{\omega}_3 = \vec{M}_{23} + \vec{M}_{D_3} \tag{3.71}$$

$$\overset{\vee}{J}_4 \cdot \vec{\alpha}_4 + \vec{\omega}_4 \times \overset{\vee}{J}_4 \cdot \vec{\omega}_4 = \vec{M}_{24} + \vec{M}_{D_4} \tag{3.72}$$

The resolution of Eqs. (3.66) and (3.67) in $F_1\left(C_1\right)$ are expressed as follows.

$$\hat{J}_1 \bar{\alpha}_1^{(1)} + \tilde{\omega}_1^{(1)} \hat{J}_1 \bar{\omega}_1^{(1)} = -\bar{M}_{1c}^{(1)} + \bar{M}_{dw}^{(1)} - \tilde{r}_{C_1Q}^{(1)} \bar{F}_{1c}^{(1)} \tag{3.73}$$

$$\bar{r}_{C_1Q}^{(1)} = \bar{u}_3 \left(l_0 - c_2\right) \tag{3.74}$$

The resolution of Eq. (3.68) in $F_c\left(Q_c\right)$ is expressed as seen below.

$$\bar{0} = \bar{M}_{1c}^{(c)} - \bar{M}_{c2}^{(c)} \;\Rightarrow\; \bar{M}_{1c}^{(c)} = \hat{C}^{(c,2)} \bar{M}_{c2}^{(2)} \tag{3.75}$$

The components of $\bar{M}_{1c}^{(c)}$ and $\bar{M}_{c2}^{(2)}$ are indicated in Eqs. (3.19) and (3.22) before and they are written again below for convenience.

$$\begin{aligned} \bar{M}_{1c}^{(c)} &= \bar{u}_1 M_{1c1} + \bar{u}_2 M_{1c2} + \bar{u}_3 T_{1c3} \\ \bar{M}_{c2}^{(2)} &= \bar{u}_1 M_{c21} + \bar{u}_2 T_{c22} + \bar{u}_3 M_{c23} \end{aligned} \tag{3.76}$$

The resolution of Eqs. (3.69) and (3.70) in $F_2\left(C_2\right)$ are expressed as follows.

$$\begin{aligned} &\hat{J}_2 \bar{\alpha}_2^{(2)} + \tilde{\omega}_2^{(2)} \hat{J}_2 \bar{\omega}_2^{(2)} = \bar{M}_{c2}^{(2)} - \bar{M}_{23}^{(2)} - \bar{M}_{24}^{(2)} \\ &+ \tilde{r}_{C_2Q}^{(2)} \bar{F}_{c2}^{(2)} - \tilde{r}_{C_2P_1}^{(2)} \bar{F}_{23}^{(2)} - \tilde{r}_{C_2P_2}^{(2)} \bar{F}_{24}^{(2)} \end{aligned} \tag{3.77}$$

The components of $\bar{M}_{23}^{(2)}$ and $\bar{M}_{24}^{(2)}$ are indicated in Eqs. (3.25) and (3.27) before and they are written again below for convenience.

$$\begin{aligned} \bar{M}_{23}^{(2)} &= \bar{u}_1 M_{231} + \bar{u}_2 M_{232} + \bar{u}_3 T_{233} \\ \bar{M}_{24}^{(2)} &= \bar{u}_1 M_{241} + \bar{u}_2 M_{242} + \bar{u}_3 T_{243} \end{aligned} \tag{3.78}$$

$$\begin{aligned}\bar{r}_{C_2Q}^{(2)} &= -c_2\bar{u}_3 \\ \bar{r}_{C_2P_1}^{(2)} &= \left(h_0 - c_2\right)\bar{u}_3 \\ \bar{r}_{C_2P_2}^{(2)} &= \left(h_0 + h_1 - c_2\right)\bar{u}_3\end{aligned} \tag{3.79}$$

The resolution of Eq. (3.71) in $F_2\left(P_1\right)$ is expressed as seen below.

$$\hat{J}_3\bar{\alpha}_3^{(2)} + \tilde{\omega}_3^{(2)}\hat{J}_3\bar{\omega}_3^{(2)} = \bar{M}_{23}^{(2)} + \bar{M}_{D_3}^{(2)} \tag{3.80}$$

The resolution of Eq. (3.72) in $F_2\left(P_2\right)$ is expressed as seen below.

$$\hat{J}_4\bar{\alpha}_4^{(2)} + \tilde{\omega}_4^{(2)}\hat{J}_4\bar{\omega}_4^{(2)} = \bar{M}_{24}^{(2)} + \bar{M}_{D_4}^{(2)} \tag{3.81}$$

3.5 Direct Dynamic Analysis

When the matrix equations indicated in the previous section are expressed as scalar equations, 30 scalar equations appear since there are 6 scalar equations for each body. Those 30 scalar equations can be collected into a single matrix equation as shown below[21].

$$\hat{N}\left(\bar{q},t\right)\ddot{\bar{q}} = \hat{A}\left(\bar{q},t\right)\bar{Q} + \hat{D}\left(\bar{q},t\right)\bar{R} + \bar{f}\left(\bar{q},\dot{\bar{q}},t\right) \tag{3.82}$$

In Eq. (3.82), $\ddot{\bar{q}}$ is the acceleration array of the generalized coordinates. As for $\bar{q}$, which is a 10×1 column matrix, it is the array of the generalized coordinates. Its elements are indicated below.

$$\bar{q} = \begin{bmatrix} x \\ y \\ z \\ \phi_1' \\ \phi_2' \\ \phi_3' \\ \phi_2 \\ \phi_3 \\ \theta_3 \\ \theta_4 \end{bmatrix} \tag{3.83}$$

In the right side of Eq. (3.82), $\bar{Q}$ is a 4×1column matrix which contains the actuating torques and expressed as seen below.

$$\bar{Q} = \begin{bmatrix} T_{1c3} \\ T_{c22} \\ T_{233} \\ T_{243} \end{bmatrix} \tag{3.84}$$

The components of $\bar{Q}$ can be seen in Eqs. (3.19)- (3.27). They are also indicated in Eqs. (3.76) and (3.78) of the preceding section.

In Eq. (3.82), $\bar{R}$ is a 20×1 column matrix and contains structural interaction forces and moments which are explained before in Section 3.2. The elements of $\bar{R}$ are listed below:

$F_{1c1}, F_{1c2}, F_{1c3}, F_{c21}, F_{c22}, F_{c23}, F_{231}, F_{232}, F_{233}, F_{241}, F_{242}, F_{243},$
$M_{1c1}, M_{1c2}, M_{c21}, M_{c23}, M_{231}, M_{232}, M_{241}, M_{242}.$

In Eq. (3.82), $\bar{f}$ is a 30×1 column matrix which contains all the other force and moment components. Moreover, $\hat{N}$, $\hat{D}$ and $\hat{A}$ are coefficient matrices with sizes of 30×10, 30×20 and 30×4 respectively.

To be able to solve the acceleration of the generalized coordinates, Eq. (3.82) is turned into the form expressed as seen below.

$$\begin{bmatrix} \hat{N}(\bar{q},t) & -\hat{D}(\bar{q},t) \end{bmatrix} \begin{bmatrix} \ddot{\bar{q}} \\ \bar{R} \end{bmatrix} = \hat{A}(\bar{q},t)\bar{Q} + \bar{f}(\bar{q},\dot{\bar{q}},t) \tag{3.85}$$

The form of Eq(3.85) is utilized to solve the direct dynamics problems required for motion simulations dealt with later in Chapter 6. Therefore, the following matrix inversion is achieved numerically in motion simulations.

$$\begin{bmatrix} \ddot{\bar{q}} \\ \bar{R} \end{bmatrix} = \begin{bmatrix} \hat{N}(\bar{q},t) & -\hat{D}(\bar{q},t) \end{bmatrix}^{-1} \begin{bmatrix} \hat{A}(\bar{q},t)\bar{Q} + \bar{f}(\bar{q},\dot{\bar{q}},t) \end{bmatrix} \tag{3.86}$$

To be able to invert the matrix $\begin{bmatrix} \hat{N}(\bar{q},t) & -\hat{D}(\bar{q},t) \end{bmatrix}$ seen in Eq. (3.86), it must be a square matrix. Since $\hat{N}$ is a 30×10 matrix and $\hat{D}$ is a 30×20 matrix, the matrix $\begin{bmatrix} \hat{N}(\bar{q},t) & -\hat{D}(\bar{q},t) \end{bmatrix}$ has a size of 30×30, which makes it a square matrix.

CHAPTER 4

CONTROL SYSTEM DESIGN

The UAV has 6 DoF described by the set of generalized coordinates $\{x, y, z; \phi_1', \phi_2', \phi_3'\}$. As it is an underactuated system, 4 of the 6 generalized coordinates, $\{x, y, z; \phi_3'\}$ are controlled indirectly by the 4 control torques by means of certain intermediate controlling variables while the other 2 generalized coordinates $\{\phi_1', \phi_2'\}$, roll and pitch angles, are left free. However, they are kept to have finite values because the UAV is passively stabilized due to the downwash effect of the propellers, the restoring effect of the gravity and damping effect of air.

4.1 Active Control Strategy

A. The Newton-Euler formulation leads to the following differential equations expressed in the generic formats indicated below.

-Propeller Shaft Angles:

$$\ddot{\phi}_3 = b_{11}T_{1c3} + b_{12}T_{c22} + b_{13}T_{233} + b_{14}T_{243} + f_1(\phi_3, \phi_2, \ ...) \tag{4.1}$$

$$\ddot{\phi}_2 = b_{21}T_{1c3} + b_{22}T_{c22} + b_{23}T_{233} + b_{24}T_{243} + f_2(\phi_3, \phi_2, \ ...) \tag{4.2}$$

-Propeller Angles:

$$\ddot{\theta}_3 = \dot{\omega}_3 = T_{233} - f_3(\omega_3) \tag{4.3}$$

$$\ddot{\theta}_4 = \dot{\omega}_4 = T_{243} - f_4(\omega_4) \tag{4.4}$$

-Orientation Angles of the UAV:

$$\ddot{\phi}_3' = b_{51}T_{1c3} + b_{52}T_{c22} + b_{53}T_{233} + b_{54}T_{243} + f_5\left(\phi_3, \phi_2, \omega_3, \omega_4, \ ...\right) \tag{4.5}$$

$$\ddot{\phi}_2' = b_{61}T_{1c3} + b_{62}T_{c22} + b_{63}T_{233} + b_{64}T_{243} + f_6\left(\phi_3, \phi_2, \omega_3, \omega_4, \ ...\right) \tag{4.6}$$

$$\ddot{\phi}_1' = b_{71}T_{1c3} + b_{72}T_{c22} + b_{73}T_{233} + b_{74}T_{243} + f_7\left(\phi_3, \phi_2, \omega_3, \omega_4, \ ...\right) \tag{4.7}$$

-Mass Center Coordinates of the UAV:

$$\ddot{x} = b_{81}T_{1c3} + b_{82}T_{c22} + b_{83}T_{233} + b_{84}T_{243} + f_8\left(\phi_3, \phi_2, \omega_3, \omega_4, \ ...\right) \tag{4.8}$$

$$\ddot{y} = b_{91}T_{1c3} + b_{92}T_{c22} + b_{93}T_{233} + b_{94}T_{243} + f_9\left(\phi_3, \phi_2, \omega_3, \omega_4, \ ...\right) \tag{4.9}$$

$$\ddot{z} = b_{101}T_{1c3} + b_{102}T_{c22} + b_{103}T_{233} + b_{104}T_{243} + f_{10}\left(\phi_3, \phi_2, \omega_3, \omega_4, \ ...\right) \tag{4.10}$$

B. The control of the above-mentioned variables (except ϕ_1' and ϕ_2') is established as follows.

Eqs. (4.8), (4.9), (4.10), and (4.5) can be written together as the following matrix equation.

$$\begin{bmatrix} \ddot{x} \\ \ddot{y} \\ \ddot{z} \\ \ddot{\phi}_3' \end{bmatrix} = \begin{bmatrix} b_{81} & b_{82} & b_{83} & b_{84} \\ b_{91} & b_{92} & b_{93} & b_{94} \\ b_{101} & b_{102} & b_{103} & b_{104} \\ b_{51} & b_{52} & b_{53} & b_{54} \end{bmatrix} \begin{bmatrix} T_{1c3} \\ T_{c22} \\ T_{233} \\ T_{243} \end{bmatrix} + \begin{bmatrix} f_8(\cdots) \\ f_9(\cdots) \\ f_{10}(\cdots) \\ f_5(\cdots) \end{bmatrix} \tag{4.11}$$

The same equation can be written compactly as follows.

$$\ddot{\bar{\xi}} = \hat{B}\bar{T} + \bar{f} \tag{4.12}$$

Here, $\bar{T} = \bar{Q}$ is the array of the actuating torques, which was defined earlier by Eq. (3.84). Let $\bar{T}$ be generated according to the following "computed torque method".

$$\bar{T} = \hat{B}^{-1}\left(\bar{u} - \bar{f}\right) \tag{4.13}$$

Then, Eq. (4.12) becomes

$$\ddot{\bar{\xi}} = \bar{u} \tag{4.14}$$

Here, $\bar{u}$ is the array of acceleration commands. It can be produced according to the following PID control law with acceleration feedforward.

$$\bar{u} = \ddot{\bar{\xi}}^* + K_d\left(\dot{\bar{\xi}}^* - \dot{\bar{\xi}}\right) + K_p\left(\bar{\xi}^* - \bar{\xi}\right) + K_i\int_0^t\left(\bar{\xi}^* - \bar{\xi}\right)d\tau \tag{4.15}$$

Let $\bar{\varepsilon} = \bar{\xi}^* - \bar{\xi}$ be the error between the desired and actual values. Then Eq. (4.15) leads to the following error equation.

$$\dddot{\bar{\varepsilon}} + K_d\ddot{\bar{\varepsilon}} + K_p\dot{\bar{\varepsilon}} + K_i\bar{\varepsilon} = \bar{0} \tag{4.16}$$

Eq. (4.16) implies that it is possible to have $\bar{\varepsilon} \to \bar{0}$ as $t \to 0$ by means of properly tuned PID gains.

Once $\bar{u}$ and $\bar{T}$ are determined according to Eqs. (4.13) and (4.15), then the following operations lead to the propeller speeds and propeller shaft angles.

1. Propeller speeds are determined by integrating the following first order differential equations.

$$\dot{\omega}_3 = T_{233} - f_3\left(\omega_3\right) \tag{4.17}$$

$$\dot{\omega}_4 = T_{243} - f_4\left(\omega_4\right) \tag{4.18}$$

2. Propeller shaft angles are determined by integrating the following second order differential equations.

$$\ddot{\phi}_3 = b_{11}T_{1c3} + b_{12}T_{c22} + b_{13}T_{233} + b_{14}T_{243} + f_1\left(\phi_3, \phi_2, ...\right) \tag{4.19}$$

$$\ddot{\phi}_2 = b_{21}T_{1c3} + b_{22}T_{c22} + b_{23}T_{233} + b_{24}T_{243} + f_2\left(\phi_3, \phi_2, ...\right) \tag{4.20}$$

As for the roll and pitch angles $\phi_1^{'}$ and $\phi_2^{'}$, they are determined by integrating the following second order differential equations.

$$\ddot{\phi}_1^{'} = b_{71}T_{1c3} + b_{72}T_{c22} + b_{73}T_{243} + f_7\left(\phi_3, \phi_2, \omega_3, \omega_4, ...\right) \tag{4.21}$$

$$\ddot{\phi}_2' = b_{61}T_{1c3} + b_{62}T_{c22} + b_{63}T_{233} + b_{64}T_{243} + f_6\left(\phi_3, \phi_2, \omega_3, \omega_4, ...\right) \tag{4.22}$$

Here, owing to the restoring and damping effects of the downwash flow of the propellers, which appear in the expressions of the functions f_6 and f_7, the angles ϕ_1' and ϕ_2' are expected to be stabilized passively.

4.2 Passive Control Strategy

As there are 2 uncontrolled generalized coordinates $\{\phi_1', \phi_2'\}$, roll and pitch angles, there arise a need to model passive stablizing effects to keep roll and pitch angles as finite values. The restoring effect of the gravity and downwash effect mentioned in Section 3.3.1 are two of the passive controls over the roll and pitch angles but they are not sufficient. Damping effects and drag forces in opposite direction of the longitudinal motion of the UAV is also modelled due to their passive stablizing effects. Damping effect on B_1 is simply added to the model as seen in Eq. (4.23)

$$\vec{M}_{1d} = -\vec{u}_1^{(1)}\left(K_d\dot{\phi}_1'\right) - \vec{u}_2^{(1)}\left(K_d\dot{\phi}_2'\right) \tag{4.23}$$

K_d is called damping effect coefficient and determined as 0.7 based on trial and errors during simulations. Moreover, the drag force assumed to be applied at the mass center of the UAV is simply included in the model as seen in Eq. (4.24).

$$F_D = -C_D\left|\dot{x}_1\right|\dot{x}_1 \tag{4.24}$$

Since, the flow is perpendicular to the stabilizing fins which condition is the same as the downwash effect, drag coefficient C_D is taken as 1.17 which is the same as the drag coefficient used to calculate downwash force in Eq. (3.33).

CHAPTER 5

SERIAL TO PARALLEL MANIPULATOR CONVERSION

Even though the serial manipulator version of the UAV is more convenient for modelling, there arises a need for the parallel manipulator version which is mentioned in Chapter 2 before. The parallel manipulator version enables the UAV to have some advantages such as roboustness and precision. Moreover, during a non-operational period, the legs can carry the weight of the upper platform and the propellers to provide a stable pose. On the other hand, the serial manipulator version requires actuation to be able to stand stable in a non-operational period which is more power-consuming than the parallel manipulator version. The conversion is applied by showing the equivalence of the two actuation systems. The first one is actuation by means of a universal joint which is a part of the serial manipulator version explained deeply in previous chapters. The second one is actuation by means of a 3-DoF parallel manipulator which will be explained comprehensively in this chapter. Continuing with the assumptions, the equivalence of the two actuation system is shown here when relatively small masses and distances are neglected for the sake of simplicty. An e-mail (M. K. Ozgoren, personal communication, July 16, 2022) confirms that the equivalence equations are accurate. On the other hand, an additonal study proves that when the small masses and distances are not neglected, the equivalency can still be shown.

5.1 Actuation by Means of a Universal Joint

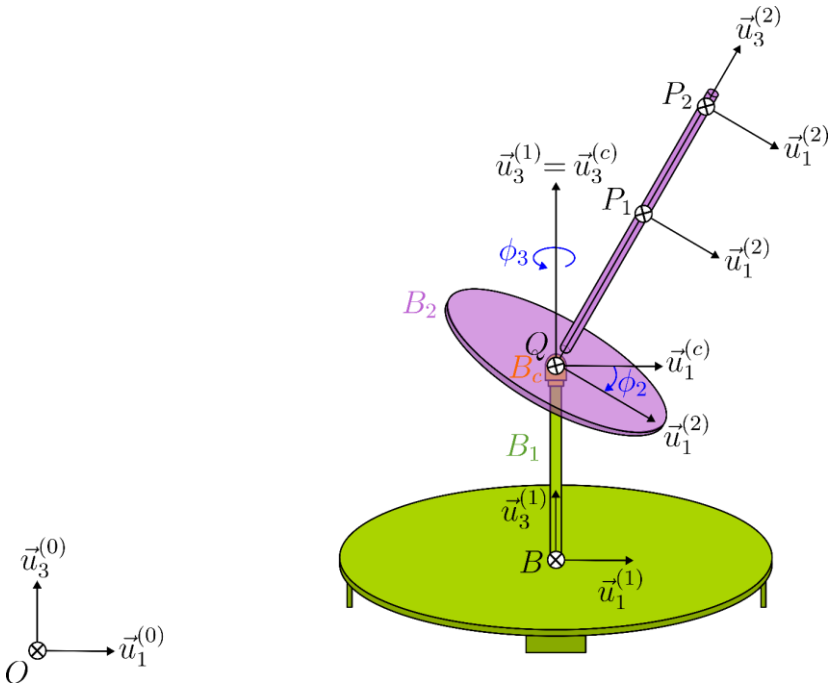

Figure 5.1. Actuation by Means of a Universal Joint

To explain the equivalence, focus is on the bodies B_1, B_c and B_2 of the serial manipulator version. That is why, only B_1, B_c and B_2 are shown in Figure 5.1.

5.1.1 Kinematics for Actuation by a Universal Joint

The orientation matrix of B_2 with respect to B_1 through B_c is expressed in Eq. (3.17) and written below again for convenience.

$$\hat{C}^{(1,2)} = \hat{C}^{(1,c)}\hat{C}^{(c,2)} = e^{\tilde{u}_3\phi_3}e^{\tilde{u}_2\phi_2} \tag{5.1}$$

5.1.2 Dynamics for Actuation by a Universal Joint

The N-E equations for B_2 expressed in Eqs. (3.5) and (3.11) are written below again for convenience.

$$m_2\vec{a}_2 = \vec{F}_{c2} - \vec{F}_{23} - \vec{F}_{24} + m_2\vec{g} \tag{5.2}$$

$$\overset{\vee}{J}_2\cdot\vec{\alpha}_2 + \vec{\omega}_2\times\overset{\vee}{J}_2\cdot\vec{\omega}_2 = \vec{M}_{c2} - \vec{M}_{23} - \vec{M}_{24} + \vec{r}_{C_2Q}\times\vec{F}_{c2} - \vec{r}_{C_2P_1}\times\vec{F}_{23} - \vec{r}_{C_2P_2}\times\vec{F}_{24} \tag{5.3}$$

Point C_2 represents the center of mass for B_2. For the sake of simplicity, the mass and the inertia tensor of B_2 can be neglected ($m_2 = 0$, $\overset{\vee}{J}_2 = \overset{\vee}{0}$). Thus, C_2 can be shifted to Q, then Eqs. (5.2) and (5.3) are simplified to the ones seen below.

$$\vec{F}_{c2} = \vec{F}_{23} + \vec{F}_{24} \tag{5.4}$$

$$\vec{M}_{c2} = \vec{M}_{23} + \vec{M}_{24} + \vec{r}_{QP_1}\times\vec{F}_{23} + \vec{r}_{QP_2}\times\vec{F}_{24} \tag{5.5}$$

In addition, the cross-link of the universal joint B_c between the base platform B_1 and upper platform B_2 is assumed massless in Chapter 3. The same assumption is valid here too. Therefore, Eqs. (3.4) and (3.10) are written again as seen below for convenience.

$$\begin{aligned} &\vec{0} = \vec{F}_{1c} - \vec{F}_{c2} \\ &\Rightarrow \vec{F}_{1c} = \vec{F}_{c2} = \vec{F}_{23} + \vec{F}_{24} \end{aligned} \tag{5.6}$$

$$\begin{aligned} &\vec{0} = \vec{M}_{1c} - \vec{M}_{c2} \\ &\Rightarrow \vec{M}_{1c} = \vec{M}_{c2} = \vec{M}_{23} + \vec{M}_{24} + \vec{u}_3^{(2)}\times\left(h_0\vec{F}_{23} + \left(h_0 + h_1\right)\vec{F}_{24}\right) \end{aligned} \tag{5.7}$$

The above force and moment vectors are resolved in the relevant frames in Eqs. (3.18) and (3.21) before and written again as follows.

$$\begin{aligned} \vec{F}_{1c} &= \vec{u}_1^{(1)}F_{1c1} + \vec{u}_2^{(1)}F_{1c2} + \vec{u}_3^{(1)}F_{1c3} \\ \vec{M}_{1c} &= \vec{u}_1^{(1)}M_{1c1} + \vec{u}_2^{(1)}M_{1c2} + \vec{u}_3^{(1)}T_{1c3} \end{aligned} \tag{5.8}$$

$$\begin{aligned}\vec{F}_{c2} &= \vec{u}_1^{(2)} F_{c21} + \vec{u}_2^{(2)} F_{c22} + \vec{u}_3^{(2)} F_{c23} \\ \vec{F}_{c2} &= \vec{u}_1^{(2)} \left(F_{231} + F_{241}\right) + \vec{u}_2^{(2)} \left(F_{232} + F_{242}\right) + \vec{u}_3^{(2)} \left(F_{233} + F_{243}\right)\end{aligned} \tag{5.9}$$

$$\begin{aligned}\vec{M}_{c2} &= \vec{u}_1^{(2)} M_{c21} + \vec{u}_2^{(2)} T_{c22} + \vec{u}_3^{(2)} M_{c23} \\ \vec{M}_{c2} &= \vec{u}_1^{(2)} \left(M_{231} + M_{241} - h_0 F_{232} - \left(h_0 + h_1\right) F_{242}\right) \\ &+ \vec{u}_2^{(2)} \left(M_{232} + M_{242} + h_0 F_{231} + \left(h_0 + h_1\right) F_{241}\right) + \vec{u}_3^{(2)} \left(T_{233} + T_{243}\right)\end{aligned} \tag{5.10}$$

Here, T_{1c3} and T_{c22} are the actuation torques applied on B_c and B_2. As for T_{233} and T_{243}, they are the actuation torques applied on the propellers. The other components are associated with the structural interaction forces and moments.

The preceding vector equations imply the following scalar equations.

$$F_{c21} = F_{231} + F_{241} \tag{5.11}$$

$$F_{c22} = F_{232} + F_{242} \tag{5.12}$$

$$F_{c23} = F_{233} + F_{243} \tag{5.13}$$

$$F_{1c1} = c_{11} F_{c21} + c_{12} F_{c22} + c_{13} F_{c23} \tag{5.14}$$

$$F_{1c2} = c_{21} F_{c21} + c_{22} F_{c22} + c_{23} F_{c23} \tag{5.15}$$

$$F_{1c3} = c_{31} F_{c21} + c_{32} F_{c22} + c_{33} F_{c23} \tag{5.16}$$

$$M_{c21} = M_{231} + M_{241} - h_0 F_{232} - \left(h_0 + h_1\right) F_{242} \tag{5.17}$$

$$M_{c22} = T_{c22} = M_{232} + M_{242} + h_0 F_{231} + \left(h_0 + h_1\right) F_{241} \tag{5.18}$$

$$M_{c23} = T_{233} + T_{243} \tag{5.19}$$

$$M_{1c1} = c_{11} M_{c21} + c_{12} M_{c22} + c_{13} M_{c23} = c_{11} M_{c21} + c_{12} T_{1c3} + c_{13} \left(T_{233} + T_{243}\right) \tag{5.20}$$

$$M_{1c2} = c_{21} M_{c21} + c_{22} M_{c22} + c_{23} M_{c23} = c_{21} M_{c21} + c_{22} T_{1c3} + c_{23} \left(T_{233} + T_{243}\right) \tag{5.21}$$

$$M_{1c3} = T_{1c3} = c_{31} M_{c21} + c_{32} M_{c22} + c_{33} M_{c23} \tag{5.22}$$

$$M_{1c3} = T_{1c3} = c_{31} M_{c21} + c_{32} M_{c22} + c_{33} \left(T_{233} + T_{243}\right) \tag{5.23}$$

In the above equations, for all $i = 1, 2, 3$ and $j = 1, 2, 3$;

$$c_{ij} = \vec{u}_i^{(1)} \cdot \vec{u}_j^{(2)} = \bar{u}_i^t e^{\tilde{u}_3 \phi_3} e^{\tilde{u}_2 \phi_2} \bar{u}_j \tag{5.24}$$

Eq. (5.24) implies that

$$\begin{aligned} c_{11} &= \bar{u}_1^t e^{\tilde{u}_3 \phi_3} e^{\tilde{u}_2 \phi_2} \bar{u}_1 = c\phi_3 c\phi_2 \\ c_{12} &= \bar{u}_1^t e^{\tilde{u}_3 \phi_3} e^{\tilde{u}_2 \phi_2} \bar{u}_2 = -s\phi_3 \\ c_{13} &= \bar{u}_1^t e^{\tilde{u}_3 \phi_3} e^{\tilde{u}_2 \phi_2} \bar{u}_3 = c\phi_3 s\phi_2 \end{aligned} \tag{5.25}$$

$$\begin{aligned} c_{21} &= \bar{u}_2^t e^{\tilde{u}_3 \phi_3} e^{\tilde{u}_2 \phi_2} \bar{u}_1 = s\phi_3 c\phi_2 \\ c_{22} &= \bar{u}_2^t e^{\tilde{u}_3 \phi_3} e^{\tilde{u}_2 \phi_2} \bar{u}_2 = c\phi_3 \\ c_{23} &= \bar{u}_2^t e^{\tilde{u}_3 \phi_3} e^{\tilde{u}_2 \phi_2} \bar{u}_3 = s\phi_3 s\phi_2 \end{aligned} \tag{5.26}$$

$$\begin{aligned} c_{31} &= \bar{u}_3^t e^{\tilde{u}_3 \phi_3} e^{\tilde{u}_2 \phi_2} \bar{u}_1 = -s\phi_2 \\ c_{32} &= \bar{u}_3^t e^{\tilde{u}_3 \phi_3} e^{\tilde{u}_2 \phi_2} \bar{u}_2 = 0 \\ c_{33} &= \bar{u}_3^t e^{\tilde{u}_3 \phi_3} e^{\tilde{u}_2 \phi_2} \bar{u}_3 = c\phi_2 \end{aligned} \tag{5.27}$$

On the other hand, according to Eq. (5.23), if $s\phi_2 \neq 0$,

$$M_{c21} = \left[\left(T_{233} + T_{243} \right) c\phi_2 - T_{1c3} \right] / s\phi_2 \tag{5.28}$$

Hence, the components of $\vec{M}_{1c}$ in the frame $F_1(B)$ become completely determined in terms of the actuation torques. That is,

$$M_{1c1} = \left[\left(T_{233} + T_{243} \right) c\phi_3 - T_{1c3} c\phi_3 c\phi_2 - T_{c22} s\phi_3 s\phi_2 \right] / s\phi_2 \tag{5.29}$$

$$M_{1c2} = \left[\left(T_{233} + T_{243} \right) s\phi_3 - T_{1c3} s\phi_3 c\phi_2 - T_{c22} c\phi_3 s\phi_2 \right] / s\phi_2 \tag{5.30}$$

$$M_{1c3} = T_{1c3} \tag{5.31}$$

5.2 Actuation by Means of a 3-DoF Parallel Manipulator

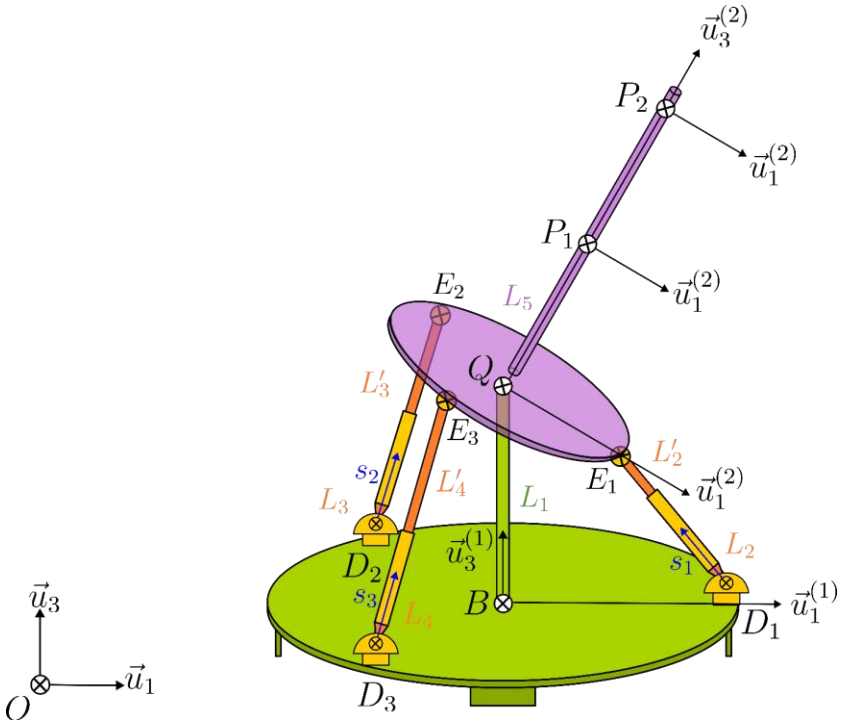

Figure 5.2. Actuation by Means of a 3-DoF Parallel Manipulator

Since the focus is on the links L_1, $\{L_2, L_2'\}$, $\{L_3, L_3'\}$, $\{L_4, L_4'\}$ and L_5 to explain the equivalence, the propellers are not shown in Figure 5.2.

5.2.1 Kinematics for Actuation by a 3-DoF Parallel Manipulator

As seen in in Figure 5.2, the 3-DoF parallel manipulator, which is installed on L_1, consists of $n = 7$ moving links, which are L_5 (upper platform) and the link pairs $\{L_2, L_2'\}$, $\{L_3, L_3'\}$ and $\{L_4, L_4'\}$ that form the three legs. It contains $j_2 = 3$ universal joints at the points D_1, D_2, D_3; $j_3 = 4$ spherical joints at the points Q, E_1, E_2, E_3; and $j_1 = 3$ prismatic joints between the upper and lower links of the legs. Thus, its DoF (μ) with respect to L_1 is verified as follows by the *Kutzbach-Grübler formula*.

$$\begin{aligned}&\mu = 6n_m - (5j_1 + 4j_2 + 3j_3)\\&\Rightarrow 6\times 7 - \left(5\times 3 + 4\times 3 + 3\times 4\right) = 42 - 39 = 3\end{aligned} \tag{5.32}$$

It is required to operate the manipulator so that L_5 has the same orientation with respect to L_1 as in the case described in Chapter 5.1. In other words, it is required to have

$$\hat{C}^{(1,2)} = e^{\tilde{u}_3\phi_3}e^{\tilde{u}_2\phi_2} \tag{5.33}$$

This requirement can be achieved by determining the leg lengths s_1, s_2 and s_3 so as to satisfy the following three independent loop closure equations.

$$\begin{aligned}&\overrightarrow{BQ} + \overrightarrow{QE_1} = \overrightarrow{BD_1} + \overrightarrow{D_1E_1} \;\Rightarrow\; l_0\vec{u}_3^{(1)} + d_0\vec{n}_1 = b_0\vec{m}_1 + s_1\vec{\mu}_1\\&\overrightarrow{BQ} + \overrightarrow{QE_2} = \overrightarrow{BD_2} + \overrightarrow{D_2E_2} \;\Rightarrow\; l_0\vec{u}_3^{(1)} + d_0\vec{n}_2 = b_0\vec{m}_2 + s_1\vec{\mu}_2\\&\overrightarrow{BQ} + \overrightarrow{QE_3} = \overrightarrow{BD_3} + \overrightarrow{D_3E_3} \;\Rightarrow\; l_0\vec{u}_3^{(1)} + d_0\vec{n}_3 = b_0\vec{m}_3 + s_1\vec{\mu}_3\end{aligned} \tag{5.34}$$

The number of independent loops is given by the following formula [17]

$$n_{IL} = j_{tot} - n_m = \left(j_1 + j_2 + j_3\right) - n_m = 10 - 7 = 3 \tag{5.35}$$

The corresponding matrix equations are written as follows.

$$\begin{aligned}&l_0\bar{u}_3^{(1/1)} + d_0\hat{C}^{(1,2)}\bar{n}_1^{(2)} = b_0\bar{m}_1^{(1)} + s_1\bar{\mu}_1^{(1)}\\&\Rightarrow l_0\bar{u}_3 + d_0\left(e^{\tilde{u}_3\phi_3}e^{\tilde{u}_2\phi_2}\right)\left(e^{\tilde{u}_3\phi_3''}\bar{u}_1\right) = b_0\bar{u}_1 + s_1\bar{\mu}_1\\&\Rightarrow s_1\bar{\mu}_1 = \bar{\lambda}_1\;;\;\bar{\lambda}_1 = \bar{\lambda}_1\left(\phi_3,\phi_2\right) = l_0\bar{u}_3 + \left(d_0e^{\tilde{u}_3\phi_3}e^{\tilde{u}_2\phi_2}e^{\tilde{u}_3\phi_3''} - b_0\hat{I}\right)\bar{u}_1\end{aligned} \tag{5.36}$$

$$\begin{aligned}&l_0\bar{u}_3^{(1/1)} + d_0\hat{C}^{(1,2)}\bar{n}_2^{(2)} = b_0\bar{m}_2^{(1)} + s_2\bar{\mu}_2^{(1)}\\&\Rightarrow l_0\bar{u}_3 + d_0\left(e^{\tilde{u}_3\phi_3}e^{\tilde{u}_2\phi_2}\right)\left(e^{\tilde{u}_3\phi_3''}e^{\tilde{u}_3\gamma}\bar{u}_1\right) = b_0e^{\tilde{u}_3\gamma}\bar{u}_1 + s_2\bar{\mu}_2\\&\Rightarrow s_2\bar{\mu}_2 = \bar{\lambda}_2\;;\;\bar{\lambda}_2 = \bar{\lambda}_2\left(\phi_3,\phi_2\right) = l_0\bar{u}_3 + \left(d_0e^{\tilde{u}_3\phi_3}e^{\tilde{u}_2\phi_2}e^{\tilde{u}_3\phi_3''} - b_0\hat{I}\right)e^{\tilde{u}_3\gamma}\bar{u}_1\end{aligned} \tag{5.37}$$

$$\begin{aligned}&l_0\bar{u}_3^{(1/1)} + d_0\hat{C}^{(1,2)}\bar{n}_3^{(2)} = b_0\bar{m}_3^{(1)} + s_3\bar{\mu}_3^{(1)}\\&\Rightarrow l_0\bar{u}_3 + d_0\left(e^{\tilde{u}_3\phi_3}e^{\tilde{u}_2\phi_2}\right)\left(e^{\tilde{u}_3\phi_3''}e^{-\tilde{u}_3\gamma}\bar{u}_1\right) = b_0e^{-\tilde{u}_3\gamma}\bar{u}_1 + s_3\bar{\mu}_3\\&\Rightarrow s_3\bar{\mu}_3 = \bar{\lambda}_3\;;\;\bar{\lambda}_3 = \bar{\lambda}_3\left(\phi_3,\phi_2\right) = l_0\bar{u}_3 + \left(d_0e^{\tilde{u}_3\phi_3}e^{\tilde{u}_2\phi_2}e^{\tilde{u}_3\phi_3''} - b_0\hat{I}\right)e^{-\tilde{u}_3\gamma}\bar{u}_1\end{aligned} \tag{5.38}$$

In the above equations, the angle γ locates the second and third legs with respect to the first one. For equally separated legs, it happens that $\gamma = 2\pi/3$ rad$\left(\text{i.e., } 120°\right)$.

As for ϕ_3'', it is the angular offset of the upper platform L_5 with respect to the base platform L_1. It may be taken to be zero, but its nonzero presence facilitates the yaw motion of the upper platform especially when the manipulator is in the zero pose with $\phi_2 = \phi_3 = 0$.

Noting that $\bar{\mu}_1$, $\bar{\mu}_2$ and $\bar{\mu}_3$ represent the unit vectors along the legs, Eqs. (5.36)-(5.38) provide the leg lengths as follows.

$$s_k = \sqrt{\bar{\lambda}_k^t \bar{\lambda}_k} \; ; k = 1,2,3. \tag{5.39}$$

Hence, the unit vectors of the legs are also obtained so that

$$\left[\vec{\mu}_k\right]^{(1)} = \bar{\mu}_k = \bar{\lambda}_k / s_k \; ; k = 1,2,3. \tag{5.40}$$

5.2.2 Dynamics for Actuation by a 3-DoF Parallel Manipulator

Similarly as in Chapter 5.1, the N-E equations for the upper platform (L_5) can be written as follows.

$$m_2 \vec{a}_2 = \vec{F}_{l_1 2} + \vec{F}_{l_2 2} + \vec{F}_{l_3 2} + \vec{F}_{l_4 2} - \vec{F}_{23} - \vec{F}_{24} + m_2 \vec{g} \tag{5.41}$$

$$\begin{aligned} \overset{\vee}{J}_2 \cdot \vec{\alpha}_2 = {} & \vec{M}_{l_1 2} + \vec{M}_{l_2 2} + \vec{M}_{l_3 2} + \vec{M}_{l_4 2} - \vec{M}_{23} - \vec{M}_{24} - \vec{r}_{C_2 P_1} \times \vec{F}_{23} - \vec{r}_{C_2 P_2} \times \vec{F}_{24} \\ & + \vec{r}_{C_2 Q} \times \vec{F}_{l_1 2} + \vec{r}_{C_2 E_1} \times \vec{F}_{l_2 2} + \vec{r}_{C_2 E_2} \times \vec{F}_{l_3 2} + \vec{r}_{C_2 E_3} \times \vec{F}_{l_4 2} \end{aligned} \tag{5.42}$$

Here, $\vec{F}_{l_k 2}$ and $\vec{M}_{l_k 2}$ are the force and moment applied by the kth leg on the upper platform (L_5). Note that the pole BQ is also treated as a leg, i.e., leg l_1.

Also as done in Section 5.1, it is reasonable to assume that the masses of the legs (l_1, l_2 l_3, l_4) and the upper platform (L_5) are negligible. Then, noting that the actuated

three legs can be treated as two-force members, C_2 may be shifted to Q and the joints at E_1, E_2, E_3 and Q are all spherical (without any moment resistance), Eqs. (5.41) and (5.42) can be written again as follows.

$$f_1\vec{\mu}_1 + f_2\vec{\mu}_2 + f_3\vec{\mu}_3 + \vec{F}_{12} = \vec{F}_{23} + \vec{F}_{24} \tag{5.43}$$

$$\begin{aligned}
&\vec{r}_{C_2E_1} \times \vec{F}_{l_2 2} + \vec{r}_{C_2E_2} \times \vec{F}_{l_3 2} + \vec{r}_{C_2E_3} \times \vec{F}_{l_4 2} \\
&= \vec{M}_{23} + \vec{M}_{24} + \vec{r}_{C_2P_1} \times \vec{F}_{23} + \vec{r}_{C_2P_2} \times \vec{F}_{24} \Rightarrow \\
&\left(d_0\vec{n}_1\right)\times\left(f_1\vec{\mu}_1\right) + \left(d_0\vec{n}_2\right)\times\left(f_2\vec{\mu}_2\right) + \left(d_0\vec{n}_3\right)\times\left(f_3\vec{\mu}_3\right) \\
&= \vec{M}_{23} + \vec{M}_{24} + \vec{u}_3^{(2)} \times \left(h_0\vec{F}_{23} + \left(h_0 + h_1\right)\vec{F}_{24}\right) \\
&\Rightarrow d_0 f_1\left(\vec{n}_1 \times \vec{\mu}_1\right) + d_0 f_2\left(\vec{n}_2 \times \vec{\mu}_2\right) + d_0 f_3\left(\vec{n}_3 \times \vec{\mu}_3\right) \\
&= \vec{M}_{23} + \vec{M}_{24} + \vec{u}_3^{(2)} \times \left(h_0\vec{F}_{23} + \left(h_0 + h_1\right)\vec{F}_{24}\right)
\end{aligned} \tag{5.44}$$

When Eqs. (5.43) and (5.44) are compared to Eqs. (5.4) and (5.5), it is seen that

$$\vec{F}_{12} = \vec{F}_{c2} - \left(f_1\vec{\mu}_1 + f_2\vec{\mu}_2 + f_3\vec{\mu}_3\right) \tag{5.45}$$

$$d_0 f_1\left(\vec{n}_1 \times \vec{\mu}_1\right) + d_0 f_2\left(\vec{n}_2 \times \vec{\mu}_2\right) + d_0 f_3\left(\vec{n}_3 \times \vec{\mu}_3\right) = \vec{M}_{c2} = \vec{M}_{1c} \tag{5.46}$$

As noticed above, Eq. (5.46) gives the actuation forces f_1, f_2 and f_3. Afterwards, Eq. (5.45) gives the force $\vec{F}_{12}$ supported by the pole BQ.

The actuation forces can be extracted from Eq. (5.46) by first writing it as the following matrix equation.

$$\begin{aligned}
&\left(\tilde{n}_1\bar{\mu}_1\right) f_1 + \left(\tilde{n}_2\bar{\mu}_2\right) f_2 + \left(\tilde{n}_3\bar{\mu}_3\right) f_3 = \bar{M}_{1c} / d_0 \\
&\Rightarrow \bar{\eta}_1 f_1 + \bar{\eta}_2 f_2 + \bar{\eta}_3 f_3 = \bar{M}_{1c} / d_0
\end{aligned} \tag{5.47}$$

Referring to Eqs. (5.36)-(5.38), note that

$$\bar{\eta}_1 = \tilde{n}_1\bar{\mu}_1 = e^{\tilde{u}_3\phi_3}e^{\tilde{u}_2\phi_2}e^{\tilde{u}_3\phi_3''}\tilde{u}_1 e^{-\tilde{u}_3\phi_3''}e^{-\tilde{u}_2\phi_2}e^{-\tilde{u}_3\phi_3}\bar{\mu}_1 \tag{5.48}$$

$$\bar{\eta}_2 = \tilde{n}_2\bar{\mu}_2 = e^{\tilde{u}_3\phi_3}e^{\tilde{u}_2\phi_2}e^{\tilde{u}_3\phi_3''}e^{\tilde{u}_3\gamma}\tilde{u}_1 e^{-\tilde{u}_3\gamma}e^{-\tilde{u}_3\phi_3''}e^{-\tilde{u}_2\phi_2}e^{-\tilde{u}_3\phi_3}\bar{\mu}_2 \tag{5.49}$$

$$\bar{\eta}_3 = \tilde{n}_3\bar{\mu}_3 = e^{\tilde{u}_3\phi_3}e^{\tilde{u}_2\phi_2}e^{\tilde{u}_3\phi_3''}e^{-\tilde{u}_3\gamma}\tilde{u}_1 e^{\tilde{u}_3\gamma}e^{-\tilde{u}_3\phi_3''}e^{-\tilde{u}_2\phi_2}e^{-\tilde{u}_3\phi_3}\bar{\mu}_3 \tag{5.50}$$

Eq. (5.47) can also written as the following more compact matrix equation.

$$\begin{bmatrix} \bar{\eta}_1 & \bar{\eta}_2 & \bar{\eta}_3 \end{bmatrix} \begin{bmatrix} f_1 \\ f_2 \\ f_3 \end{bmatrix} = \hat{H}\bar{f} = \bar{M}_{1c} / d_0 \tag{5.51}$$

Hence, $\bar{f}$ is found as follows depending on the components of $\bar{M}_{1c}$ expressed in Chapter 5.1.

$$\bar{f} = \hat{H}^{-1}\bar{M}_{1c} / d_0 \tag{5.52}$$

CHAPTER 6

SIMULATION RESULTS

Kinematic, dynamic analysises and control algoritms discussed previously, are coded and simulated via MATLAB, Simulink and Simscape Multibody. In the simulations, negative torque values are applied on the lower propeller while positive torque values are applied on the upper propeller to cancel net torque applied on the lower and upper platforms when yaw motion is not intended. 3-D animations of MATLAB Mechanics Explorer is used to realize the motion of the UAV as seen in Figure 6.1.

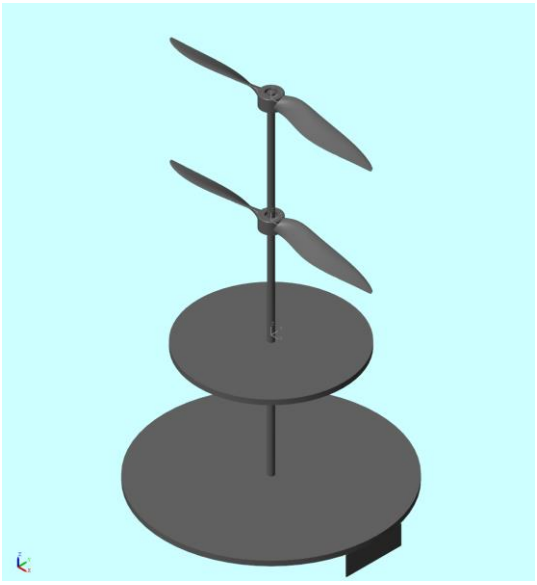

Figure 6.1. Screen Shot Taken from MATLAB Mechanics Explorer Animation

6.1 Simulation Parameters

Propeller sizing with the overall scaling of the UAV is inspired from a coaxial drone study [23]. However, exact dimensions of the propeller are decided according to the experimental performance data published from a supplier [24]. Therefore, APC 9x6

propeller [25] is selected from the catalog. The selected parameters for simulations of the UAV are shown in Table 6.1.

Table 6.1 Numerical Parameters of the UAV

Parameters	*Values*	*Parameters*	*Values*
$m_1\,[kg]$	0.5243	$b_0\,[m]$	0.1100
$m_2\,[kg]$	0.2567	$l_0\,[m]$	0.1200
$m_3, m_4\,[kg]$	0.0221	$d_0\,[m]$	0.0750
$J_{11},\ J_{12}\left[kg\cdot m^2\right]$	0.0016	$h_0,\ h_1\,[m]$	0.1100
$J_{13}\left[kg\cdot m^2\right]$	0.0031	$h_{hub}\,[m]$	0.0120
$J_{21},\ J_{22}\left[kg\cdot m^2\right]$	6.1739e-4	$r_{shaft}\,[m]$	0.0030
$J_{23}\left[kg\cdot m^2\right]$	6.7377e-4	$t_p\,[m]$	0.0050
$J_{31},\ J_{32},\ J_{41},\ J_{42}\left[kg\cdot m^2\right]$	7.2749e-7	$h_f\,[m]$	0.0200
$J_{33},\ J_{43}\left[kg\cdot m^2\right]$	3.4093e-5	$l_f\,[m]$	0.0569
$c_1\,[m]$	0.0010	C_D	1.17
$c_2\,[m]$	0.0076	$g\left[m/s^2\right]$	9.8100

6.2 Open Loop Simulations

Firstly, the torques and angular velocities of the propellers required for hovering are calculated as seen in Eqs (6.1) and (6.2).

$$T_{233,h} = -0.6101 \left[N \cdot m\right]$$
$$T_{243,h} = 0.6101 \left[N \cdot m\right] \tag{6.1}$$

$$\omega_{3,h} = -627.8005 \left[rad / s\right]$$
$$\omega_{4,h} = 627.8005 \left[rad / s\right] \tag{6.2}$$

OL (open-loop) simulations are started in hovering state. Newton – Euler equations derived in Chapter 3 are simulated by 2 different scenarios. In the first scenario, the universal joint actuator inputs T_{1c3} and T_{c22} are increased to observe the 10 states of the UAV. The inputs for the first scenario are shown in

Figure 6.2. The position states $\{x, y, z, \phi_1', \phi_2', \phi_3', \phi_2, \phi_3\}$ are both measured by the sensor blocks of the Simscape and calculated by the derived Newton-Euler equations. The two results are shown in the same plots to show the consistency. Those plots can be seen in Figure 6.3 and Figure 6.4. Similarly, plots for the velocity states are illustrated in Figure 6.5, Figure 6.6 and Figure 6.7.

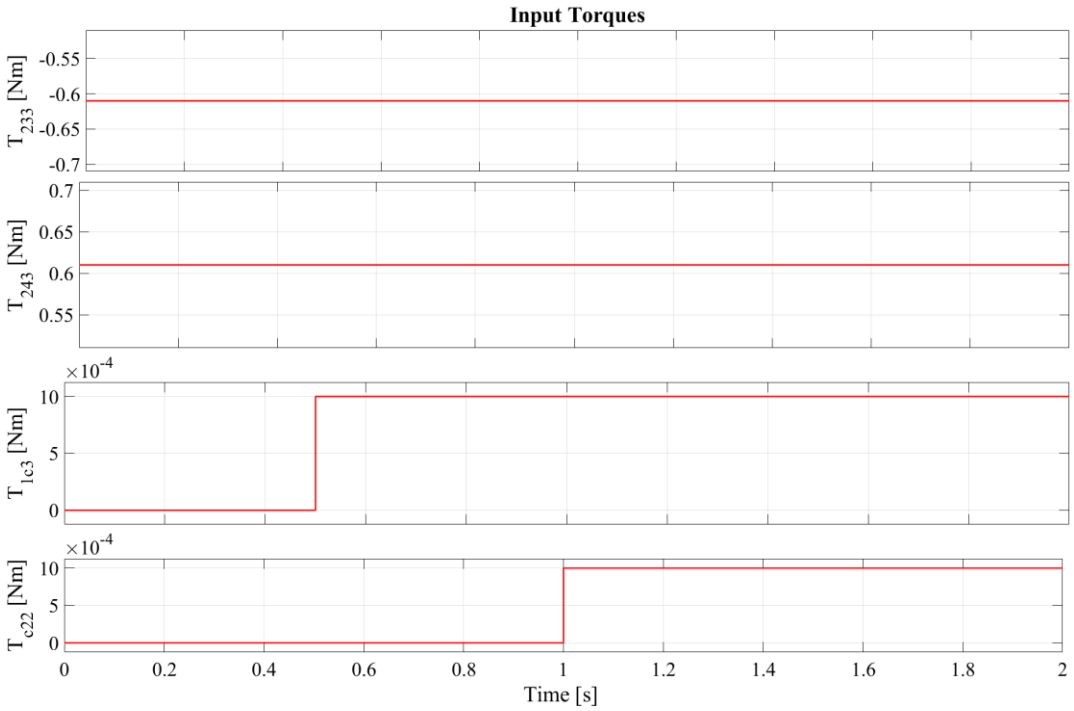

Figure 6.2. Input Torques for the OL Simulation

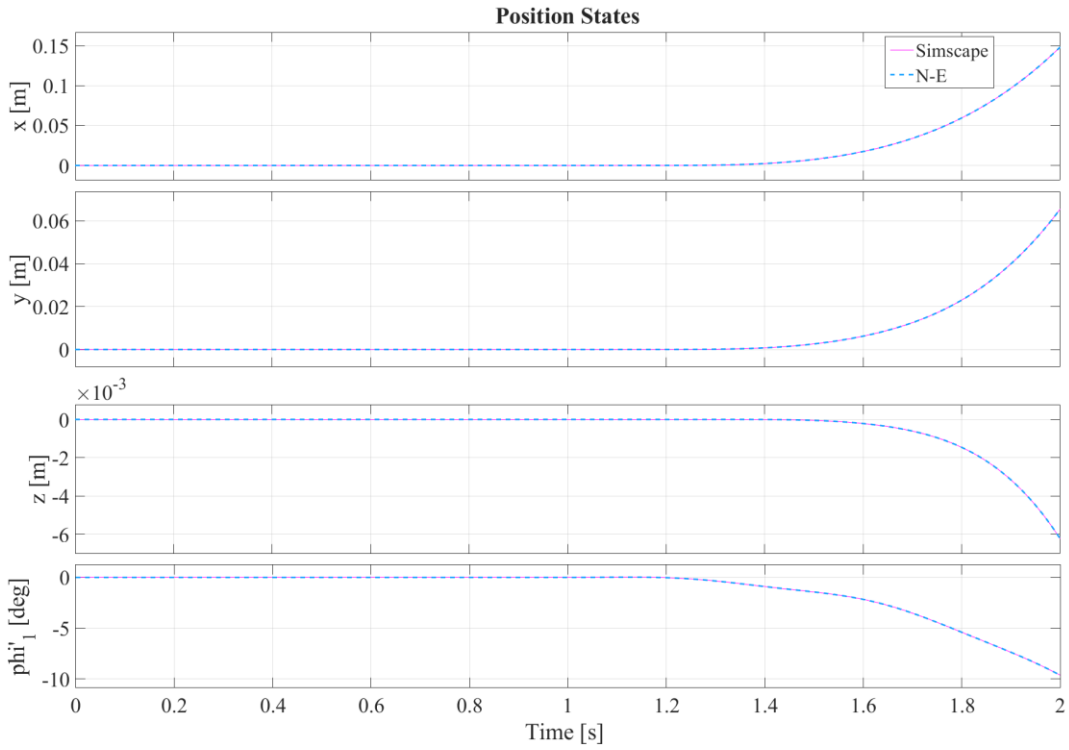

Figure 6.3. First Set of Position States for the OL Simulation

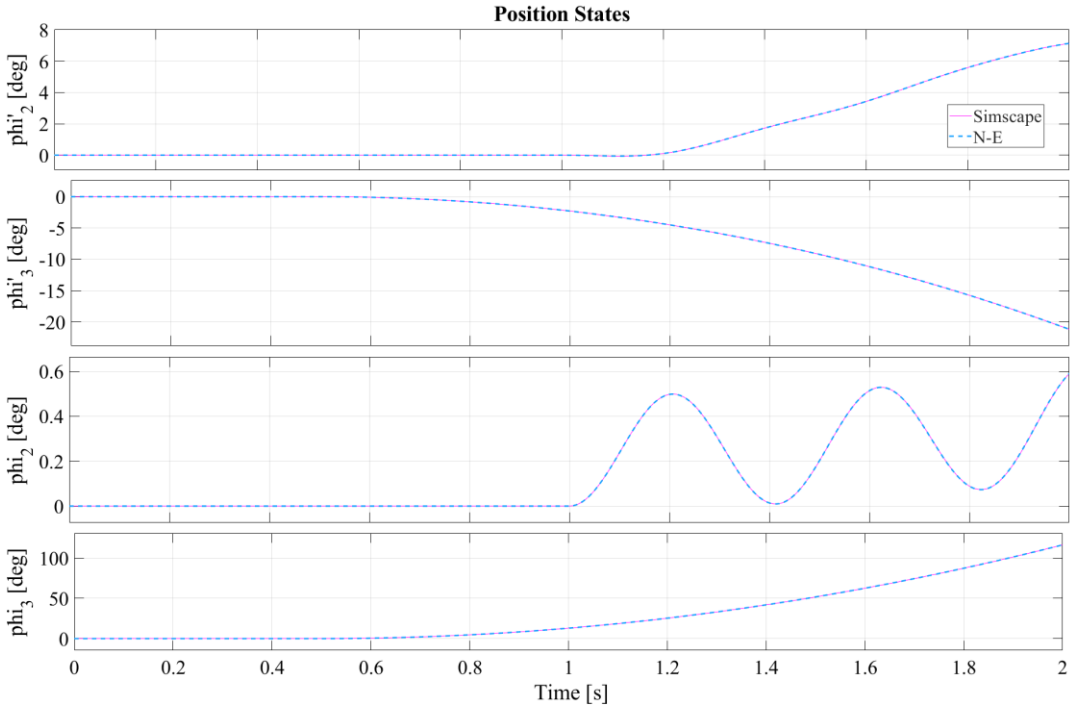

Figure 6.4. Second Set of Position States for the OL Simulation

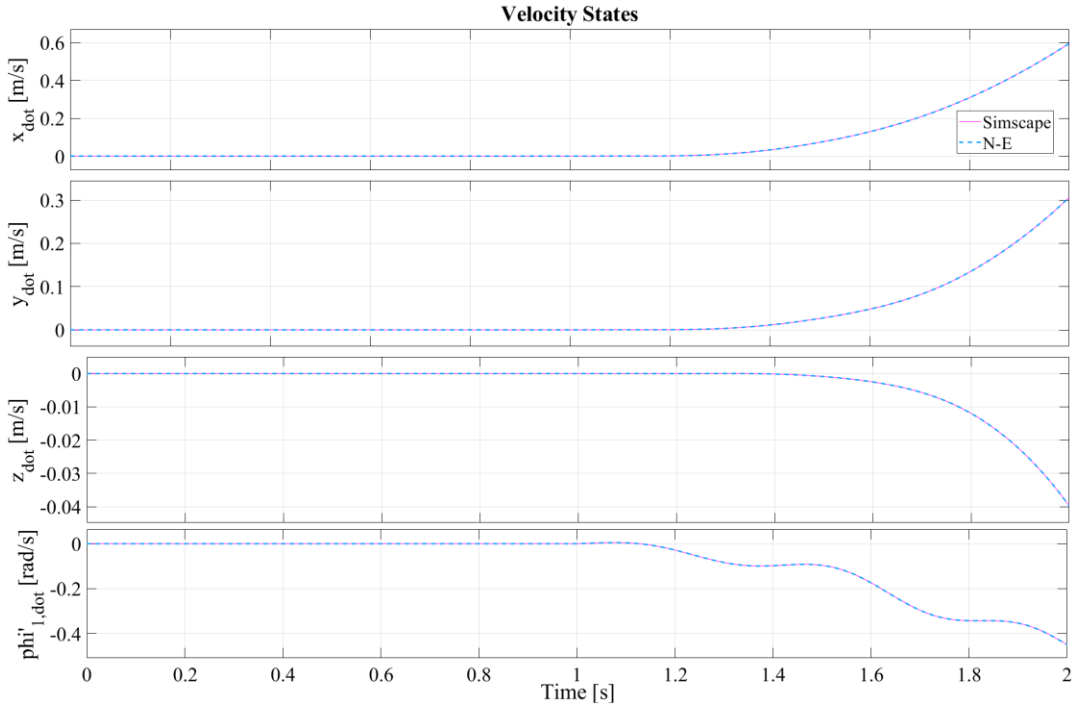

Figure 6.5. First Set of Velocity States for the OL Simulation

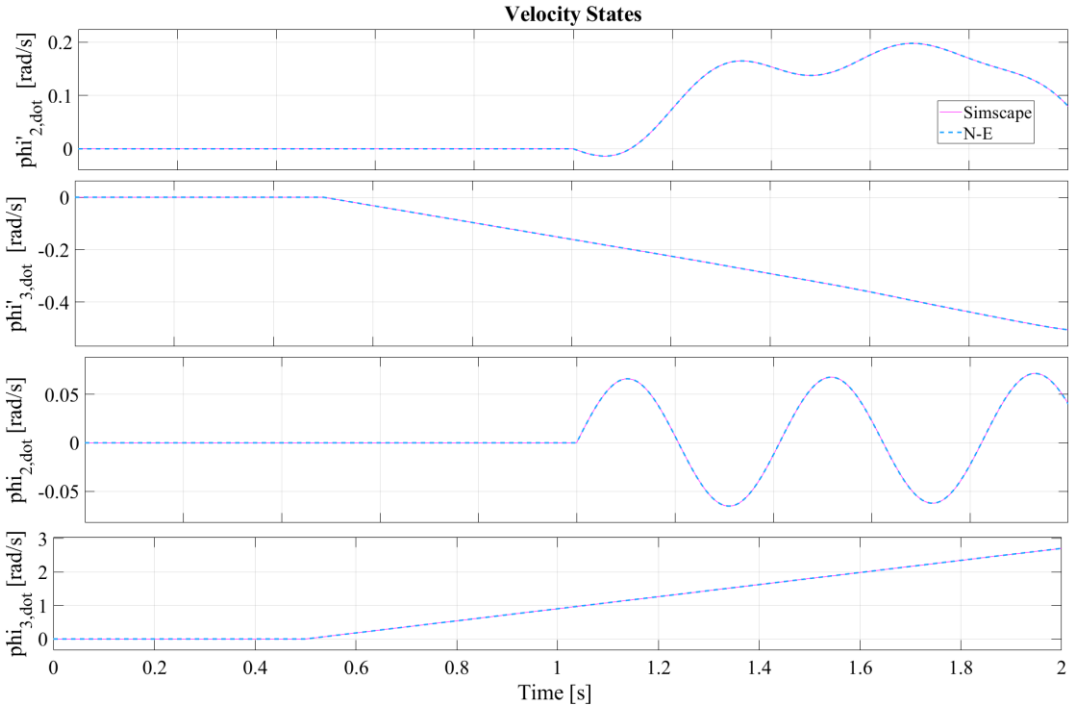

Figure 6.6. Second Set of Velocity States for the OL Simulation

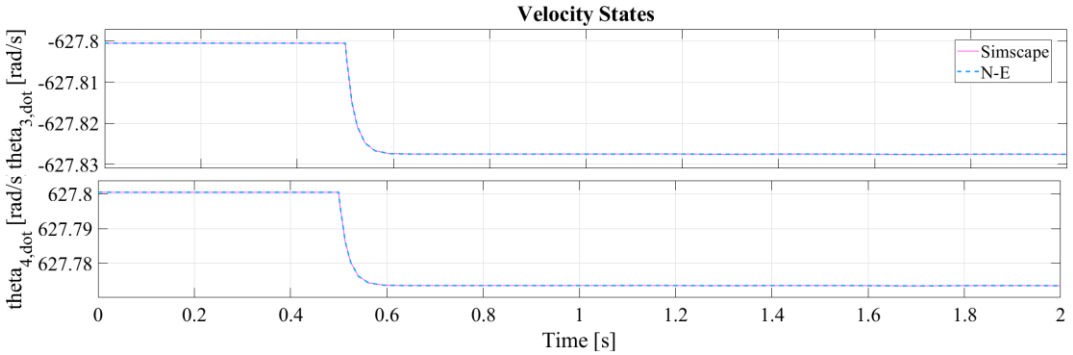

Figure 6.7. Third Set of Velocity States for the OL Simulation

6.3 Closed Loop Simulations

The computed torque control method explained in Chapter 4 is utilized in the simulations. The desired trajectory is tracked by the frame of the base platform and the results are shown in following sections.

6.3.1 Altitude Control

A polynomial trajectory block from Simulink is utilized for trajectory planning of the altitude. Reference altitude position, velocity and acceleration values are generated by this block. To acquire altitude control, gains for PID control law are selected as seen below according to the pole placement of the characteristic equation for the error function which is the third order polynomial for PID control law.

$$\begin{aligned} K_{p,z} &= 3178.4268 \\ K_{i,z} &= 33457.1247 \\ K_{d,z} &= 98.4643 \end{aligned} \tag{6.3}$$

Altitude data from a Simscape sensor block and desired positional trajectory is shown in the same plot to evaluate the reference position tracking. This plot is illustrated in Figure 6.8.

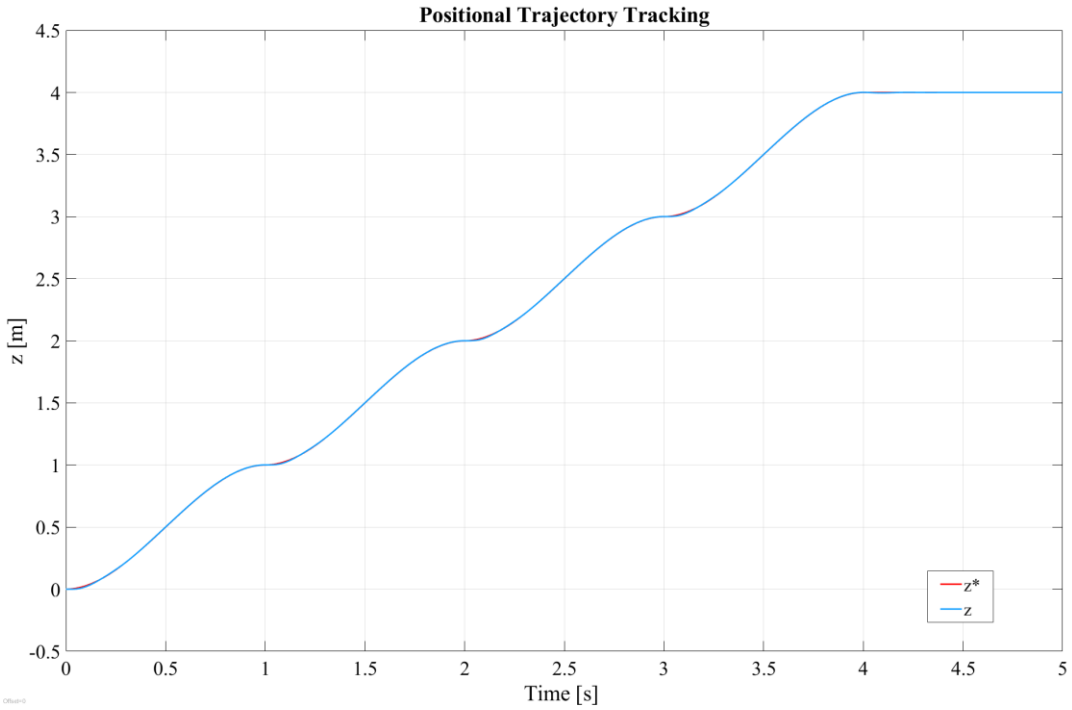

Figure 6.8. Reference Altitude Position Tracking of the UAV

Moreover, velocity data in z direction is taken from another Simscape sensor block and plotted with the desired velocity in z direction which is shown in Figure 6.9 to evaluate the reference velocity tracking.

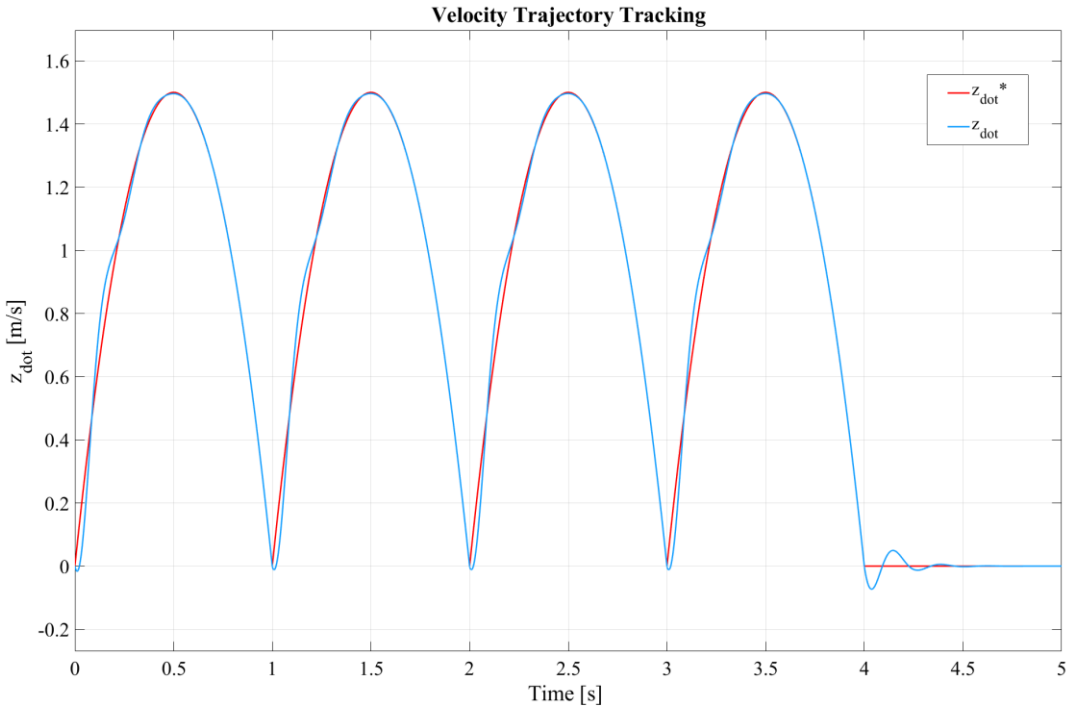

Figure 6.9. Reference Velocity Tracking of the UAV in Z Direction

6.3.2 Yaw Motion Control

A rotation trajectory block from Simulink is used for angular trajectory planning of the yaw motion. Reference yaw angle, angular velocity and acceleration values are generated by this block. During designing yaw motion control, gains for PD control law are selected as seen below according to the pole placement of the characteristic equation for the error function which is the second order polynomial for PD control law.

$$\begin{aligned} K_{p,yaw} &= 34.6021 \\ K_{d,yaw} &= 11.7647 \end{aligned} \tag{6.4}$$

Yaw angle data from a Simscape sensor block and desired angular trajectory is shown in the same plot to evaluate the reference angle tracking. This plot is illustrated in Figure 6.10

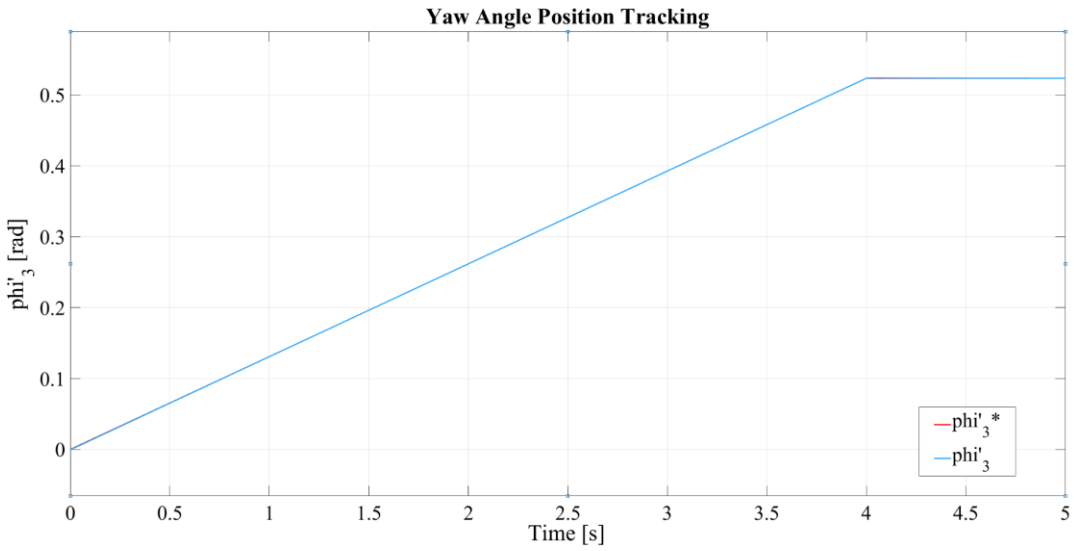

Figure 6.10. Reference Yaw Angle Tracking of the UAV

In addition, yaw angular velocity data is taken from another Simscape sensor block and plotted with the desired yaw angular velocity which is shown in Figure 6.11 to evaluate the tracking of the reference yaw angular velocity.

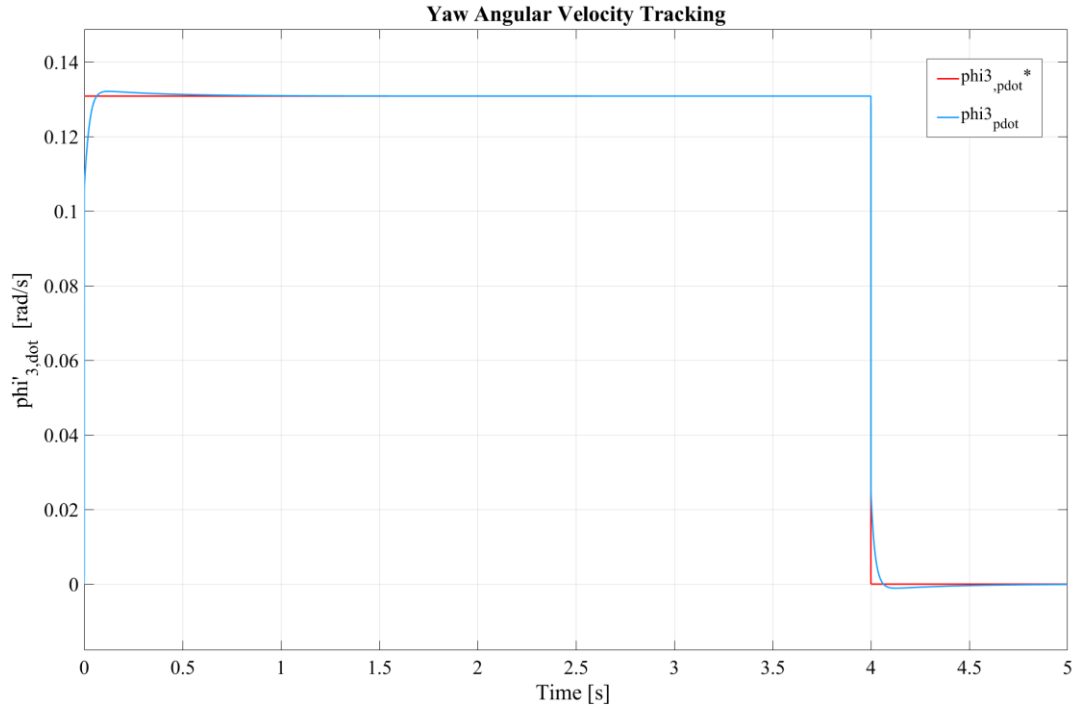

Figure 6.11. Reference Yaw Angular Velocity Tracking of the UAV

6.3.3 Motion Control in X-Y Plane

PID control is applied to x velocity feedback then output becomes reference angle ϕ_2^* and is fed to the PD controller. Reference angular velocity $\dot{\phi}_2^*$ is taken as 0. Thus, final output is required torque T_{c22} to tilt the upper platform. The gains can be seen in Eq. (6.5). Here, T_{1c3} is taken as zero for simplicity.

$$\begin{aligned} K_{p,\dot{x}} &= 1.5 \\ K_{i,\dot{x}} &= 0.1 \\ K_{d,\dot{x}} &= 0.2 \\ K_{p,\phi_2} &= 200 \\ K_{p,\dot{\phi}_2} &= 50 \end{aligned} \tag{6.5}$$

x position data from a Simscape sensor block and desired x trajectory is shown in the same plot to evaluate the reference position tracking. This plot is illustrated in

Figure 6.12. Moreover, $\dot{x}$ data from Simscape sensor block and desired $\dot{x}$ reference velocity is plotted in Figure 6.13 to show the reference velocity tracking in x direction.

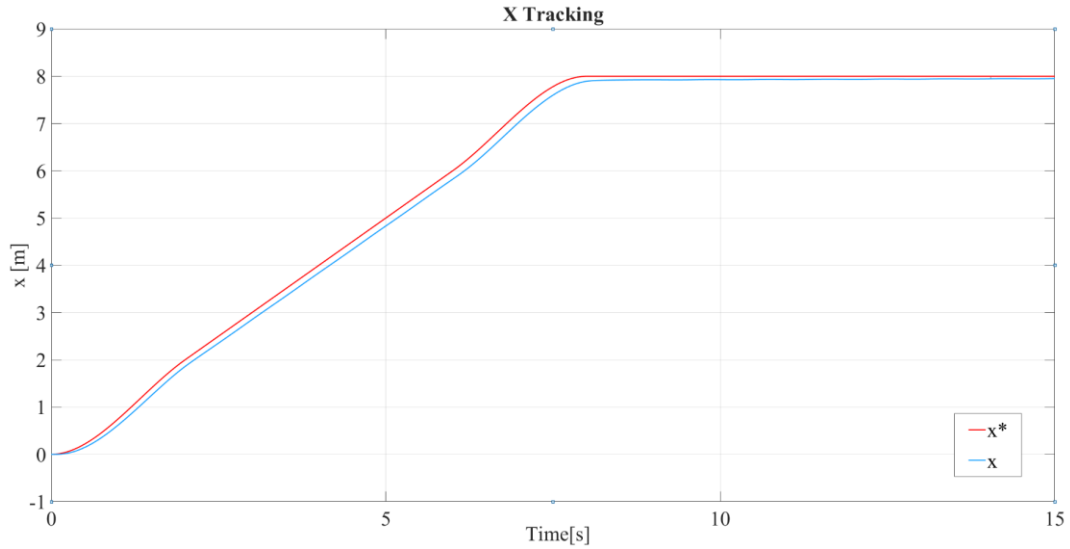

Figure 6.12. Reference X Position Tracking of the UAV

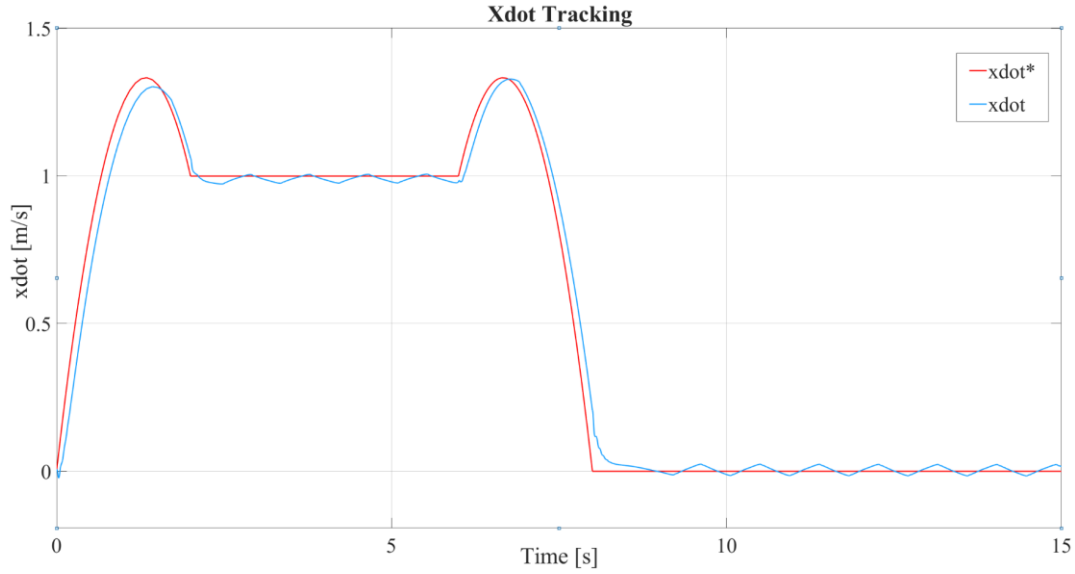

Figure 6.13. Reference X Velocity Tracking of the UAV

CHAPTER 7

CONCLUSION AND FUTURE WORKS

7.1 Conclusion

The UAV design consists of 3 actuated prismatic joints and 4 spherical joints as connecting base platform to upper platform along with 2 coaxial propellers on the shaft of the upper body. Since there is a parallel manipulator configuration, it creates a complexity while modelling the UAV, some simplifications are done such as eliminating the 3 legs and leaving only one leg. Moreover, to eliminate redundancy, the spherical joint at the center is replaced by a universal joint. After processing the simplifications, kinematic analysis is conveyed for the serial manipulator configuration. In the kinematic analysis part, as a result, linear and angular acceleration equations are obtained and expressed in closed form.

Then, in the Dynamic Analysis part, Newton-Euler equations are derived. The interaction forces along with the downwash and other aerodynamic forces and moments are expressed in the N-E model. After that, Direct Dynamic Analysis method is utilized to solve the N-E equations in a matrix form. Structural forces and moments are eliminated from the resulting matrix to proceed with solution for generalized coordinates and velocities only.

Afterwards, the *computed torque method* is proposed in order to guide the UAV so that it tracks specified variations of the mass center coordinates and yaw angle. Meanwhile, the equivalency is verified between the actual UAV design involving a 3-DoF parallel manipulator and a simplified design involving a serial configuration. In the Simulation studies, open-loop and closed-loop simulations are done to realize the motion of the UAV in MATLAB, Simulink and Simscape environment. For the sake of simplicity, the closed-loop simulations are done within two distinct case studies. In the first case study, only the controls of the altitude and yaw motions are

simulated. In the second case study, only controls of the x and y motions are simulated. The results of the Simulations are listed as below.

- Kinematic expressions are compatible with the results obtained from the MATLAB symbolic toolbox.
- N-E equations are compared with the Simscape model and results are consistent with each other in terms of position and velocity generalized coordinates.
- After validating Simscape model with N-E equations, PID with PD controller is applied to the model to control the UAV in x direction by tilting the upper platform. Reference input tracking is shown and the results are satisfactory in terms of position and velocity generalized coordinates.
- Proposed Computed Control Algorithm is applied for yaw and altitude motion of the UAV in Simscape and Simulink environment. Reference input tracking is shown and the results are satisfactory in terms of position and velocity generalized coordinates.
- The overall motion of the UAV is simulated by yaw motion control to change the heading angle then motion control in x-direction of the UAV to track reference position and velocity inputs in x-y plane while controlling the altitude motion simultaneously throughout the task.
- Since the UAV is underactuated, roll and pitch angles of the UAV is uncontrolled actively but to keep them in finite values, passive stabilizing effects are necessary in the model. The restoring effect of the gravity and downwash effect are modelled initially as passive stabilizing effects but simulation results show that, damping effect of the air on the roll and pitch angles of the UAV is crucial for passive stabilization. Moreover, drag force in the opposite direction of the longitudinal motion is also included in the model later to have more satisfactory results in terms of motion in x-y plane.

7.2 Future Works

- The aerodynamic forces and moments modelled in N-E equations can be validated by CFD analysis. Especially the stabilizing coefficient to model damping effect of the air is based on engineering judgement and trial and error thus, this coefficient can be found more precisely via CFD analysis.
- A prototype can be manufactured along with the test bench to validate the simulations by experiments.

REFERENCES

[1] O. A. Martinez and M. Cardona, “State of the Art and Future Trends on Unmanned Aerial Vehicle,” *Proceedings of the 2018 3rd IEEE International Conference on Research in Intelligent and Computing in Engineering, RICE 2018*, Oct. 2018, doi: 10.1109/RICE.2018.8509091.

[2] “Curtiss-Sperry Aerial Torpedo at the Cradle of Aviation Museum.” https://www.cradleofaviation.org/history/exhibits/exhibit-galleries/world_war_i/curtiss_sperry_aerial_torpedo.html (accessed Aug. 25, 2022).

[3] X. Y. Liu, M. Z. Liu, X. G. Tuo, and J. Wang, “The recent advance of unmanned quadrocopter,” *Applied Mechanics and Materials*, vol. 574, pp. 564–568, 2014, doi: 10.4028/WWW.SCIENTIFIC.NET/AMM.574.564.

[4] S. Norouzi Ghazbi, Y. Aghli, M. Alimohammadi, and A. A. Akbari, “Quadrotors unmanned aerial vehicles: A review,” *International Journal on Smart Sensing and Intelligent Systems*, vol. 9, no. 1, pp. 309–333, Mar. 2016, doi: 10.21307/IJSSIS-2017-872.

[5] W. Johnson, *Helicopter Theory*. Dover Publications, 1994. doi: 10.1108/eb030686.

[6] G. D. Padfield and C. Eng, *HELICOPTER FLIGHT DYNAMICS The Theory and Application of Flying Qualities and Simulation Modelling Second Edition*, Second Edition. Blackwell Publishing, 2007.

[7] P. Pounds, R. Mahony, and P. Corke, “Modelling and control of a large quadrotor robot,” *Control Eng Pract*, vol. 18, no. 7, pp. 691–699, Jul. 2010, doi: 10.1016/j.conengprac.2010.02.008.

[8] M. Soliman, T. Matsue, S. Andou, and S. Yoshikawa, “Analysis and optimization of coaxial propeller-driven drones,” in *AIAA Scitech 2021 Forum*, 2021, pp. 1–6. doi: 10.2514/6.2021-0210.

[9] B. Sababha, H. Alzubi, O. Rawashdeh, B. H. Sababha, H. M. al Zu'bi, and O. A. Rawashdeh, "A rotor-Tilt-free tricopter UAV: Design, modelling, and stability control," *Int. J. Mechatronics and Automation*, vol. 5, no. 3, pp. 107–113, 2015, doi: 10.1504/IJMA.2015.075956.

[10] W. Ong, S. Srigrarom, and H. Hesse, "Design methodology for heavy-lift unmanned aerial vehicles with coaxial rotors," 2019. doi: 10.2514/6.2019-2095.

[11] F. Bohorquez, P. Samuel, J. Sirohi, D. Pines, L. Rudd, and R. Perel, "Design, analysis and hover performance of a rotary wing micro air vehicle," *Journal of the American Helicopter Society*, vol. 48, no. 2, pp. 80–90, 2003, doi: 10.4050/JAHS.48.80.

[12] K. Malandrakis, R. Dixon, A. Savvaris, and A. Tsourdos, "Design and Development of a Novel Spherical UAV," *IFAC-PapersOnLine*, vol. 49, no. 17, pp. 320–325, 2016, doi: 10.1016/j.ifacol.2016.09.055.

[13] J. Paulos, B. Caraher, and M. Yim, "Emulating a Fully Actuated Aerial Vehicle Using Two Actuators," in *Proceedings - IEEE International Conference on Robotics and Automation*, Sep. 2018, pp. 7011–7016. doi: 10.1109/ICRA.2018.8462975.

[14] S. George and P. Samuel, "On the design and development of a coaxial nano rotorcraft," 2012. doi: 10.2514/6.2012-585.

[15] "(1004) Coaxial UAV - YouTube." https://www.youtube.com/watch?v=P2z2p_0XXwA (accessed May 23, 2021).

[16] "(1004) Coaxial drone - YouTube." https://www.youtube.com/watch?v=6FU_HeXyI-Y&t=4s (accessed May 23, 2021).

[17] M. K. Ozgoren, *Kinematics of General Spatial Mechanical Systems*. John Wiley & Sons, 2020.

[18] “Model Rocket Weather Cocking.” https://www.grc.nasa.gov/www/k-12/VirtualAero/BottleRocket/airplane/rktcock.html (accessed Aug. 06, 2022).

[19] C. C. Chen and H. H. T. Liu, “Model of UAV and Downwash for Multi-UAV Path Planning,” *AIAA Science and Technology Forum and Exposition, AIAA SciTech Forum 2022*, 2022, doi: 10.2514/6.2022-0757.

[20] P. Gerhart, A. Gerhart, and J. Hochstein, *Munson, Young and Okiishi’s fundamentals of fluid mechanics*, 8th ed. John Wiley & Sons, 2016.

[21] M. Kemal Özgören, *ROBOT MANİPÜLATÖRLERİN DİNAMİĞİ VE KONTROLU*. Makina Teorisi Derneği ve Gazi Üniversitesi, 2016.

[22] M. K. Ozgoren, “Comparative study of attitude control methods based on Euler angles, quaternions, angle–axis pairs and orientation matrices:,” *https://doi.org/10.1177/0142331218773519*, vol. 41, no. 5, pp. 1189–1206, Jun. 2018, doi: 10.1177/0142331218773519.

[23] V. H. Dominguez, O. Garcia-Salazar, L. Amezquita-Brooks, L. A. Reyes-Osorio, C. Santana-Delgado, and E. G. Rojo-Rodriguez, “Micro Coaxial Drone: Flight Dynamics, Simulation and Ground Testing,” *Aerospace*, vol. 9, no. 5, May 2022, doi: 10.3390/AEROSPACE9050245.

[24] “Performance Data - APC Propellers.” https://www.apcprop.com/technical-information/performance-data/ (accessed Sep. 10, 2022).

[25] “9x6 - APC Propellers.” https://www.apcprop.com/product/9x6/ (accessed Sep. 10, 2022).